



UNIVERSITY OF LEEDS

Incipient Slip Detection and Grasping Automation for Robotic Surgery

Ian Waters

The University of Leeds

Faculty of Engineering and Physical Sciences

School of Mechanical Engineering

Date of Submission: 24/10/2022

Abstract

Robotic minimally invasive surgery provides multiple improvements over traditional laparoscopic procedures, but one significant issue still encountered is their limited force control during the grasping and retraction of tissue, as the surgeon is separated from the instrument, and therefore denuded of their sense of touch and the applied forces. Prior solutions have largely looked towards haptic feedback to resolve this issue, but an alternative approach is to detect and monitor the occurrence of tissue slip events. This would allow the force to be automatically adjusted to prevent slip, minimising the clamp force used to maintain control, thus reducing the probability of tissue trauma. The aim of this work is to develop a method for the early detection and mitigation of tissue slip during robotic surgical manipulation tasks, helping to reduce tissue trauma and minimise tissue slip events.

Initial investigations into literature, and evaluation of the slip mechanics when grasping soft, lubricated, deformable materials, indicated that small localised slips occur before the onset of macro slip. Two phenomena were identified in the slip mechanics investigation that could be employed to induce these slip in a measurable and repeatable manner. Firstly through using the tissue's deformable properties to create slip differentials between the front and rear of the grasper face, and secondly through using a curved surface to create a variation in the normal force, and thus frictional force, across the surface.

Two instrumented grasper faces were developed, based on each of these phenomena, that were capable of monitoring the occurrence of localised tissue slip through monitoring the displacement of a series of independent movable islands that made up the grasper face.

These were then demonstrated to be capable of automatically detecting slip events for a range of test conditions with tissue simulants, before being utilised to automatically control the grasping forces during a tissue retraction task. Both sensor systems provided similar levels of tissue control to one which utilised the maximum clamp force throughout the task, whilst applying lower forces during the early stages of retraction, reducing the probability of tissue damage. In addition the normal force based method, with the curved grasper face, was demonstrated to be effective for the early detection of slip when grasping porcine liver tissue, successfully detecting incipient slip in 77% of cases.

This work provides a strong basis for further development of incipient slip sensing for surgical applications. It provides novel contributions in the understanding of slip mechanics of soft tissues, as well as presenting two separate novel sensing approaches for the automatic detection and mitigation of slip events, offering an opportunity for reducing the occurrence of tissue slip events whilst minimising tissue trauma, as well as surgeon fatigue.

Acknowledgements

I would first like to thank my supervisors, Peter Culmer and Ali Alazmani for their advice and encouragement over the past three and a half years, without whom this work wouldn't have been possible. Pete Culmer in particular has provided countless assistance in reviewing and refining my publications. Peter Culmer and Nik Kapur should also be commended for keeping me sane through the COVID-19 lockdowns, by employing me to work on the LEVE mechanical ventilator project, which let me get out of the house a little more, and was some of the best work I've ever had the pleasure to be part of. William Davis-Birch, the people at Mengo hospital, Medaid, and within the NHS at Leeds General Infirmary, should also receive recognition for this amazing piece of work.

Next, I'd like to thank the members of the healthcare mechatronics lab, in particular Dominic Jones who has been helping me right from Day 1, and has been a constant sounding board for my ideas, and even more of my problems.

Finally to my family and friends who've always given me support throughout the years, and never fail to cheer me up or help distract me from my work when I most need it, especially through the isolation we've all been through over the past few years.



Acronyms

RAMS Robotically Assisted Minimally Invasive Surgery

MIS Minimally Invasive Surgery

DoF Degrees of Freedom

CoF Coefficient of Friction

FA Fast Adapting

SA Slow Adapting

PVDF Polyvinylidene Fluoride

DIC Digital Image Correlation

SITS Soft Inductive Tactile Sensor



Contents

1	Background	1
1.1	Introduction	2
1.1.1	Contributions	4
1.2	Literature Review	4
1.2.1	Clinical Need	5
1.2.2	Tactile Sensing in Surgical Graspers	6
1.2.3	Slip Mechanics	9
1.2.4	Incipient Slip Detection	13
1.2.5	Automation	22
1.2.6	Summary of Literature	22
1.3	Aims and Objectives	24
1.3.1	Thesis Outline	24
2	Engineering Incipient Slip Into Surgical Graspers to Enhance Grasp Performance	37
2.1	Introduction	38
2.2	Methods	41
2.2.1	Background	41
2.2.2	Grasper Design	41
2.2.3	Experimental Setup	42
2.2.4	Experimental Parameters	42
2.2.5	Analysis Method	43

2.3	Results	44
2.4	Discussion	46
2.5	Conclusion	47
2.6	Appendix	51
3	Incipient Slip Sensing for Improved Grasping in Robot Assisted Surgery	55
3.1	Introduction	56
3.2	System Development	59
3.2.1	Concept	59
3.2.2	System Design and Fabrication	60
3.2.3	Data Processing	62
3.2.4	Slip Detection	63
3.3	System Evaluation	65
3.3.1	Experimental Set Up and Analysis	65
3.3.2	Data Analysis	65
3.3.3	Experimental Parameters	67
3.3.4	Results	69
3.4	Case Study: Automation	71
3.5	Discussion	73
3.6	Conclusions and Further Work	77
3.7	Appendix	82
4	Encouraging and Detecting Preferential Incipient Slip for Use in Slip Prevention in Robot-Assisted Surgery	85
4.1	Introduction	86
4.2	System Development	89
4.2.1	Concept and Requirements	89
4.2.2	System Design and Fabrication	90
4.2.3	Signal Processing	92
4.2.4	Slip Detection	93

4.3	Materials and Methods	95
4.3.1	Experimental Set Up	95
4.3.2	Experiment I: Silicone Tissue Simulants	96
4.3.3	Experiment II: Porcine Liver	97
4.4	Results	98
4.4.1	Experiment I: Silicone Tissue Simulants	98
4.4.2	Experiment II: Porcine Liver	102
4.5	Discussion	104
4.6	Conclusions and Further Work	107
4.7	Appendix	112
5	Utilising Incipient Slip for Grasping Automation in Robot Assisted Surgery	115
5.1	Introduction	116
5.2	System Development	119
5.2.1	Concept and Requirements	119
5.2.2	System Design and Fabrication	119
5.2.3	Signal Processing	122
5.2.4	Slip Detection & Mitigation	122
5.3	System Evaluation	127
5.3.1	Experimental Set Up and Analysis	127
5.3.2	Experimental Parameters	128
5.3.3	Data Processing	129
5.3.4	Results	130
5.4	Discussion	133
5.5	Conclusions and Further Work	135
5.6	Appendix	140
6	Discussion and Conclusions	143
6.1	Introduction	144

6.2	Comparison of Developed Slip Sensing Methods	145
6.3	Comparison With Alternative Slip Sensing Systems	148
6.4	Evaluation against the Mechanics of Slip Theory	150
6.5	Assessment of Research Objectives	151
6.6	Future Work	153
6.7	Conclusions	156

List of Figures

1.1	Example of a RAMS platform, the Da Vinci Surgical System [9]	2
1.2	Left: Example of a typical robotic surgical grasper (Double Fenestrated Grasper, Intuitive) Right: A cross-section of histological tissue samples of porcine colon, displaying the effect of clamping force on colon tissue damage during laparoscopic grasping [15]	3
1.3	Left: Graph indicating the ‘Safe Grasp’ region where the force is sufficient to hold the tissue without causing tissue trauma or a loss of control. Right: (A) Arrangement of the heater and thermistors in a temperature based slip detection system. (B) Principle of operation of slip detection system based on hot wire anemometry	8
1.4	Diagram of contact mechanics between an elastic cylinder and a rigid flat plate under normal and tangential loads demonstrating how incipient slip can occur.	10
1.5	Coulomb’s model of friction indicating that the frictional force is independent of the sliding velocity	13
1.6	Change in the ratio of stuck area (Dark Grey) to the slipping area (light grey) as the contact of a finger progresses from incipient to macro slip	14
1.7	Diagram of the various mechanoreceptors present within the human glaborous skin	14
1.8	Left: Diagram of slip sensor.Right: Diagram of slip sensor	16
1.9	Left: Strain Based slip sensor.Right: Slip sensor based on epidermal ridges	18
1.10	Left: Schematic of Biotac. Right: Biotac finger	19

1.11	Left: Principle of operation of optical slip sensor. Right: Output of Gelslim sensor during manipulation task	20
1.12	Principle of operation PapillArray. (A) Uncompressed State. (B) Compressed state with no tangential load, the normal force experienced by the right hand pillar is greater due to the larger compression. (C) Tangential load is applied, and friction force at the right pillar is higher due to higher normal load based on Amontons Law, therefore it will take a higher tangential load for this pillar to lose contact	21
1.13	Diagram displaying the relationship between the chapters and publications presented within this thesis.	26
2.1	Diagram of surgical grasper and the various grasper face designs investigated. Top: Control ("All Hex"). Middle: Convex. Bottom: Centre Hex. The colour map shows an example of the relative displacement of tissue across a convex grasper face due to incipient slip, prior to macro slip occurring.	39
2.2	Schematic of the control system used for the simulated grasping environment.	43
2.3	Image displaying the grid of 35 dots used for tracking the displacement, with the major metrics used for the calculation of local and general distortion marked on, as well as the relevant equations.	44
2.4	Affect of grasper design on the level of incipient slip, indicated by the magnitude of tissue distortion. The colour maps show typical y displacements for each grasper face. (a) Local Distortion. (b) General Distortion.	45
2.5	Typical response for displacement over time of the central and outer points for Lines 1 and 7 of the Convex grasper face. Colour maps show how the y displacement of the whole face changes over time.	46

2.6	Influence of grasper design on the level of incipient slip, indicated by the magnitude of both local and general tissue distortion. Affect of: (a) Variation in force, using Mat A with a 5 mm/s retraction speed. (b) Variation in speed, using Mat A with a 20 N clamp load. (c) Variation in tissue simulant stiffness, with a 20N clamp load and 5 mm/s retraction speed.	53
3.1	Concept of the slip sensor's mechanical operation; the grasper face is separated into movable islands that can be tracked to detect the difference in slip between the front and rear of the grasper (The scale indicates the relative displacement of the colours used in the diagram).	57
3.2	Top: Dimensioned grasper face islands. Middle: Exploded model of the different components making up the sensor system. Bottom: Illustration of the principle of operation of SITS sensors.	61
3.3	Example trace showing the displacement of the front and rear sensor islands, as well as the change in the separation between the two. Test conditions: Mat A, 20 N clamp load, and 2 mm/s retraction speed.	64
3.4	Model of the testing setup used for simulating the clamping and retraction of tissue.	66
3.5	Graphs showing average sensor displacement, with the shaded area representing the standard deviation. The vertical dotted lines indicate the time incipient slip occurs, while the solid vertical line indicates the time of macro slip, the shaded areas around each show range of slip times/displacements. a) Sensor displacement vs time for changes in force and material stiffness at a retraction speed of 2 mm/s. b) Sensor displacement vs linear stage displacement (retraction distance) for variations in retractions speed for Mat A under a 20 N clamping load.	68
3.6	Graphs showing the mean time difference between the detection of incipient and macro slip (N=5), the error bars indicate the standard deviation. (a) Variation of force and material stiffness at 2 mm/s retraction speed. (b) Variation of speed and material stiffness at 20 N clamp load.	69

3.7	Graphs show the average tissue displacement at the front, central and rear islands measured using DIC. The dotted line indicates the point of incipient slip while the solid line indicates macro slip. Colour maps show displacement profiles, 1 is the point of incipient slip, 2 is midway between incipient and macro slip, and 3 is the point of macro slip (a) Mat A, 20 N, 2 mm/s. (b) Mat C, 20 N, 2 mm/s.	70
3.8	Variation in shear and clamp loads for automated and fixed load control methods. The black vertical lines indicate the times of macro slip for each case. Mat A with a 1 mm/s retraction speed.	72
3.9	Comparison of tissue displacement for automated and fixed load control methods. Test carried out on Mat A with a 1 mm/s retraction speed. (a) Average displacement of tissue under the front, central, and rear islands. (b) Colour map showing tissue displacements.	73
3.10	Configuration of the multi-axis sensor calibration system. Adapted from [24]	82
3.11	Graphs showing comparison between the output of the trained neural network and the displacement measured by the calibration rig in x,y and z for the validation data set for the SITS sensor.	83
4.1	Diagram demonstrating the concept of encouraging incipient slip across grasper face through the variation of normal force using a curved surface.	87
4.2	Detailed drawing of grasper design showing independently movable islands, the grey circles indicate the positions of the magnetic sensing nodes (All dimensions are in mm). Section A-A: Cross section displaying the design of the sensed and passive islands. Section B-B: Cross section showing how the magnetic field moves through the Hall effect sensor as force is applied to the island.	91

- 4.3 Example of typical displacement characteristics for the front left, middle, and right islands of the grasper, under a 20N clamp load with a retraction speed of 2 mm/s (using Mat A). The inset shows how the variation of the slip ratio changes the time at which incipient slip of the edge islands is detected. 93
- 4.4 (a) A schematic showing key components of the experimental system. (b) An image of the experimental system used for simulating surgical grasping and retraction. 95
- 4.5 Graphs showing typical sensor displacements. The vertical dashed and dotted lines indicate the time slip is first detected at the outer and middle islands respectively, while the solid vertical line indicates the time of macro slip. The horizontal arrows indicate the time difference between the detection of incipient slip and the occurrence macro slip ($\Delta t_{mitigation}$), and the time between the detection of incipient slip of one of the front outer islands and the front middle island (Δt_{front}). (a) Sensor displacement vs time for changes in force and material stiffness at a retraction speed of 2 mm/s. (b) Sensor displacement vs linear stage displacement (retraction distance) for variations in retractions speed for Mat A under a 20 N clamping load. 99
- 4.6 Graphs showing the mean time difference (N=5) between: (a) Detection of slip at the outer and middle grasper islands (Δt_{front}) for variation of force and material stiffness with a 2 mm/s retraction speed. (b) Available mitigation time ($\Delta t_{mitigation}$) for variation of force and material stiffness with a 2 mm/s retraction speed. (c) Δt_{front} for variation of retraction speed and material stiffness with a 20 N clamp load. (d) $\Delta t_{mitigation}$ for variations of retraction speed and material stiffness with a 20 N clamp load. The error bars indicate the standard deviation 100

4.7	Typical results for average tissue displacement at the front, middle and rear of the grasper face measured using DIC. The vertical dashed and dotted lines indicate the time slip is first detected at the outer and middle islands respectively, while the solid vertical line indicates the time of macro slip. The colour maps show the change in displacement profiles over time. (a) Mat A, 20 N, 2 mm/s. (b) Mat C, 20 N, 2 mm/s.	101
4.8	Graphs showing example sensor displacement for cases in which the early detection of slip was successful for porcine liver samples for various load cases. The vertical dashed and dotted lines indicate the time slip is first detected at the outer and middle islands respectively, while the solid vertical line indicates the time of macro slip.	102
4.9	Graphs showing sensors displacements for cases in which early slip detection was unsuccessful, or there was abnormal sensor responses for liver tissue retractions.	103
4.10	Graphs showing the mean time difference (N=10) between: (a) Detection of slip at the outer and middle grasper islands (Δt_{front}). (b) Available mitigation time ($\Delta t_{mitigation}$). For variation of the clamp force with a 2 mm/s retraction speed. The error bars indicate the standard deviation.	103
4.11	Graphs showing comparison between the output of the trained neural network and the displacement measured by the calibration rig in x,y and z for the validation data set for the magnetic sensor.	112
5.1	Diagram demonstrating the concept of encouraging incipient slip across independently moveable sections of the grasper face through the variation of normal force using a curved surface.	120

5.2	Dimensioned drawing of the grasper separated into 5×3 grid of independently moveable islands, the grey circles indicate the positions of the sensing nodes (All dimensions in mm). Section A-A: cross section across the width displaying the design of the sensed and passive islands. Section B-B: Principle of operation of the sensing system, displaying how the magnetic field moves through the Hall effect sensor as force is applied to the island.	121
5.3	Example of typical displacement characteristics for the front left, middle and right islands of the grasper under a 20N clamp load with a retraction speed of 2 mm/s (using Mat C). The inset shows how variation of the slip ratio changes when incipient slip of the edge islands is detected.	123
5.4	A schematic showing the grasping and slip regimes defined by ϕ slip ratios and the associated response of the automated system. Uppermost, the diagrams show how the relative velocity of the islands, in the direction of retraction, differ in these regimes.	125
5.5	Graphs showing the effect on the shear force required to induce macro slip for the automated grasper during surgical retraction for: (a) Variation in gain. The dashed vertical lines indicate the gains identified for each retraction speed. (b) Variation of ϕ_T lower bound.	126
5.6	Image of the experimental set up used for simulating surgical grasping. Inset shows view of tissue simulant from video extensometer.	127
5.7	Typical grasping characteristics recorded for the automated and fixed test cases for variations in tissue simulant material stiffness and grasper retraction speed. Vertical lines indicated the point of macro slip.	130
5.8	Summary of the results for the average maximum shear force and average impulse, between $t=0$ and the point of macro slip, across all test conditions. The percentages indicate the relative decrease in metric between the 30N hold and automated test cases.	131

-
- 5.9 Representative displacement data for the tissue over the front, central and rear sections of the grasper, for the automated and non-automated control methods. The dashed vertical line indicates the point at which the automated system reaches the maximum 30N clamp force. (a) Low stiffness simulant (Mat A) with a 2mm/s retraction speed. (b) High stiffness simulant (Mat C) with a 2mm/s retraction speed. 132
- 5.10 Typical force characteristics during a retract and hold of tissue simulant for: (a) Low stiffness simulant (Mat A). (b) High stiffness simulant (Mat C). The black vertical lines indicate the point of macro slip, whilst the purple shaded areas indicate when the tissue is being retracted at 2 mm/s. 132
- 5.11 Representative displacement data for the tissue over the front, central and rear sections of the grasper, for the automated and non-automated control methods, for variations in material stiffness and retraction speed. The dashed vertical line indicates the point at which the automated system reaches the maximum 30N clamp force. 141

List of Tables

1.1	Summary of instrumented graspers for robotic surgery	7
1.2	Summary of methods for encouraging the preferential occurrence of incipient slips in a controlled and predictable manner	12
1.3	Summary of the major receptors in the glabrous skin of the fingertip . .	15
2.1	Experimental Parameters.	52

Chapter 1

Background

1.1 Introduction

Robotically Assisted Minimally Invasive Surgery (RAMS) is a burgeoning new technology that offers the opportunity to revolutionize the field of surgery, by making procedures faster [1], safer [1; 2; 3], and with shorter & less painful recoveries compared to traditional laparoscopic procedures [2; 3; 4; 5].

RAMS is an evolution of standard Minimally Invasive Surgery (MIS), however, rather than the instruments being manipulated directly by the surgeon they are connected to a robotic arm, which is then controlled via a telemanipulator system. The use of RAMS allows the introduction of features like 3D vision, articulated instruments, tremor elimination, and computer-assisted scaling, all of which help improve the level of accuracy and dexterity available to the surgeon, improving surgical outcomes[6; 7; 8].



Figure 1.1: Example of a RAMS platform, the Da Vinci Surgical System [9]

Despite the advantages offered by RAMS there has been limited uptake of the technology within hospitals. One of the main reasons cited by surgeons for this is the lack of haptic feedback [8; 10; 11], as there is no direct contact between the surgeon and the patient, so the surgeon is denuded of their sense of touch. This can result in multiple issues during surgery, but one of the most prominent is a lack of force control during grasping actions [12; 13]. The over-application of force can lead to tissue trauma, due to the crushing of the tissue by the grasper [12], or a lack of force can result in the occurrence of tissue slip

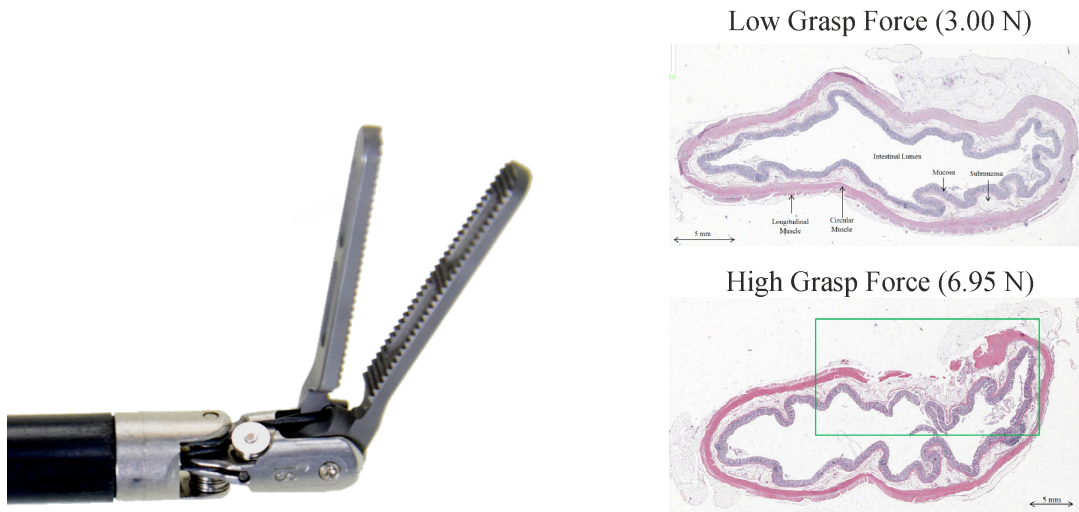


Figure 1.2: Left: Example of a typical robotic surgical grasper (Double Fenestrated Grasper, Intuitive) Right: A cross-section of histological tissue samples of porcine colon, displaying the effect of clamping force on colon tissue damage during laparoscopic grasping [15].

events, which can lead to surgical delays, or further adverse events [13; 14].

Although haptic feedback of the grasping forces has been demonstrated to be an effective means of reducing tissue trauma caused by excessive grasping forces, there has been limited investigation of its ability to reduce the occurrence of slip events during surgical grasping [16; 17; 18]. A more direct method of preventing slip, whilst minimizing the grasp forces applied, would be through detecting the occurrence of tissue slip. If slip can be detected early, then the grasping force can be adjusted to prevent further slips from occurring. This would allow the grasper to utilize reduced grasping forces, whilst preventing slip events, resulting in reduced tissue trauma, and minimizing the occurrence of loss of tissue control due to slip. This would also open up the possibility for automation of the force control during the grasping action, allowing them to focus on more critical surgical tasks, helping to reduce surgeon fatigue [19].

Therefore, the following work will investigate methods for detecting the slip of soft deformable tissues during surgical manipulation, so that mitigating actions can be taken to prevent slip, whilst aiming to also reduce tissue trauma.

1.1.1 Contributions

This dissertation makes the following contributions in the fields of surgical robotics, grasping, and sensing:

- Characterisation of the slip mechanics when grasping soft, deformable, lubricated materials, with various grasper face designs. The results of this work indicated two viable methods of inducing incipient slip when grasping these materials. This work provides a useful basis for future sensor designs for the detection of slip of deformable materials.
- A novel incipient slip sensing approach that utilizes the grasped materials' deformable nature to create measurable levels of incipient slip. This can be used to detect tissue slip early so that mitigating actions can be taken to prevent it, whilst reducing the applied grasping force, helping prevent tissue trauma during surgical grasping.
- A second novel slip sensing approach that uses a curved grasper face to create areas of high and low normal, and thus frictional force, to induce predictable incipient slips towards the outer edge of the grasper face, when grasping deformable materials. This system has been demonstrated to effectively detect the presence of incipient slip when grasping porcine liver samples, and has been used to fully automate the force control during grasping actions, under conditions representative of those used in surgical practice.

1.2 Literature Review

This literature review first evaluates the major clinical issues associated with robotic surgical graspers, to demonstrate the clinical need for improved slip detection, with a focus on the grasper's limited force control, which has been identified as a major issue during surgical manipulation tasks. The review then analyses current research that aims to resolve this issue, before presenting a novel alternative approach that utilizes detecting

tissue slip events through the induction and monitoring of localized incipient slips. The fundamentals of slip mechanics are then discussed, followed by a review of how both humans, and the latest conventional robotic grippers, encourage and detect incipient slip events.

1.2.1 Clinical Need

One of the main problems encountered within robotic and laparoscopic surgery is the limited force control available during tissue manipulation tasks, this can result in tissue trauma due to the over-application of force [12], or lead to tissue slip if insufficient grasping forces are used [12; 14].

The over-application of force has been shown to be the cause of up to 55% of consequential errors in surgical trainees [12]. During surgery excessive clamp forces can lead to tissue trauma, resulting in blood supply issues and localized necrosis [20], or even perforation and haemorrhaging of the tissue [12; 21], which can lead to far more serious issues like infection and sepsis.

In addition, the limited force control can result in tissue slip if insufficient gripping forces are used during manipulation and retraction tasks. Although these don't usually lead to consequential errors one study found them to be responsible for 21% of inconsequential errors [12], whilst another found them to account for 7% of failed grasping actions [22]. Slip during surgery is an undesirable event as it can lead to tearing of the grasped tissue, or result in further adverse events as the surgeon will not be expecting the tissue to slip [23]. Tissue slips also disrupt surgical procedures, leading to delays while the tissue is found and re-grasped, which results in longer surgeries with higher costs [19].

The main source of the limited force control during RAMS is the lack of haptic feedback available to the surgeon, denuding them of their sense of touch and an understanding of the forces being applied. Instead, surgeons rely on visual cues to estimate the force, but these have been demonstrated to provide insufficient information to reliably predict the magnitude of force being used for the task [24]. This is supported by trials done by *King*

et al. [16], where a tactile feedback system consisting of silicone balloons to simulate the force measured at the tips of the graspers was employed to provide force feedback to the surgeon. When moving an object from one peg to another, the study found that the addition of the tactile feedback mechanism reduced the mean applied force from 15.3 N to 6.4 N, a reduction of 58% [16]. *Wottowa et al.* [25] used a similar system to evaluate the effect of grasping force on tissue damage using porcine bowel samples, and found a direct correlation between the force applied and the amount of tissue damage present. The addition of haptic feedback to the system reduced the median number of tissue damage sites per sample from 3 to 1 [25].

1.2.2 Tactile Sensing in Surgical Graspers

A large amount of research has focused on the addition of sensors around the grasper jaws, a range of these sensors are summarised in Table 1.1. From the sensing modalities column, it can be seen that the majority of these systems focus on either measuring the pressure distribution, for palpitation and force control, or monitoring the shear and normal forces, with the aim of reducing tissue trauma caused by the over-application of force.

Although some of these systems have been demonstrated to effectively reduce the forces applied, and the levels of tissue trauma observed [16; 25], they still haven't seen inclusion within RAMS platforms. We believe a better method of controlling the grasping force is through monitoring and detecting the occurrence of tissue slip. If slip can be detected early then the grasping force can be adjusted to prevent it, this would also help to minimize the grasp force used to maintain a stable grip of the tissue, as only just enough force is being used to prevent tissue slip, thus reducing tissue trauma. Only a small number of graspers were identified that specifically focused on the detection of tissue slip (Table 1.1).

Table 1.1: Summary of instrumented graspers for robotic surgery

Researchers	Sensing Modality	Sensing Technology	Sensor Location/planned
<i>Howe et al.</i> [26]	Pressure Distribution	Capacitive tactile array 8x8	Grasper Jaws
<i>Kim et al.</i> [27; 28]	Normal and Shear Force (3 DoF)	Capacitive Sensor	Grasper Jaws
<i>Burkhard et al.</i> [29; 19]	Gross Slip	Heater and Thermistors (Similar to hot wire anemometry)	Grasper Jaws
<i>Dai et al.</i> [30]	Normal and Shear Force (3 DoF)	Capacitive Sensor	Grasper Jaws
<i>Khadem et al.</i> [31]	Grasp Force and Pull Force to estimate when close to slip point	Load Cell + 6 DoF Force Torque Sensor	Joint actuation unit + Robot arm
<i>Lee et al.</i> [32]	Normal and Shear Force (3 DoF)	Capacitive Sensor	Grasper Jaws
Hong and Jo [33]	Normal and Shear (2 DoF)	Strain Gauges	Articulated Joint
<i>Hammond et al.</i> [34]	Pressure Distribution	Conductive liquid filled microchannels 2x4	Grasper Jaw
<i>Qasaimeh et al.</i> [35]	Pressure Distribution	PVDF Array 3x3	Grasper Jaw
<i>King et al.</i> [16; 17]	Normal/Grasp Force	Piezoresistive with 2x3 electrode array	Grasper Jaw
<i>Schostek et al.</i> [36]	Pressure Distribution	Change in contact area between conductive polymer and spherical electrode array (33 electrodes)	Grasper Jaw
<i>Dargahi et al.</i> [37]	Pressure Distribution	PVDF Film with electrode array	Grasper Jaw
<i>Jones et al.</i> [38]	Normal and Shear (2 DoF)	Soft inductive tactile sensor (2 DoF)	Grasper Jaw
<i>Sokhanvar et al.</i> [39]	Pressure Distribution	PVDF film mounted on beams	Grasper Jaw
<i>Jones et al.</i> [40]	Gross Slip	Soft inductive tactile sensor (2 DoF)	Grasper Jaw

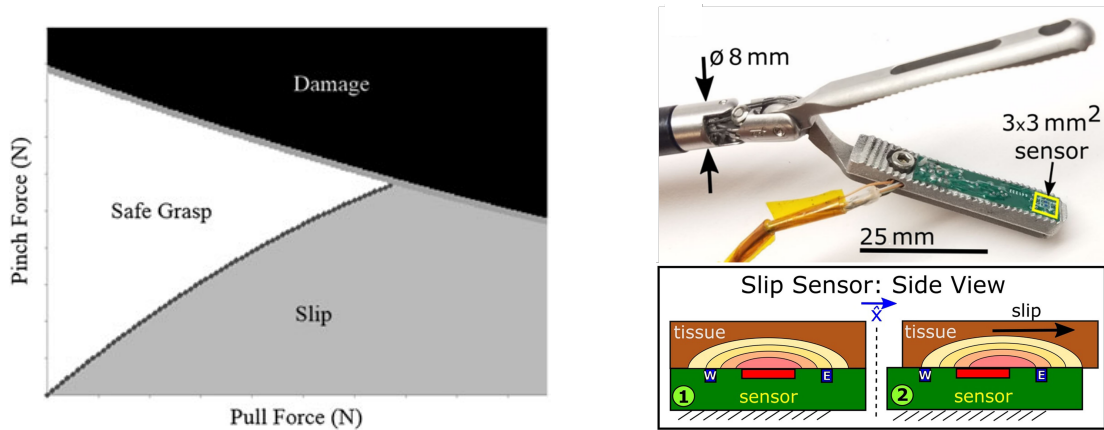


Figure 1.3: Left: Graph indicating the ‘Safe Grasp’ region where the force is sufficient to hold the tissue without causing tissue trauma or a loss of control [14]. Top Right: Slip sensor for use in surgical grasper developed by [29]. Bottom Right: Principle of operation of slip detection system based on hot wire anemometry [29].

Khadem et al. [31] developed an automated grasper system that automatically adjusts the applied gripping force, depending on the current retraction force, to remain within a pre-defined safe grasping zone (Figure 1.3). The system consists of two sensors, a load cell contained within the joint actuation unit, which measures the grasping force via the tension in the cable, and a 6 DoF force/torque sensor, connected at the interface between the robot arm and tool, to monitor the retraction forces [31]. The main issue with this system is it requires prior knowledge of the tissue being grasped, the safe grasping zone is pre-determined for each tissue, making it unable to adapt to different tissue types, or those with significant variation from the ‘average’, which is likely given the high variability between patients [41].

A more direct method of monitoring tissue slip was developed by *Burkhard et al.* [42; 29; 19], this uses a thermal sensor technology, based on hot wire anemometry, to detect the occurrence of tissue slip. The basic principle relies on a heater with thermistors placed either side (Fig. 1.3), during static grasping both thermistors will detect the same heat flux from the heater. However, when the tissue slips the heated section of the tissue will move closer to one of the thermistors, increasing the heat flux detected by it, whilst decreasing it at the thermistor opposite [23]. Through monitoring these changes in heat flux it is possible to detect the occurrence and direction of slip, in trials on ex-vivo porcine samples it was able to detect slip after less than 2 mm of displacement [29].

Another reactive approach to detecting the presence of tissue slip was developed by *Jones et al.* [40], this utilised a 2 DoF soft inductive tactile sensor to monitor the normal and shear forces applied at the grasper face. Slip was indicated when the Coefficient of Friction first peaked.

Although both of these systems show some promise for direct slip detection during robotic surgery, they are both reliant on gross slip occurring before it can be detected. Given the small size of most robotic surgical graspers, the occurrence of only a small number of slip events could result in a complete loss of grip control. If it is possible to predict slip, or detect early indicators that suggest slip is imminent, then mitigating actions can be taken to prevent it before a loss of tissue control can occur, ensuring a more complete control during tissue manipulation tasks, whilst reducing the probability of tissue trauma.

1.2.3 Slip Mechanics

To be able to develop a robust and reliable sensor for the early detection of slip events during tissue grasping, it is essential that the mechanics of slip are first well understood.

For two bodies to remain in contact all points along the contacting surface, for each body, must move with the same tangential velocity, if any two coincident points along the contact have different tangential velocities, then slip is occurring [43; 44]. Whether an object slips or not is determined by the ratio between the static friction force (F_F) at the surface, and the shear force (F_S) that is being applied, when $F_S > F_F$ slip will occur [43; 44; 45].

The frictional force of the contact is determined by Amonton's Law of friction, which states that F_F is directly proportional to the normal force (F_n), the ratio between these is determined by the static coefficient of friction (μ_s), see Equation 1.1. It was previously thought that this value was constant for a particular pair of materials in contact, however it is now believed that μ_s can vary with normal load, sliding velocity, apparent contact area, temperature, humidity, age of contact, and the rate of change of tangential force [46; 47]. Amonton's law though is a reasonable first order approximation for a model

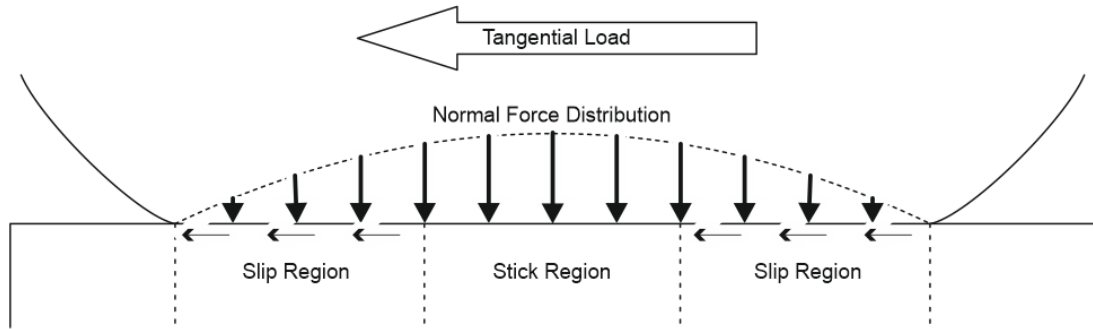


Figure 1.4: Diagram of contact mechanics between an elastic cylinder and a rigid flat plate under normal and tangential loads demonstrating how incipient slip can occur.

of friction between two solid elastic bodies, the inclusion of elastomers and lubrication will reduce its accuracy [48], however it should function sufficiently as a model to help understand the problem.

$$F_F = F_n \mu_s \quad (1.1)$$

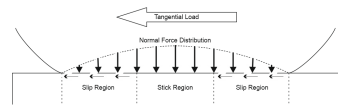
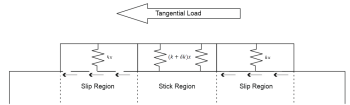
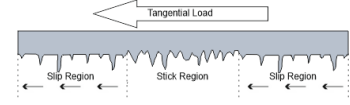
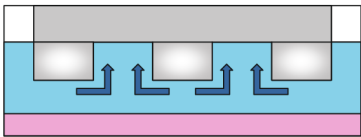
Slip can be broken down into two main stages [44]; there is macro or gross slip, which occurs when the total shear force exceeds the total friction force. In this case the whole of the surface loses grip, and the contacting bodies will move relative to each other. The other form of slip is incipient or micro-slip, this generally occurs prior to the onset of macro slip, when the local shear force exceeds the local frictional force, leading to localised relative displacements between two contacting points on the surface, whilst the remainder of the contacting surface remains static [43; 44; 45] (See Fig. 1.4).

Observation of the mechanics of a Hertzian contact, demonstrates how these incipient slips develop. Hertz theory describes the contact between two elastic spheres contacting at a point, or as an elastic sphere contacting a rigid plane (Fig. 1.4). As a normal force is applied the sphere deforms resulting in an increase in the contact area, the points towards the centre of the contact deform more, leading to a greater pressure at this point due to the greater material displacement, and therefore strain. This pressure distribution decreases towards the outer edge of the contact, with a parabolic distribution, tending

to zero and the edge contact where there is no compression of the elastic sphere, and so there is zero normal force acting at this point. Combining this Hertzian contact with Amanton's law of friction, when a tangential load is applied to the sphere the points of zero normal force at the very edge of the contact will slip first, as they will have zero frictional force to resist the tangential load. However, the remainder of the contact will still remain static due to the frictional force acting on the contacting surface. As the tangential load is increased the slip will then propagate towards the centre of the contact where the material deformation, and therefore normal and frictional forces, are greatest. Hertzian contact theory contains a number of assumptions and simplifications, but provides a good model for understanding how the normal force distribution, that result in incipient slip, develops.

If incipient slip can be created and controlled in a predictable manner, then it should be possible to cause preferential incipient slips to first occur on a particular part of the grasper face. These incipient slips can then be detected before the onset of macro slip, whilst grip is still maintained by the remainder of the grasper face. Based on Amonton's Law there are two main ways of encouraging incipient slip, through variation of the normal force, or through variation of the coefficient of friction, the methods we identified for altering these are summarised in Table 1.2.

Table 1.2: Summary of methods for encouraging the preferential occurrence of incipient slips in a controlled and predictable manner

Normal Force	Surface Shape	The contacting shape can create a distribution of normal load which results in a variation in friction force across the surface	
	Material stiffness	Stiffer materials will create a higher normal load for the same displacement. This only works when grasping rigid objects	
Coefficient of Friction	Surface Roughness	Change in surface roughness through different finishing methods can cause variation in the coefficient of friction	
	Surface Features	The addition of large scale features similar to tyre treads can reduce hydroplaning and increase friction in wet/lubricated environments	

The other major law that governs slip is Coulomb's model of friction. This states that the kinematic frictional force is independent of the sliding velocity, therefore if the normal force remains constant after the point of macro slip, then the frictional force acting between the sliding surfaces will also remain constant.

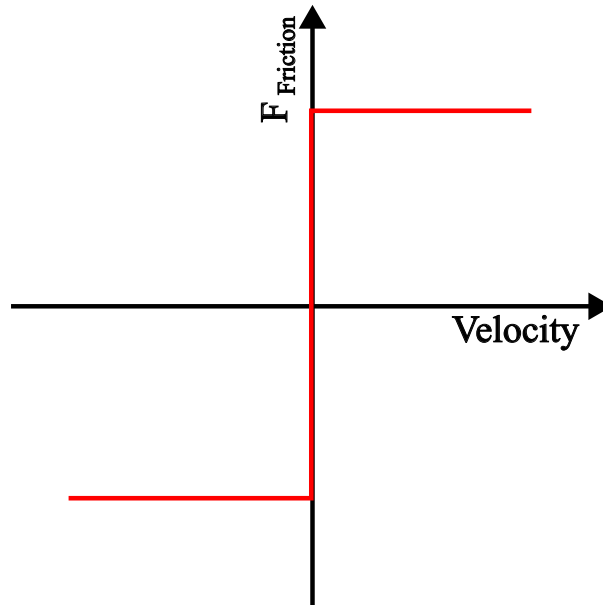


Figure 1.5: Coulomb's model of friction indicating that the frictional force is independent of the sliding velocity

1.2.4 Incipient Slip Detection

Human Slip Sensing

The human finger is able to automatically detect the occurrence of localised incipient slips, and make adjustments with minimal displacement of the grasped object [49; 50], using a force only 10-40% above the minimum required to prevent slip [49]. The convex shape of the human finger pad encourages the onset of these incipient slips, as the higher normal force at the centre of the finger pad results in an increased frictional force compared to the edges. Therefore, when shear force is applied the edge is seen to break contact first, and starts to slip, while the centre maintains the grip on the grasped object [51; 52].

Delhaye et al. [52] showed that once the tangential force reaches a certain value there is a linear decrease in the ratio between the contact area that is stuck, and that which is slipping, this is otherwise known as the stick ratio. Once the stick ratio reaches zero the

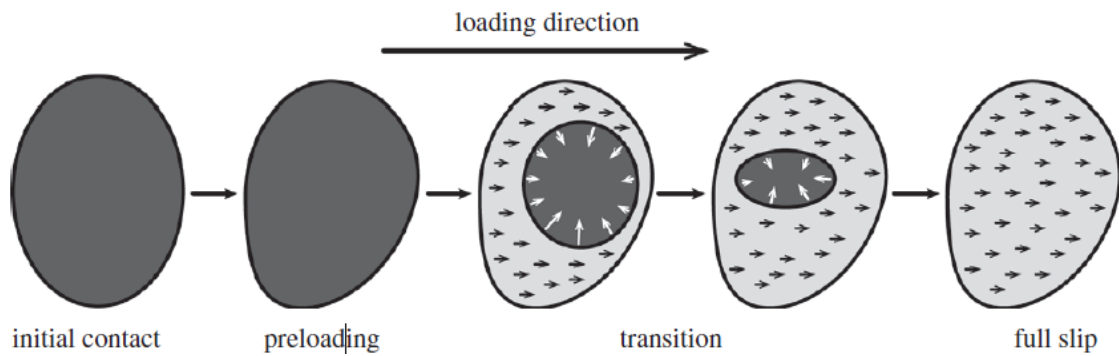


Figure 1.6: Change in the ratio of stuck area (dark grey) to the slipping area (light grey) as the contact of a finger progresses from incipient to macro slip [51].

finger goes from an incipient slip regime to a macro slip one, this took between 90 and 980 ms depending on the sliding velocity, normal force, and direction of movement [52].

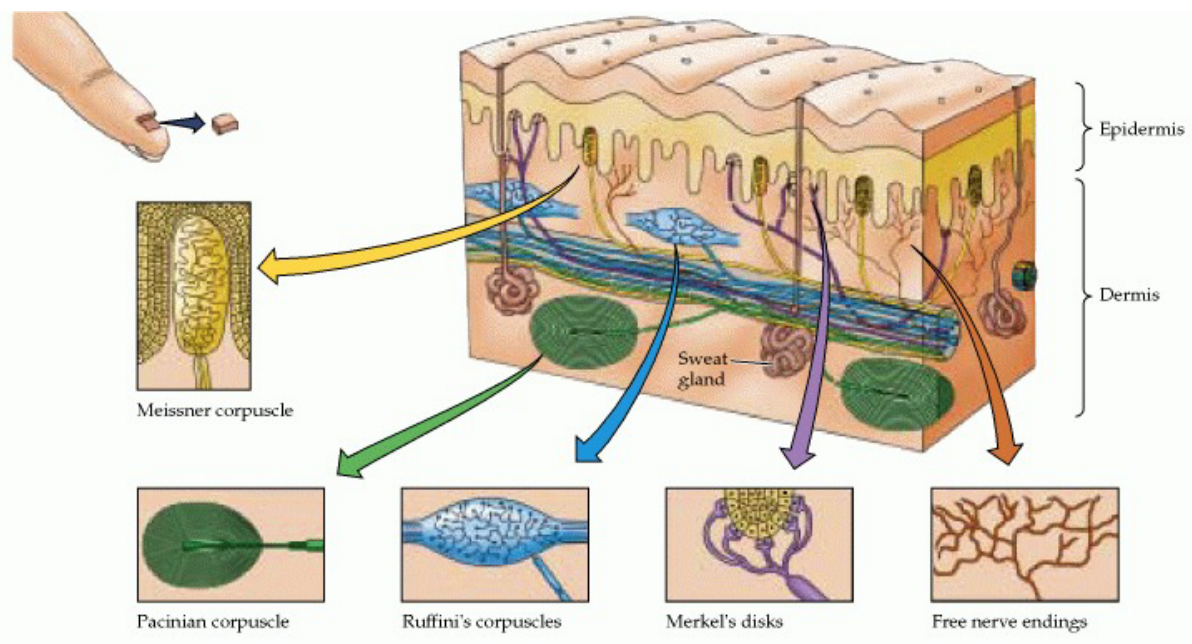


Figure 1.7: Diagram of the various mechanoreceptors present within the human glabrous skin [53].

Humans are able to detect the occurrence of these incipient slips through the mechanoreceptors within the glabrous skin of the finger pad. There are 4 different types of receptors which can be classified as either fast adapting (FA) or slow adapting (SA), with a small or large receptive field [54] (Fig. 1.7 & Table 1.3).

In a study carried out by *Johansson and Westling* [50] the signals coming from these four main mechanoreceptors were monitored. It was observed that just prior to the occurrence

Table 1.3: Summary of the major receptors in the glabrous skin of the fingertip. Adapted from [49; 55]

Receptor	Class	Field Diameter (mm)	Sensitive Frequency (Hz)	Receptors per cm ²	Probable Sensory Modality
Meissner Corpuscle	FAI	1-100 (12.6)	5-50	140	Touch/Contact
Pacinian Corpuscle	FAII	10-1000 (100)	40-400	21	Vibrations
Merkel Disk	SAI	2-100 (11)	<5	70	Pressure & Shape
Ruffini Endings	SAII	10-500 (60)	7	10	Skin Stretch

of slip there was a spike in responses from a large number of FAI and SAI receptors. It was suspected that these were the result of localised slips occurring prior to the onset of macro slip, as higher activity was seen towards the edge of the contact [50]; this is further supported by the work done by *Delhaye et al.* [52].

Once macro slip occurred responses from the FAII receptors also spiked as a result of high frequency vibrations caused by the macro slip, but they barely triggered during the incipient stage [50]. This suggests that localised slips are detected through changes in the local strain, rather than any vibrations given off from localised slips, possibly due to the damping of vibration when a solid contact is present [50]. However, another study by *Srinivasan et al.* [56] showed that the surface texture of the grasped object has a significant effect on whether or not a particular mechanoreceptor detects the presence of incipient slip. For FAII receptors to function a textured surface was required to induce sufficient vibrations that could be detected during the incipient slip stage [56], if the objects used by *Johansson and Westling* lacked the appropriate texture then the FAII receptors would not fire during incipient slip.

Robotic Slip Sensing

For robots to be able to grasp unknown objects securely, whilst using the minimal possible force, they need to be able to detect the occurrence of slip [45]. There are two main approaches taken to detect slip, through monitoring of macro slip or by detecting the incipient slips [45]. The issue with a reliance on detecting macro slip is that it requires the loss of stable control of the grasped object before mitigating actions can be taken.

This is particularly relevant for surgical graspers given the inherently low levels of friction [57], and small size of the grasper face [58], there is very little margin for error before complete loss of control occurs. Therefore the focus of this section will be on methods of incipient slip detection, for a review of methods of macro slip detection see [43; 45].

One of the key elements of an incipient slip sensor is its ability to encourage detectable levels of incipient slip; it must be able to cause some areas of the contact to slip whilst maintaining a secure grip in others. The majority of incipient slip sensing systems focus on human inspired methods to try to encourage the occurrence of localised slip, employing finger like or hemispherical/cylindrical grasper jaws to create a distribution of normal load [45]. However, the detection methods and methodologies used vary significantly.

One of the earliest attempts to monitor incipient slip by *Tremblay and Cutkosy* [59] used accelerometers placed below a curved contacting surface to detect the vibrations that occur as a result of incipient slips, similar to how FAII receptors work [50]. The sensor consisted of a hemicylindrical deformable core, covered in a rubber skin with an array of ‘nibs’ on its surface. The curve of this structure created a normal distribution to try and encourage incipient slip, and then when localised slips occurred the ‘nibs’ helped amplify any vibrations that occurred to make detection easier [59; 60].

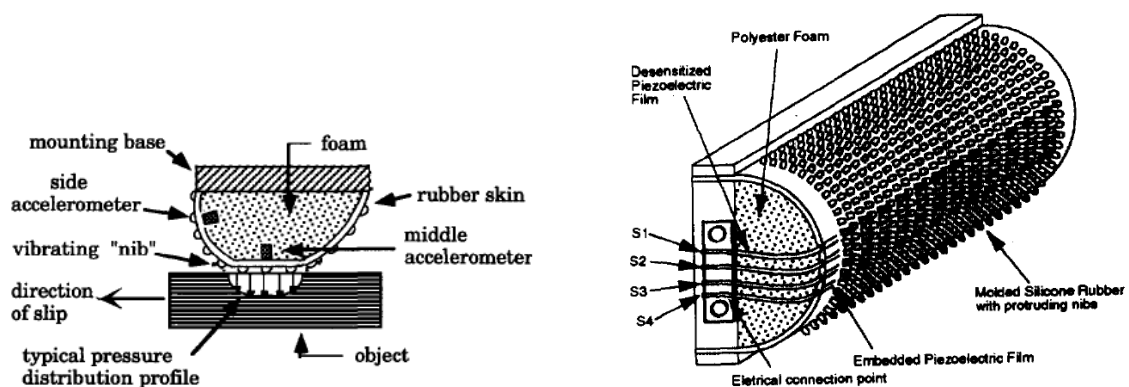


Figure 1.8: Left: Diagram of slip sensor from [59] Right: Diagram of slip sensor from [61]

Two accelerometers were used to detect the vibrations, one was placed at the centre of contact whilst the other was placed on the side of the cylinder [59]. This set up was used to differentiate between external vibrations, and those that are the result of incipient slip.

If a signal is detected at both accelerometers then the result of the vibration is likely not due to slip but general motion, however if it was caused by incipient slip then a signal would be detected at the side accelerometer, whilst the central one was damped due to its contact with the grasped object [59]. The system was able to detect the occurrence of incipient slip and take mitigating actions to prevent it, as well as differentiate between actual slip and general movement vibrations.

Son et al. [61] further developed this design, replacing the 2 accelerometers with 4 Polyvinylidene fluoride (PDVF) piezoelectric strips along the length of the cylinder, which function as stress sensors. This design was intended to try and detect more localised events, like incipient slip, instead of the global vibrations [61]. To test the sensor they pressed it against a linear slide and applied a constant tangential force, the normal force was then reduced until sliding occurred [61]. They were able to detect a loss of contact at the edge of the region due to stress relaxation measured by the PVDF, up to 95 ms before any motion was detected, a sufficient time window to make any adjustments to prevent slip [61].

Marconi and Melchiorri [62] developed a 16x16 taxel matrix which was covered in a layer of piezoresistive rubber, this was capable of detecting incipient slip through monitoring changes in the centre of pressure. This method appeared able to identify incipient slip before the onset of macro slip, even in highly lubricated conditions [62]. However, the sensor design is flat and was only tested for grasping a curved object, it would be less likely to work on flat objects, as there would be minimal occurrence of incipient slip that could be detected before macro slip occurs.

Another method of detecting incipient slip is through monitoring of the strain field, as the amount of strain present across the curved surface should vary, as different tangential loads are being experienced across the surface due to the variation of normal force [63]. *Maeno et al.* [63] developed a curved elastomeric sensor to mimic the human finger, then implanted strain gauges along its length so that the distribution of shear strain could be monitored.

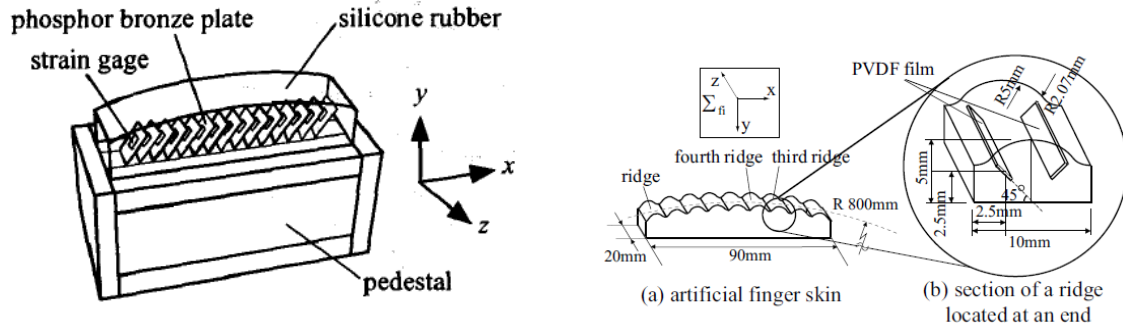


Figure 1.9: Left: Strain Based slip sensor from [63] Right: Slip sensor based on epidermal ridges from [64]

Fujimoto et al. [64] also developed a strain monitoring sensor for incipient slip detection, using an artificial skin that mimicked the epidermal ridges in human fingers. Both the overall sensor and the individual ridges were curved to encourage the occurrence of incipient slips. To detect the slips 2 PVDF strips were placed within each epidermal ridge, mimicking the position of FAI receptors in human skin [64]. An artificial neural network was then used to monitor and detect the occurrence of incipient slip based on both the high and low frequency response of the PVDF strips [64]. The system was able to detect incipient slip, but there is no indication over what length or time scales it was able to achieve this.

One of the most advanced tactile sensors currently available is the Biotac finger. This uses a multitude of sensors for detecting a range of different tactile sensations, it consists of 19 electrodes to measure the contact positions of the finger, a hydro-acoustic pressure transducer to measure the overall contact pressure and vibrations, and a thermistor to measure temperature at the fingertip [65; 66]. *Veiga et al.* [66] used the Biotac finger, combined with machine learning, to try and develop a system that could predict slip, using inputs from all of the available sensors to detect it, and then automatically adjusting the grip force to prevent it. Analysis of the channel relevance, to understand the contribution of each in predicting slip, indicated that the array of localised electrodes on the finger dominated prediction. They were the most significant signal for slip detection in 6 out of 7 trial objects, though there was also significant input from the low and high frequency pressure channels [66]. This indicates that a more localised sensing methodology is a

better detector of slip, but a combination of sensors has the greatest overall success rate, similar to how mechanoreceptors in the human hand work in tandem to detect slip.

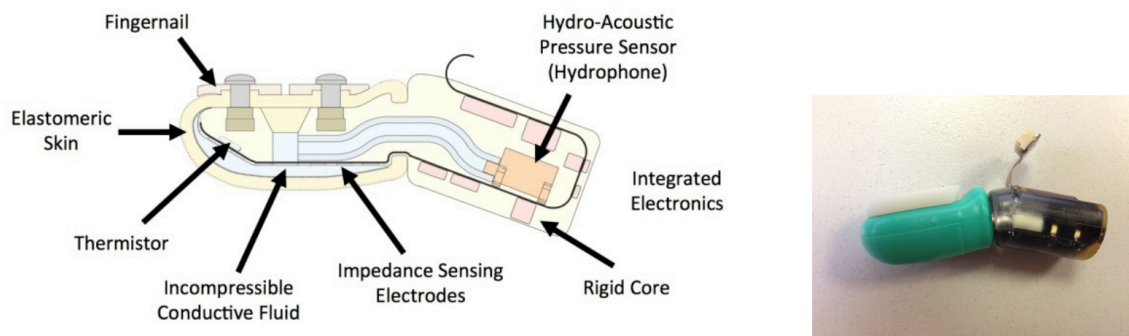


Figure 1.10: Left: Schematic of Biotac [67]. Right: Biotac finger [65]

Work done by *Su et al.* [68] investigating slip using the same Biotac finger showed that the high frequency pressure gave the earliest indication of slip, up to 35 ms before macro slip, whereas the electrodes were only able to detect incipient slip 8 ms before its onset. This is likely because for slip prediction the electrode values were combined into a single normal force value, rather than being analysed individually as in [66], removing the advantage offered by localised measurement.

Several research groups have looked into optical methods for detecting the occurrence of incipient slip. *William et al.* [69] developed a slip sensor that measures the change in light intensity, which varies depending on the deformation of translucent ridges on the sensor's surface. This method was able to detect incipient slip up to 600 ms before the onset of macro slip [69], however it is reliant on the consistency of an external light source which in many cases may be inconsistent, particularly during robotic surgery.

Another optical based method is that developed by *Watanabe and Obinata* [71] which consists of a camera positioned behind a transparent semi-spherical body, with an array of dots on its surface. Through monitoring the displacement of each dot from its initial position it is possible to detect when slips occur [71]. The major issue with this technique though is images can only be taken every 32 ms due to the high computational time required to process them, this was sufficient for slow slip rates, but might struggle for sudden slips where a much more rapid response time is required [71].

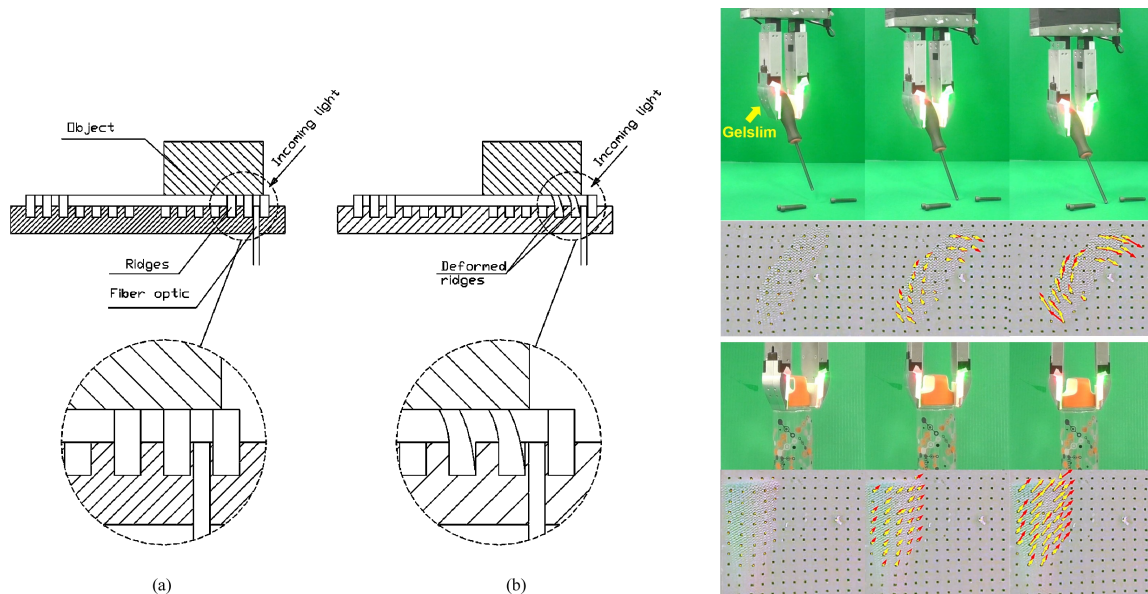


Figure 1.11: Left: Principle of operation of optical slip sensor from [69] Right: Output of Gelslim sensor during manipulation task [70]

The GelSlim tactile sensor also uses a camera combined with an array of dots, but uses a flat grasper filled with a soft gel rather than an elastomer [70]. The sensor is able to detect the object's shape through the imprint pattern, and through monitoring the relative movement of the dots compared to an expected rigid transform is able to detect the occurrence of both translational and rotational incipient slips [70]. The GelSlim was able to detect the occurrence of incipient slip with 86.25% accuracy. However, this method is reliant on the grasped object being rigid, and is less reliable on objects with a small contact patch [70].

Rigi et al. [72] developed a vision-based system that used a rectangular silicone block as the grasper interface, and then to detect slip an event-based camera was positioned at 45 degrees looking through the rear of the block. This offset filtered out any external light so it was significantly easier to measure the contact area through image processing [72]. This system proved capable of detecting slip on a variety of objects, up to 44 ms prior to the onset of macro slip [72].

One design that strays from the standard hemicylindrical/spherical shape for inducing incipient slip is the PapillArray. Rather than using a single curved surface to create a normal force distribution, an array of deformable pillars is used instead [73]. This creates

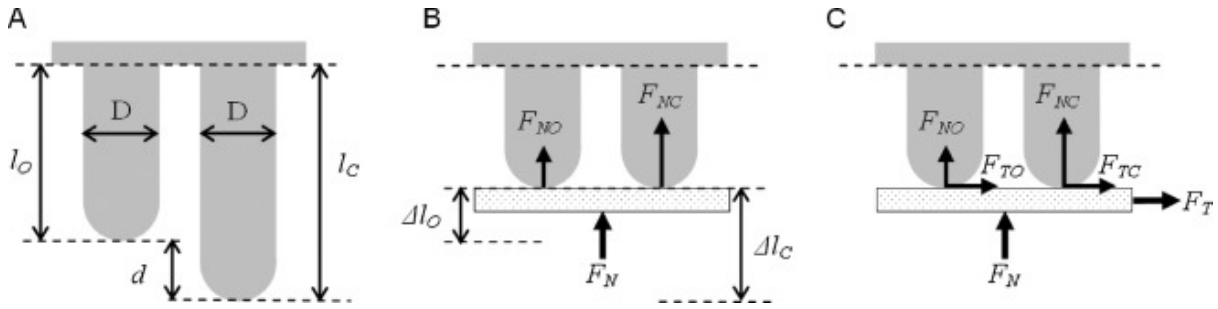


Figure 1.12: Principle of operation PapillArray. (A) Uncompressed State. (B) Compressed state with no tangential load, the normal force experienced by the right hand pillar is greater due to the larger compression. (C) Tangential load is applied, and friction force at the right pillar is higher due to higher normal load based on Amontons Law, therefore it will take a higher tangential load for this pillar to lose contact [73].

a step change in the normal load, rather than a continuous distribution, as the central pillar is 1 mm taller than the surrounding pillars. During tests it was observed that in high friction cases, there was a significant difference between the time each pillar slipped, over 2 seconds in some cases [73]. However, for low friction lubricated conditions, both pillars slipped at almost the exact same time [73]. A pinhole camera is then used to monitor pillar deflection through changes in a spot of light projected into the tip of the pillar [74].

Although a large number of these sensors have results that prove their ability to detect incipient slip, it is difficult to compare the performance of the various sensors as they use a variety of different metrics. These include:

- Time delay that occurs between incipient and macro slip [68; 72].
- The relative displacement of different parts of the sensor surface [73].
- How often the sensors identify incipient slip correctly [66; 70].

As well as the different metrics used there is no standard grasped object, test method, or clamping force, used in the assessment of grasping performance, making comparisons between different sensing methods almost impossible as too many variables change between experiments.

1.2.5 Automation

Humans are able to react to the onset of slips very quickly when they do occur, with the onset of slip, and the occurrence of adjustments to mitigate the slip, approximately 0.06-0.08 s apart, this indicates that the neural response occurs automatically as part of a reflex arc [75]. This suggests that slip detection and response should be managed via closed loop controls, to minimise the reaction time to slip. In contrast, involving the surgeon in the feedback and response loop would increase the response time, unless the system is able to achieve almost complete feedback transparency between the surgeon and sensors.

The automation of the force control during the grasping action could also provide several surgical benefits. Primarily the surgeon will no longer need to focus on accurately controlling the force during grasping, helping to reduce surgeon fatigue, and allowing surgeons to focus on more critical surgical tasks [19]. Grasping automation could also provide additional utilisation from extra robotic arms on the surgical platform. Currently, the Davinci Surgical System (Intuitive) has a total of 3 instrumented arms, but the surgeon only has direct control over two of these at any one time. The inclusion of grasping automation would allow the third arm to be utilised for simple retraction and hold tasks, whilst the surgeon manipulates the other arms without concern of the tissue slipping or releasing [19], helping to speed up surgeries, and possibly even allowing more complex manipulation tasks to be conducted.

1.2.6 Summary of Literature

From the analysis of the literature there is a clear clinical need for improved force control within robotic surgical graspers, as poor force control results in tissue trauma from excessive grasping loads, or can lead to tissue slip if insufficient forces are used. Evaluation of current systems developed for force control in surgical graspers, indicates that the majority aim to utilise haptic feedback of the grasping forces to the surgeon to try and avoid excessive clamping forces, and therefore tissue trauma. However, the key aim of a

surgical grasper is to securely clamp and hold tissue, so that it can be manipulated reliably, therefore a better indication of a successful grasp is the measurement and detection of tissue slip events. If tissue slip can be detected early then grasp forces can be adjusted to prevent them, also helping to reduce the applied gripping force and thus limit tissue trauma.

Research into the theoretical mechanics of slip indicates that before macro slip occurs multiple smaller incipient slips occur where the local shear forces exceed local frictional forces, whilst the remainder of the contact is still being held securely. This is how human fingers detect slip early, helping us to manipulate fragile objects in a controlled manner without damaging them. The curved pad of the human finger causes slip to occur preferentially towards the outer edges, where there is lower normal forces as a result of its curved surface. The large majority of robots designed to detect incipient slip mimic the human finger for this reason, to encourage the occurrence of incipient slips so they can then be detected.

Although the majority of robots use the same shape to encourage incipient slip there is a significant variety of different sensing methodologies used to detect their occurrence. The main three methods utilised are:

- Pressure distribution - This is similar to how humans detect incipient slip by monitoring the overall contact area present.
- Localised vibration - This was the most common method used for detecting slip in early robotic graspers, and is the main method humans use to detect macro slips, and possibly incipient slips depending on the texture of the contacting surface.
- Localised strain - Using localised strain measurements it is possible to detect a relaxation that occurs as grip is lost on the contacting surface as there is no longer any tension being applied.

Any slip detection and mitigation system would also require closed loop control automation, as the inclusion of the surgeon in the loop would increase the reaction time, which

could result in insufficient time for the surgeon to react in time to prevent slip.

1.3 Aims and Objectives

The main aim of this work is to develop, and demonstrate, a methodology that can be used to detect the occurrence of tissue slip early during robotic surgical manipulation tasks, so that mitigating actions can be taken to prevent it.

The purpose of this is to try and prevent slip events during the grasping and retraction task in robotic surgery, whilst minimising excessive grasping forces, which can lead to tissue trauma. Given the short reaction time required to prevent slip events the force control during grasping should be automated.

Objectives

The objectives defined for the work presented are as follows:

- Develop a system for simulating the surgical grasping and retraction of tissue, that is capable of directly monitoring the tissue slip occurring at the grasper face.
- Investigate the slip mechanics of soft, lubricated, deformable materials like biological tissue, and how variations in grasper face profile can influence the induction of incipient slips.
- Utilising knowledge of the slip mechanics develop an instrumented grasper(s) capable of inducing and then detecting incipient slip of soft tissues.
- Develop an algorithm for the automatic detection and mitigation of slip events during robotic surgery, and demonstrate its ability to reduce the forces applied to tissue during grasping and retraction, whilst preventing the occurrence of slip.

1.3.1 Thesis Outline

The following manuscripts have been published in relation to this work, these form the core chapters of this Doctoral Thesis:

- **Chapter 2:** Engineering Incipient Slip Into Surgical Graspers to Enhance Grasp Performance. Ian Waters, Ali Alazmani, and Peter Culmer. *IEEE Transactions on Medical Robotics and Bionics*. 2020 [76].
- **Chapter 3:** Incipient Slip Sensing for Improved Grasping in Robot Assisted Surgery. Ian Waters, Lefan Wang, Dominic Jones, Ali Alazmani, and Peter Culmer. *IEEE Sensors*. 2022 [77].
- **Chapter 4:** Encouraging and Detecting Preferential Incipient Slip for Use in Slip Prevention in Robot-Assisted Surgery. Ian Waters, Dominic Jones, Ali Alazmani, and Peter Robert Culmer. *MDPI Sensors*. 2022 [78].
- **Chapter 5:** Utilising Incipient Slip for Grasping Automation in Robot Assisted Surgery. Ian Waters, Dominic Jones, Ali Alazmani, and Peter Robert Culmer. *IEEE Robotics and Automation Letters*. 2022 [79].

A graphical outline of the relationship between these publications is presented in Figure 1.13. The chapters are listed in the chronological order in which the work was conducted, although the publication dates don't align with this due to particular journal deadlines.

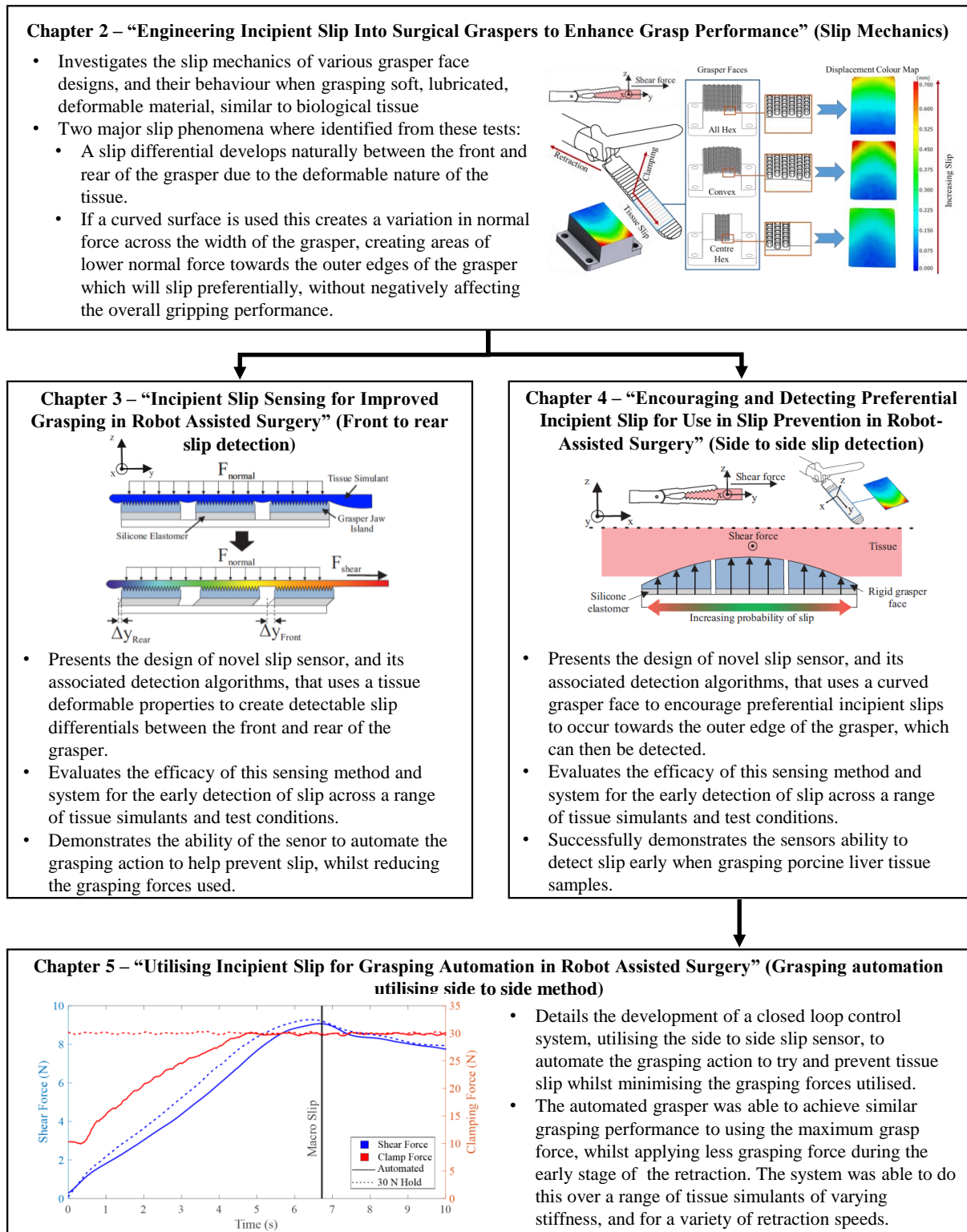


Figure 1.13: Diagram displaying the relationship between the chapters and publications presented within this thesis.

References

- [1] John W Yaxley, Geoffrey D Coughlin, Suzanne K Chambers, Stefano Occhipinti, Hema Samaratunga, Leah Zajdlewicz, Nigel Dungleison, Rob Carter, Scott Williams, Diane J Payton, Joanna Perry-Keene, Martin F Lavin, and Robert A Gardiner. Robot-assisted laparoscopic prostatectomy versus open radical retropubic prostatectomy: early outcomes from a randomised controlled phase 3 study. *The Lancet*, 388(10049):1057–1066, September 2016.
- [2] Jacob A. Greenberg. From Open to MIS: Robotic Surgery Enables Surgeons to Do More With Less. *Annals of Surgery*, 267(2):220, February 2018.
- [3] Ferdinand Köckerling. Robotic vs. Standard Laparoscopic Technique - What is Better? *Frontiers in Surgery*, 1, May 2014.
- [4] Alfredo M. Carbonell, Jeremy A. Warren, Ajita S. Prabhu, Conrad D. Ballecer, Randy J. Janczyk, Javier Herrera, Li-Ching Huang, Sharon Phillips, Michael J. Rosen, and Benjamin K. Poulouse. Reducing Length of Stay Using a Robotic-assisted Approach for Retromuscular Ventral Hernia Repair: A Comparative Analysis From the Americas Hernia Society Quality Collaborative. *Annals of Surgery*, 267(2):210–217, February 2018.
- [5] Vincenzo Ficarra, Giacomo Novara, Raymond C. Rosen, Walter Artibani, Peter R. Carroll, Anthony Costello, Mani Menon, Francesco Montorsi, Vipul R. Patel, Jens-Uwe Stolzenburg, Henk Van der Poel, Timothy G. Wilson, Filiberto Zattoni, and Alexandre Mottrie. Systematic Review and Meta-analysis of Studies Reporting Urinary Continence Recovery After Robot-assisted Radical Prostatectomy. *European Urology*, 62(3):405–417, September 2012.
- [6] John C. Byrn, Stefanie Schluender, Celia M. Divino, John Conrad, Brooke Gurland, Edward Shlasko, and Amir Szold. Three-dimensional imaging improves surgical performance for both novice and experienced operators using the da Vinci Robot System. *The American Journal of Surgery*, 193(4):519–522, April 2007.

- [7] Tamás Haidegger, Balázs Benyó, Levente Kovács, and Zoltán Benyó. Force Sensing and Force Control for Surgical Robots. *IFAC Proceedings Volumes*, 42(12):401–406, 2009.
- [8] Daniel M Herron and Michael Marohn. Prepared by the SAGES-MIRA Robotic Surgery Consensus Group. page 24, 2006.
- [9] Intuitive. Press Resources. URL: <https://www.intuitive.com/en-us/about-us/newsroom/press-resources>. Accessed: 6/15/2022.
- [10] P-J Fager and Per von Wowern. The use of haptics in medical applications. *The International Journal of Medical Robotics and Computer Assisted Surgery*, 1(1):36–42, June 2004.
- [11] O. A. J. van der Meijden and M. P. Schijven. The value of haptic feedback in conventional and robot-assisted minimal invasive surgery and virtual reality training: a current review. *Surgical Endoscopy*, 23(6):1180–1190, June 2009.
- [12] B. Tang, G.B. Hanna, and A. Cuschieri. Analysis of errors enacted by surgical trainees during skills training courses. *Surgery*, 138(1):14–20, July 2005.
- [13] E.A.M. Heijnsdijk, J. Dankelman, and D.J. Gouma. Effectiveness of grasping and duration of clamping using laparoscopic graspers. *Surgical Endoscopy*, 16(9):1329–1331, September 2002.
- [14] E. A. M. Heijnsdijk, H. de Visser, J. Dankelman, and D. J. Gouma. Slip and damage properties of jaws of laparoscopic graspers. *Surgical Endoscopy And Other Interventional Techniques*, 18(6):974–979, June 2004.
- [15] Louise Russell. *The Design and Development of an Intelligent Atraumatic Laparoscopic Grasper*. Doctor of Philosophy, University of Leeds, April 2015.
- [16] C.-H. King, M.O. Culjat, M.L. Franco, C.E. Lewis, E.P. Dutson, W.S. Grundfest, and J.W. Bisley. Tactile Feedback Induces Reduced Grasping Force in Robot-Assisted Surgery. *IEEE Transactions on Haptics*, 2(2):103–110, April 2009.

-
- [17] C.-H. King, M.O. Culjat, M.L. Franco, J.W. Bisley, G.P. Carman, E.P. Dutson, and W.S. Grundfest. A Multielement Tactile Feedback System for Robot-Assisted Minimally Invasive Surgery. *IEEE Transactions on Haptics*, 2(1):52–56, January 2009.
- [18] Verena Nitsch and Berthold Farber. A Meta-Analysis of the Effects of Haptic Interfaces on Task Performance with Teleoperation Systems. *IEEE Transactions on Haptics*, 6(4):387–398, October 2013.
- [19] Natalie T. Burkhard, J. Ryan Steger, and Mark R. Cutkosky. The Role of Tissue Slip Feedback in Robot-Assisted Surgery. *Journal of Medical Devices*, 13(2):021003, June 2019.
- [20] G.S. Fischer, T. Akinbiyi, S. Saha, J. Zand, M. Talamini, M. Marohn, and R. Taylor. Ischemia and Force Sensing Surgical Instruments for Augmenting Available Surgeon Information. In *The First IEEE/RAS-EMBS International Conference on Biomedical Robotics and Biomechanics, 2006. BioRob 2006.*, pages 1030–1035, Pisa, Italy, 2006. IEEE.
- [21] T et al Kimura. Intraabdominal contamination after gallbladder perforation during laparoscopic cholecystectomy and its complications. page 4.
- [22] E.A.M. Heijnsdijk. *Tissue manipulation in laparoscopic surgery*. Doctor of Philosophy, Delft University of Technology, 2004.
- [23] Natalie T. Burkhard. *Sensing slip of grasped biological tissue in minimally invasive surgery*. Doctor of Philosophy, Stanford University, 2018.
- [24] C.R. Wagner, N. Stylopoulos, and R.D. Howe. The role of force feedback in surgery: analysis of blunt dissection. In *Proceedings 10th Symposium on Haptic Interfaces for Virtual Environment and Teleoperator Systems. HAPTICS 2002*, pages 68–74, Orlando, FL, USA, 2002. IEEE Comput. Soc.
- [25] Christopher R. Wottawa, Bradley Genovese, Bryan N. Nowroozi, Steven D. Hart, James W. Bisley, Warren S. Grundfest, and Erik P. Dutson. Evaluating tactile

- feedback in robotic surgery for potential clinical application using an animal model. *Surgical Endoscopy*, 30(8):3198–3209, August 2016.
- [26] R.D. Howe, W.J. Peine, D.A. Kantarinis, and J.S. Son. Remote palpation technology. *IEEE Engineering in Medicine and Biology Magazine*, 14(3):318–323, June 1995.
- [27] Uikeyum Kim, Dong-Hyuk Lee, Woon Jong Yoon, Blake Hannaford, and Hyouk Ryeol Choi. Force Sensor Integrated Surgical Forceps for Minimally Invasive Robotic Surgery. *IEEE Transactions on Robotics*, 31(5):1214–1224, October 2015.
- [28] Uikeyum Kim, Yong Bum Kim, Jinho So, Dong-Yeop Seok, and Hyouk Ryeol Choi. Sensorized Surgical Forceps for Robotic-Assisted Minimally Invasive Surgery. *IEEE Transactions on Industrial Electronics*, 65(12):9604–9613, December 2018.
- [29] Natalie T. Burkhard, Mark R. Cutkosky, and J. Ryan Steger. Slip Sensing for Intelligent, Improved Grasping and Retraction in Robot-Assisted Surgery. *IEEE Robotics and Automation Letters*, 3(4):4148–4155, October 2018.
- [30] Yuan Dai, Ahmad Abiri, Siyuan Liu, Omeed Paydar, Hyunmin Sohn, Eric P. Dutton, Warren S. Grundfest, and R.N. Candler. Grasper integrated tri-axial force sensor system for robotic minimally invasive surgery. In *2017 39th Annual International Conference of the IEEE Engineering in Medicine and Biology Society (EMBC)*, pages 3936–3939, Jeju Island, South Korea, July 2017. IEEE.
- [31] Seyed Mohsen Khadem, Saeed Behzadipour, Alireza Mirbagheri, and Farzam Farahmand. A modular force-controlled robotic instrument for minimally invasive surgery - efficacy for being used in autonomous grasping against a variable pull force: Modular force-controlled robotic instrument. *The International Journal of Medical Robotics and Computer Assisted Surgery*, 12(4):620–633, December 2016.
- [32] Dong-Hyuk Lee, Uikeyum Kim, Hyungpil Moon, Ja Choon Koo, Woon Jong Yoon, and Hyouk Ryeol Choi. Preliminary design of multi-axial contact force sensor for minimally invasive robotic surgery grasper. In *2013 IEEE International Conference*

-
- on Robotics and Automation*, pages 1019–1024, Karlsruhe, Germany, May 2013. IEEE.
- [33] Man Bok Hong and Yung-Ho Jo. Design and Evaluation of 2-DOF Compliant Forceps With Force-Sensing Capability for Minimally Invasive Robot Surgery. *IEEE Transactions on Robotics*, 28(4):932–941, August 2012.
- [34] Frank L. Hammond, Rebecca K. Kramer, Qian Wan, Robert D. Howe, and Robert J. Wood. Soft tactile sensor arrays for micromanipulation. In *2012 IEEE/RSJ International Conference on Intelligent Robots and Systems*, pages 25–32, Vilamoura-Algarve, Portugal, October 2012. IEEE.
- [35] M.A. Qasaimeh, S. Sokhanvar, J. Dargahi, and M. Kahrizi. PVDF-Based Microfabricated Tactile Sensor for Minimally Invasive Surgery. *Journal of Microelectromechanical Systems*, 18(1):195–207, February 2009.
- [36] Sebastian Schostek, Chi-Nghia Ho, Daniel Kalanovic, and Marc O. Schurr. Artificial tactile sensing in minimally invasive surgery – a new technical approach. *Minimally Invasive Therapy & Allied Technologies*, 15(5):296–304, January 2006.
- [37] J. Dargahi, S. Najarian, and K. Najarian. Development and three-dimensional modelling of a biological-tissue grasper tool equipped with a tactile sensor. *Canadian Journal of Electrical and Computer Engineering*, 30(4):225–230, 2005.
- [38] Dominic Jones, Hongbo Wang, Ali Alazmani, and Peter R. Culmer. A soft multi-axial force sensor to assess tissue properties in RealTime. In *2017 IEEE/RSJ International Conference on Intelligent Robots and Systems (IROS)*, pages 5738–5743, Vancouver, BC, September 2017. IEEE.
- [39] Saeed Sokhanvar, Muthukumaran Packirisamy, and Javad Dargahi. MEMS Endoscopic Tactile Sensor: Toward *In-Situ* and *In-Vivo* Tissue Softness Characterization. *IEEE Sensors Journal*, 9(12):1679–1687, December 2009.
- [40] D Jones, A Alazmani, and P Culmer. A Soft Inductive Tactile Sensor for Slip Detection Within a Surgical Grasper Jaw. page 4, 2019.

- [41] Yi-Je Lim, Dhanannjay Deo, Tejinder P. Singh, Daniel B. Jones, and Suvranu De. In situ measurement and modeling of biomechanical response of human cadaveric soft tissues for physics-based surgical simulation. *Surgical Endoscopy*, 23(6):1298–1307, June 2009.
- [42] Natalie Burkhard, Ryan Steger, and Mark Cutkosky. Sensing slip of grasped wet, conformable objects. In *2017 IEEE/RSJ International Conference on Intelligent Robots and Systems (IROS)*, pages 5744–5749, Vancouver, BC, September 2017. IEEE.
- [43] Maria Teresa Francomano, Dino Accoto, and Eugenio Guglielmelli. Artificial Sense of Slip—A Review. *IEEE Sensors Journal*, 13(7):2489–2498, July 2013.
- [44] K. L. Johnson. *Contact mechanics*. Cambridge University Press, Cambridge Cambridgeshire New York, 1987.
- [45] Wei Chen, Heba Khamis, Ingvars Birznieks, Nathan F. Lepora, and Stephen J. Redmond. Tactile Sensors for Friction Estimation and Incipient Slip Detection – Towards Dexterous Robotic Manipulation: A Review. *IEEE Sensors Journal*, pages 1–1, 2018.
- [46] M. J. Adams, S. A. Johnson, P. Lefevre, V. Levesque, V. Hayward, T. Andre, and J.-L. Thonnard. Finger pad friction and its role in grip and touch. *Journal of The Royal Society Interface*, 10(80):20120467–20120467, December 2012.
- [47] Subrahmanyam M. Pasumarty, Simon A. Johnson, Simon A. Watson, and Michael J. Adams. Friction of the Human Finger Pad: Influence of Moisture, Occlusion and Velocity. *Tribology Letters*, 44(2):117–137, November 2011.
- [48] Valentin Popov. *Contact mechanics and friction: physical principles and applications*. Springer Berlin Heidelberg, New York, NY, 2017.
- [49] Roland S. Johansson and J. Randall Flanagan. Coding and use of tactile signals from the fingertips in object manipulation tasks. *Nature Reviews Neuroscience*, 10(5):345–359, May 2009.

-
- [50] R.S. Johansson and G. Westling. Signals in tactile afferents from the fingers eliciting adaptive motor responses during precision grip. *Experimental Brain Research*, 66(1), March 1987.
- [51] T. Andre, V. Levesque, V. Hayward, P. Lefevre, and J.-L. Thonnard. Effect of skin hydration on the dynamics of fingertip gripping contact. *Journal of The Royal Society Interface*, 8(64):1574–1583, November 2011.
- [52] B. Delhaye, P. Lefevre, and J.-L. Thonnard. Dynamics of fingertip contact during the onset of tangential slip. *Journal of The Royal Society Interface*, 11(100):20140698–20140698, September 2014.
- [53] *Neuroscience (Book with CD-ROM)*. Sinauer Associates Inc, January 2001.
- [54] Roland S. Johansson and Åke B. Vallbo. Tactile sensory coding in the glabrous skin of the human hand. *Trends in Neurosciences*, 6:27 – 32, 1983.
- [55] D.G. Caldwell, N. Tsagarakis, and A. Wardle. Mechano thermo and proprioceptor feedback for integrated haptic feedback. In *Proceedings of International Conference on Robotics and Automation*, volume 3, pages 2491–2496, Albuquerque, NM, USA, 1997. IEEE.
- [56] M. A. Srinivasan, J. M. Whitehouse, and R. H. LaMotte. Tactile detection of slip: surface microgeometry and peripheral neural codes. *Journal of Neurophysiology*, 63(6):1323–1332, June 1990.
- [57] W. Li, Z.G. Jia, J. Wang, L. Shi, and Z.R. Zhou. Friction behavior at minimally invasive grasper/liver tissue interface. *Tribology International*, 81:190–198, January 2015.
- [58] Andrew W. Brown, Stuart I. Brown, Donald Mclean, Zhigang Wang, and Alfred Cuschieri. Impact of fenestrations and surface profiling on the holding of tissue by parallel occlusion laparoscopic graspers. *Surgical Endoscopy*, 28(4):1277–1283, April 2014.

- [59] M.R. Tremblay and M.R. Cutkosky. Estimating friction using incipient slip sensing during a manipulation task. In *[1993] Proceedings IEEE International Conference on Robotics and Automation*, pages 429–434, Atlanta, GA, USA, 1993. IEEE Comput. Soc. Press.
- [60] M R Tremblay, Corinne E. Packard, M. Rabiei, and M Cutkosky. Utilizing Sensed Incipient Slip Signals for Grasp Force Control. page 7.
- [61] J.S. Son, E.A. Monteverde, and R.D. Howe. A tactile sensor for localizing transient events in manipulation. In *Proceedings of the 1994 IEEE International Conference on Robotics and Automation*, pages 471–476, San Diego, CA, USA, 1994. IEEE Comput. Soc. Press.
- [62] L. Marconi and C. Melchiorri. Incipient Slip Detection and Control Using a Rubber-Based Tactile Sensor. *IFAC Proceedings Volumes*, 29(1):475–480, June 1996.
- [63] T. Maeno, T. Kawai, and K. Kobayashi. Analysis and design of a tactile sensor detecting strain distribution inside an elastic finger. In *Proceedings. 1998 IEEE/RSJ International Conference on Intelligent Robots and Systems. Innovations in Theory, Practice and Applications (Cat. No.98CH36190)*, volume 3, pages 1658–1663, Victoria, BC, Canada, 1998. IEEE.
- [64] I. Fujimoto, Y. Yamada, T. Morizono, Y. Umetani, and T. Maeno. Development of artificial finger skin to detect incipient slip for realization of static friction sensation. In *Proceedings of IEEE International Conference on Multisensor Fusion and Integration for Intelligent Systems, MFI2003.*, pages 15–20, Tokyo, Japan, 2003. IEEE.
- [65] Jens Reinecke, Alexander Dietrich, Florian Schmidt, and Maxime Chalon. Experimental comparison of slip detection strategies by tactile sensing with the BioTac[®] on the DLR hand arm system. In *2014 IEEE International Conference on Robotics and Automation (ICRA)*, pages 2742–2748, Hong Kong, China, May 2014. IEEE.

-
- [66] Filipe Veiga, Jan Peters, and Tucker Hermans. Grip Stabilization of Novel Objects using Slip Prediction. *IEEE Transactions on Haptics*, pages 1–1, 2018.
- [67] Meghan C. Jimenez and Jeremy A. Fishel. Evaluation of force, vibration and thermal tactile feedback in prosthetic limbs. In *2014 IEEE Haptics Symposium (HAPTICS)*, pages 437–441, Houston, TX, USA, February 2014. IEEE.
- [68] Zhe Su, Karol Hausman, Yevgen Chebotar, Gerald E Loeb, Gaurav S Sukhatme, Artem Molchanov, and Stefan Schaal. Force Estimation and Slip Detection for Grip Control using a Biomimetic Tactile Sensor. page 7.
- [69] Hani William, Yousef Ibrahim, and Barry Richardson. A Tactile Sensor for Incipient Slip Detection. *International Journal of Optomechatronics*, 1(1):46–62, March 2007.
- [70] Siyuan Dong, Daolin Ma, Elliott Donlon, and Alberto Rodriguez. Maintaining Grasps within Slipping Bound by Monitoring Incipient Slip. *arXiv:1810.13381 [cs]*, October 2018. arXiv: 1810.13381.
- [71] Norinao Watanabe and Goro Obinata. Grip Force Control Based on the Degree of Slippage Using Optical Tactile Sensor. In *2007 International Symposium on Micro-NanoMechatronics and Human Science*, pages 466–471, Nagoya, Japan, November 2007. IEEE.
- [72] Amin Rigi, Fariborz Baghaei Naeini, Dimitrios Makris, and Yahya Zweiri. A Novel Event-Based Incipient Slip Detection Using Dynamic Active-Pixel Vision Sensor (DAVIS). *Sensors*, 18(2):333, January 2018.
- [73] Heba Khamis, Raquel Izquierdo Albero, Matteo Salerno, Ahmad Shah Idil, Andrew Loizou, and Stephen J. Redmond. PapillArray: An incipient slip sensor for dexterous robotic or prosthetic manipulation – design and prototype validation. *Sensors and Actuators A: Physical*, 270:195–204, February 2018.
- [74] Heba Khamis, Benjamin Xia, and Stephen J. Redmond. A novel optical 3D force and displacement sensor – Towards instrumenting the PapillArray tactile sensor. *Sensors and Actuators A: Physical*, 291:174–187, June 2019.

- [75] R.S. Johansson and G. Westling. Roles of glabrous skin receptors and sensorimotor memory in automatic control of precision grip when lifting rougher or more slippery objects. *Experimental Brain Research*, 56(3), October 1984.
- [76] Ian Waters, Ali Alazmani, and Peter Culmer. Engineering incipient slip into surgical graspers to enhance grasp performance. *IEEE Transactions on Medical Robotics and Bionics*, pages 1–1, 2020.
- [77] Ian Waters, Lefan Wang, Dominic Jones, Ali Alazmani, and Peter Culmer. Incipient Slip Sensing for Improved Grasping in Robot Assisted Surgery. *IEEE Sensors Journal*, pages 1–1, 2022.
- [78] Ian Waters, Dominic Jones, Ali Alazmani, and Peter Culmer. Encouraging and Detecting Preferential Incipient Slip for Use in Slip Prevention in Robot-Assisted Surgery. *Sensors*, 22(20):7956, October 2022.
- [79] Ian Waters, Dominic Jones, Ali Alazmani, and Peter Robert Culmer. Utilising Incipient Slip for Grasping Automation in Robot Assisted Surgery. *IEEE Robotics and Automation Letters*, 7(2):1071–1078, April 2022.

Chapter 2

Engineering Incipient Slip Into Surgical Graspers to Enhance Grasp Performance

Preface

This chapter was published as the journal paper:

Engineering incipient slip into surgical graspers to enhance grasp performance. Ian Waters, Ali Alazmani, and Peter Culmer. *IEEE Transactions on Medical Robotics and Bionics*. 2020.

Sections 2.1 through 2.5 constitute the main body of this publication, whilst the appendix provides details on the selection of the grasper face pattern, and additional results on the influence of various parameters on the development of slip. This paper investigates the slip mechanics of deformable tissue like materials, to better understand how tissue slips during retraction, and how the design of the grasper can be utilised to influence tissue slip.

Abstract

The surgical community has long reported the need for improved control of surgical graspers when handling delicate soft tissues, both to avoid the over application of force which leads to trauma, and to avoid tissue slip. The majority of research has sought to mitigate these issues through the integration of force feedback into the graspers. In this work we investigate an alternative strategy in which the grasper design is engineered to create preferential localised slip, also known as incipient slip, on the premise that this can be detected before the onset of macro slip, allowing graspers to use the minimum force required to maintain stable control.

We demonstrate the ability to encourage incipient slip in a predictable and repeatable manner through the design of the grasper face profile and pattern. This provides an important foundation for the development of sensing systems capable of detecting these slips during surgery to improve operative outcomes.

2.1 Introduction

Robotic surgical devices provide significant improvements for procedures in Minimally Invasive Surgery (MIS), but the lack of haptic feedback is still considered a major issue by surgeons. Robotic surgical devices mechanically separate the surgeon and the patient, completely denuding the surgeon of their sense of touch. This leads to issues with the over application of force, limited grasp control and an inability to palpate tissue to identify abnormalities [1; 2].

Over application of force has been identified as a major issue within robotic and laparoscopic surgery causing up to 55% of consequential errors in surgical trainees [2]. The lack of haptic feedback means the surgeon is fully reliant on visual cues to estimate the magnitude of applied forces, which are insufficient for force regulation, resulting in increased tissue damage [3]. Equally, the use of too little force is also a common occurrence where as many as 17% of grasping actions fail as a result of tissue slip [4], which could lead to

the occurrence of adverse events during surgery.

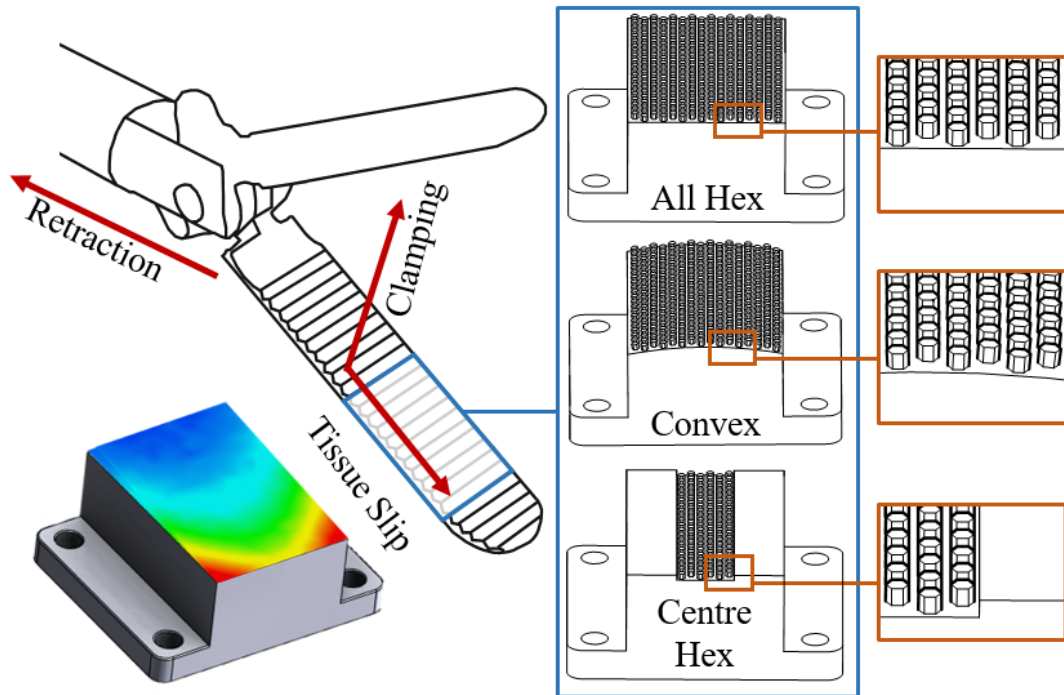


Figure 2.1: Diagram of surgical grasper and the various grasper face designs investigated. Top: Control ("All Hex"). Middle: Convex. Bottom: Centre Hex. The colour map shows an example of the relative displacement of tissue across a convex grasper face due to incipient slip, prior to macro slip occurring.

Efforts to improve grasping performance have predominantly sought to use haptic feedback strategies in which sensors provide force information to the surgeon. For example, *King et al.* [5] measured force at the grasper jaws with an array of capacitive sensors, which then relayed this information to the surgeon via small pneumatic balloons in contact with the surgeons fingers, this was found to reduce the mean force applied during grasping by 58%. However, such strategies increase cognitive loading on the surgeon, increasing the risk of fatigue and operative errors [6]. Automation can help to mitigate this effect, one approach to this is to automate grasp force using predetermined 'safe zones' [7]. Whilst this method has been successful it is constrained by the need to predetermine appropriate tissue-specific limits.

Less prescriptive approaches have been developed which look to detect tissue slip at the grasper interface. *Burkhard et al* [8] used thermal sensing to detect slip at the grasper face. In trials on porcine samples tissue slip could be detected after less than 2mm of

displacement. Similarly, *Jiang et al.* [9] developed a slip sensor using hexagonal micro structures on the surface, coupled to a piezoelectric substrate, to detect vibrations arising due to surface movement. However, these approaches rely on 'macro slip' in which the whole surface is moving before mitigating action can be taken, which risks a loss of grip stability.

An alternative strategy is to sense the occurrence of *incipient slip*, the small localised slips which occur prior to the onset of macro slip. This phenomenon helps human fingers detect slip [10] and has been exploited by the wider robotics community to improve object manipulation [11; 12]. The majority of such systems use biomimicry of the human finger to encourage incipient slip, using curved finger-like surfaces to create a normal force distribution under contact [11], whilst others use pillars to produce stepped changes in the normal force [13]. However, the application of this phenomenon is limited in surgical manipulation, with the only example of its use looking to monitor change in stiffness as an indicator of incipient slip [14].

We propose that if conditions can be created to promote incipient slips in a predictable and repeatable manner, these can be detected and mitigated prior to macro slip and a loss of grip occurring. Ultimately this offers the opportunity for closed-loop grip control independently of predetermined usage thresholds. In this paper we therefore investigate the efficacy of using incipient slip as the basis for monitoring and controlling surgical tissue manipulation. Informed by the basic mechanics of slip, we develop different grasper profiles designed to encourage preferential slip behaviour. These are evaluated experimentally using simulated soft tissues to determine the potential for using this technique in applied surgical contexts.

2.2 Methods

2.2.1 Background

Our concept is based on a biomimetic strategy of preferentially promoting incipient slip at targeted regions of the contact surface [10], achieved through appropriate mechanical design of the grasper jaw. Slip mechanics is thus critical to inform the grasper design.

The development of a slipping contact has two key phases, incipient slip and macro slip [15]. Incipient slip occurs when local shear forces exceed the local friction forces, leading to localised relative displacements between two contacting points on the surface, while the body as a whole remains static. Then macro slip occurs when the total shear force begins to exceed the total friction force at the contact, and the two contacting bodies move relative to each other [15]. Thus to encourage incipient slip there must be a variation in the frictional force between adjacent points across the contacting surface.

2.2.2 Grasper Design

From Amontons' Laws of Friction two key methods of encouraging preferential incipient slip were identified;

- (a) Through variation of the normal force via changes to the grasper profile or,
- (b) Through varying macro surface features to vary the Coefficient of Friction (CoF).

Informed by preliminary work which explored a wide array of potential jaw configurations, a set of jaw profiles were selected to correspond with each method, together with a representative control surface (Fig. 2.1). The control ("All Hex") uses an array of hexagonal pillars (0.75mm width and height) to create a 'patterned' high friction surface similar to a toothed grasper. To vary the distribution of normal force a shallow convex profile ("Convex") was used (radius 50.5mm) with the same hexagonal pattern across the face. To vary the CoF, a flat grasper face was used with a central 8mm strip of hexagonal patterning and smooth borders on either side ("Centre Hex").

The three grasper designs were fabricated using a 3D printer (Form 2, Formlabs) from solid plastic resin (Rigid Resin 1L, Formlabs) at $\times 2$ scale to enable visualisation of slip, such that each contact face was $20\text{mm}\times 30\text{mm}$.

2.2.3 Experimental Setup

A test rig was developed to provide a controlled simulation of tissue grasping and retraction, as shown in Figure 2.2. A linear load tester (Instron 5940, Instron) controlled retraction motion, whilst a pneumatic cylinder (MGPM20TF-75Z, SMC) was used to clamp a tissue simulant between the grasper face and an optically clear acrylic sheet at constant load. An electro-pneumatic regulator (ITV1030, SMC) was used to control clamping pressure, regulated with an embedded control system (MyRIO, National Instruments). The system was pre-calibrated against a load cell. To monitor the slip of the tissue simulant a video extensometer (AVE2, Instron) was positioned behind the acrylic plate, recording images at a rate of 50Hz, whilst the retraction force was measured using a 500N Load cell on the load tester.

The tissue simulant was fabricated from three layers of silicone elastomer (Ecoflex 00-30, Smooth-on), each 1mm thick, with a reinforcement mesh embedded between each layer to represent the gross mechanical and strain-limiting characteristics of human tissue [16], this was done using the film application technique from [17]. Samples were laser cut (VLS 3.50, Universal Laser Systems) in $20\text{mm}\times 100\text{mm}$ strips. A speckle pattern was then applied to the outer layer using black enamel spray paint for motion tracking. Surfactant lubricant was applied to the sample surface prior to each test to represent the serous fluid that coats most organs and provide representative surface adhesion characteristics [18].

2.2.4 Experimental Parameters

A set of test conditions were defined to emulate surgical practice; a 20N compression force was applied to simulate the pressure range used during surgical grasping [19] combined with a retraction speed of 5 mm/s [20]. In each test, the clamping force was slowly applied

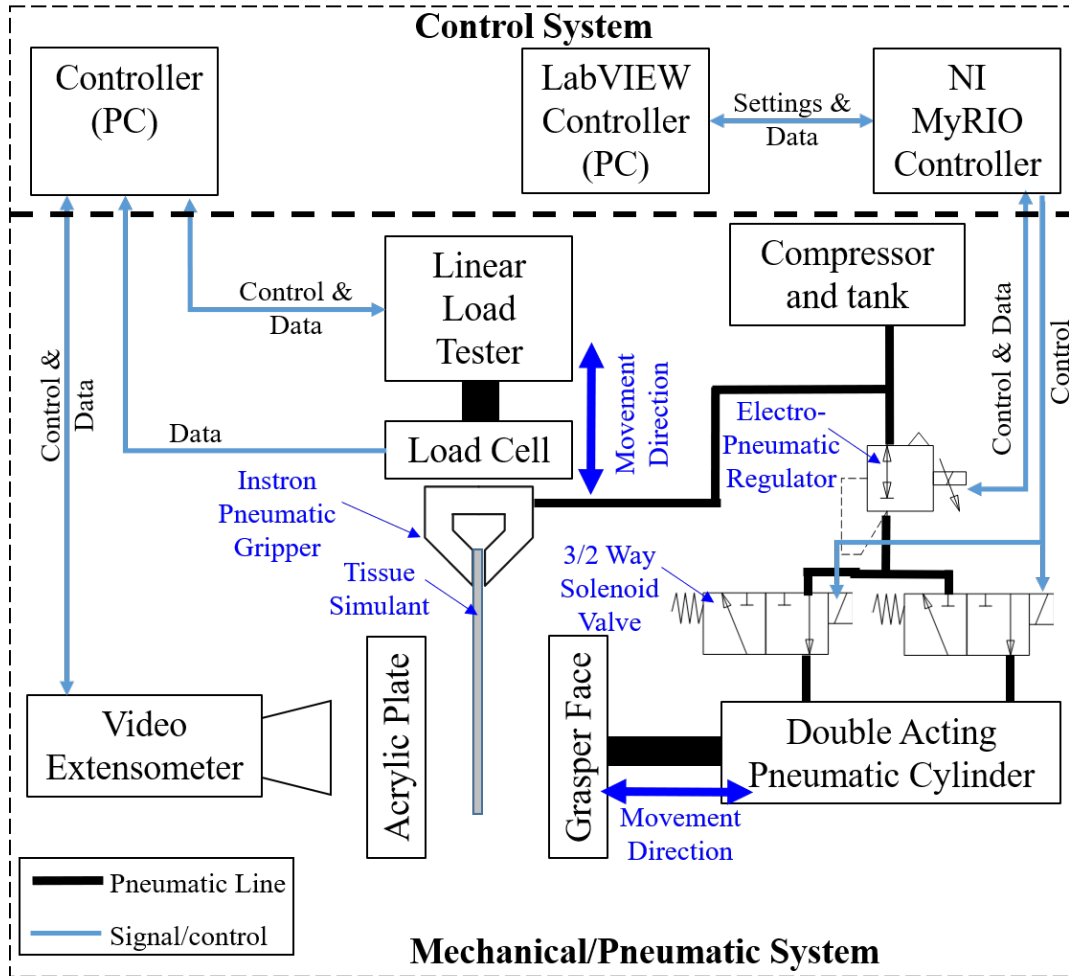


Figure 2.2: Schematic of the control system used for the simulated grasping environment.

to the tissue before retracting the tissue by 30 mm using the load tester. 5 repeats were carried out for each test condition investigated.

2.2.5 Analysis Method

Digital Image Correlation (DIC) was used to track the displacement, and thus slip, of the tissue simulant. Data from the video extensometer was processed using DIC software (GoM Correlate, GoM), enabling the displacements in x and y of a grid of 35 points to be extracted for each video frame. Results were analysed up to the onset of macro slip (defined as when all points had moved $>0.05\text{mm}$).

To characterise the incipient slip we determined the distortion of the tissue as the relative displacement between points. Both local distortion (δ_{Local}) and general distortion (δ_{Gen})

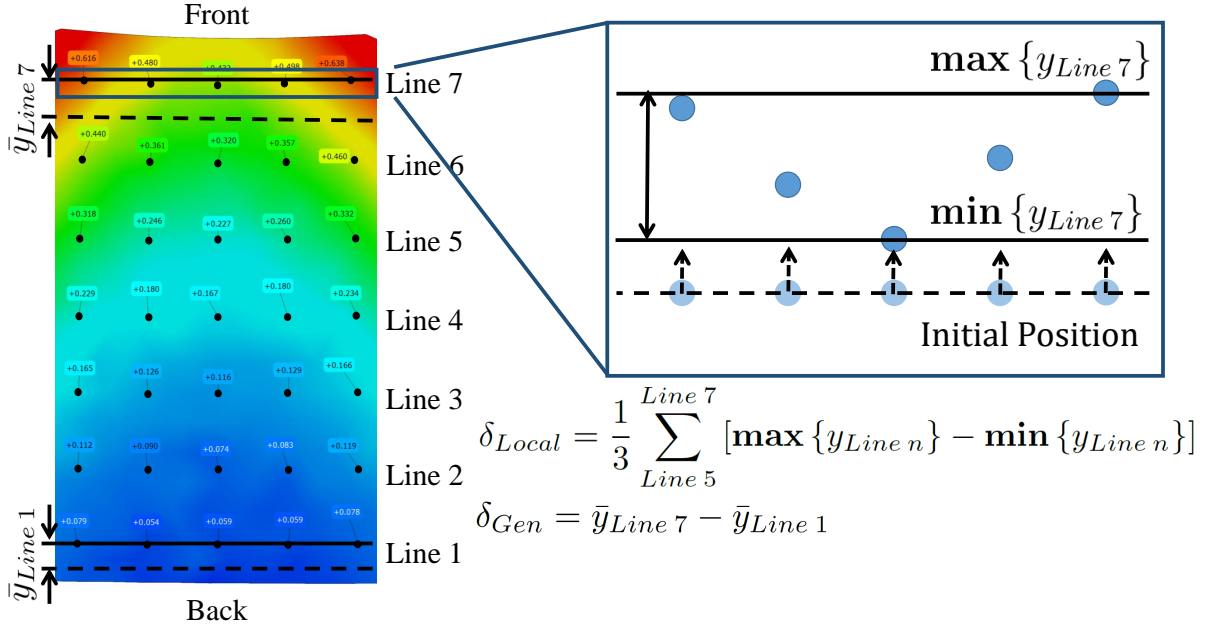


Figure 2.3: Image displaying the grid of 35 dots used for tracking the displacement, with the major metrics used for the calculation of local and general distortion marked on, as well as the relevant equations.

were calculated to monitor relative slip across the width of the grasper, and between the front and back edges respectively. Local distortion was based on the difference between the maximum and minimum displacement of points along each of the front three lines, and general distortion was calculated from the average displacement of the lines ($\bar{y}_{Line\ n}$) at the front and back edge of the sample (Fig. 2.3).

2.3 Results

Results from the study are presented in Figure 2.4 which shows the average local and general distortions for the three grasper faces under nominal conditions after 5 repeats. It is evident that both methods of promoting incipient slip are effective with respect to the control surface when looking at local distortion. However, the Convex profile yields significantly more local distortion, and thus incipient slip across the width of the grasper. The magnitude of the general distortions just prior to macro slip is significantly higher than that observed for local distortion, particularly for the All Hex and Convex graspers, indicating that greater relative slip occurs between the front and back edge than across

the width.

The mean CoF (at the onset of slip) was calculated for each grasper profile to assess their overall grip stability with respect to the high friction control. This gave CoFs of $\mu_{All_Hex} = 0.33$, $\mu_{Convex} = 0.31$ and, $\mu_{Centre_Hex} = 0.14$, indicating that changing profile from flat to convex had little effect but the addition of low friction sections impaired grip stability.

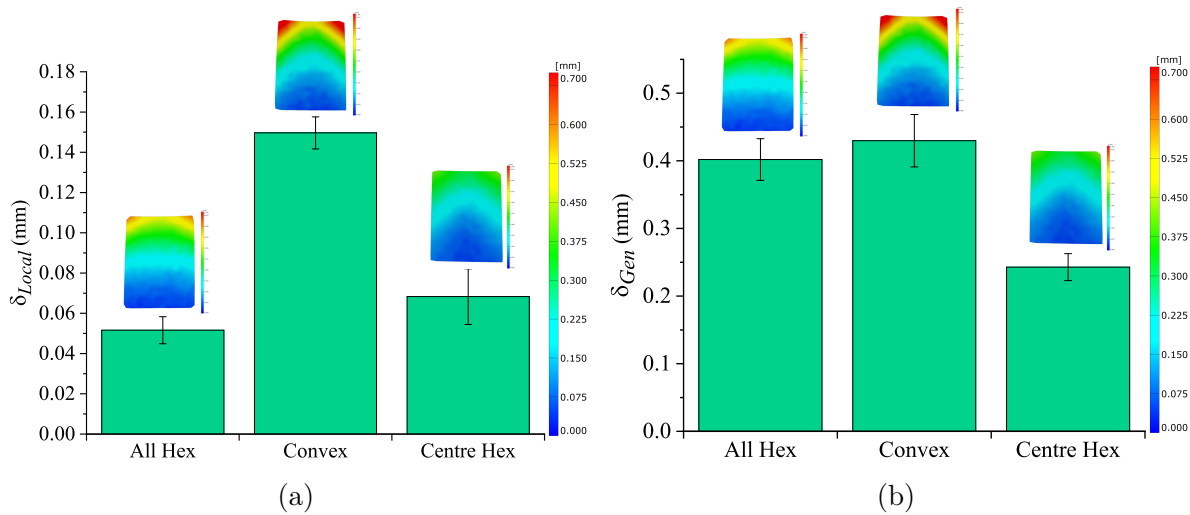


Figure 2.4: Affect of grasper design on the level of incipient slip, indicated by the magnitude of tissue distortion. The colour maps show typical y displacements for each grasper face. (a) Local Distortion. (b) General Distortion.

Figure 2.5 shows a typical temporal slip response for the Convex grasper face. The plot shows six lines representing the displacement of the left, right and central points at the front and back edges of the grasper face. These show an increasing displacement between the front and back edge of the profile, reaching ca. 0.5mm prior to macro slip. Similarly, the relative displacement across the width increases, showing a difference between central and outer sides reaching ca. 0.15mm when macro slip starts after 1 second. The All Hex grasper has a similar response but for the Centre Hex pattern macro slip occurs far earlier, after only 0.2 seconds, indicating lower grip stability.

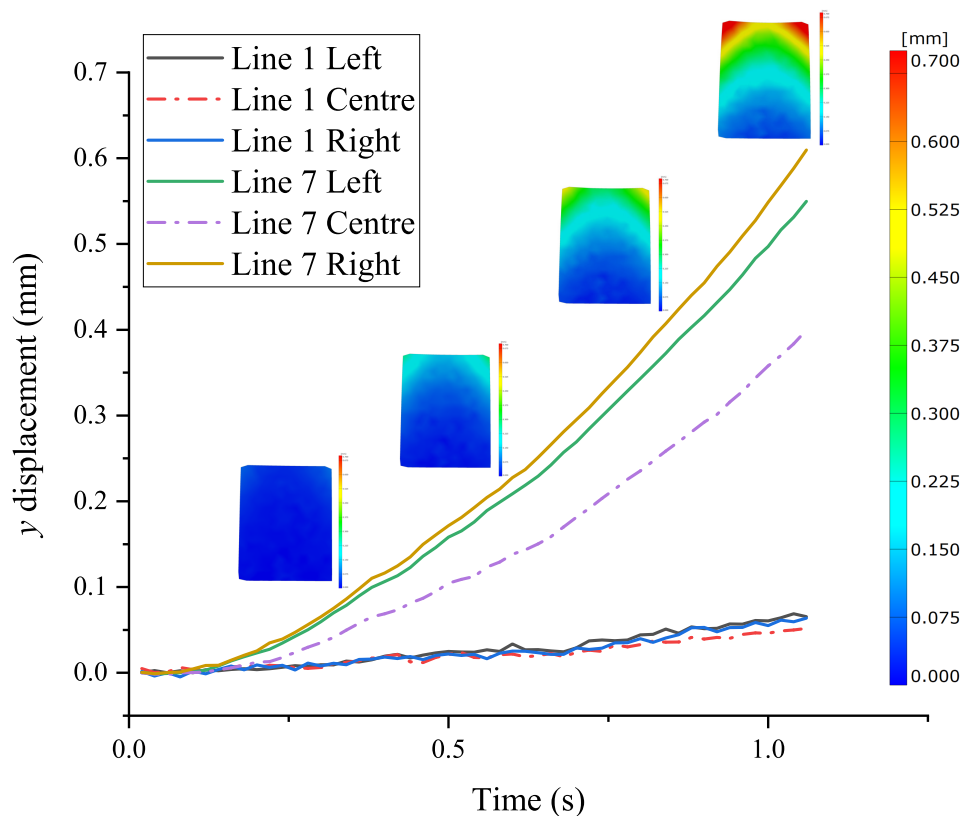


Figure 2.5: Typical response for displacement over time of the central and outer points for Lines 1 and 7 of the Convex grasper face. Colour maps show how the y displacement of the whole face changes over time.

2.4 Discussion

The results of this study demonstrate that incipient slip can be promoted in contact conditions representing a grasper contacting soft tissue. It is interesting to note that the incipient slip manifests both between the front and back edges, and across the width, with respect to the direction of pull (see Fig. 2.1). Prior to macro slip, both grasper profiles exhibited significantly higher general distortion, indicating greater incipient slip between the front and back edges due to the natural slip progression of the elastomer (Fig. 2.4). This indicates that sensing slip differentials between the front and back edges of a grasper face may be preferable to maximise the time required to effect mitigating action. For this configuration, the Convex and All Hex profiles provide the greatest slip differential, likely due to their high CoF slowing the propagation of the slip front along the grasper.

Both spatial and temporal characteristics of the incipient slip are important when consid-

ering how they could be exploited in a potential sensing system for tissue manipulation. A sensing configuration would be required with sufficient spatial sensitivity to detect the displacement differential which indicates incipient slip. This initial study indicates that sub millimetre sensitivity would be necessary. Similarly, based on the temporal development of slip (Fig. 2.5) and DIC framerate, a sensing frequency of 60+ Hz would be required, although it is noted that this will also be a function of retraction speed.

The work presented here is intended to show proof of principle, demonstrating the potential for using incipient slip as a mechanism to sense, and thus avoid, macro slip during grasping. Accordingly, this work focuses on a narrow set of experimental conditions based on preliminary testing. Our ongoing research aims to investigate and characterise the effect of a wider range of factors, including aspects of natural tissue variability, grasper profile and surface design and the operating conditions (e.g. lubricants). These findings will be used to inform the design of a macro slip sensing system which utilises incipient slip and is optimised toward soft tissue interaction.

2.5 Conclusion

his pilot work shows that it is possible to induce incipient slip in a predictable manner using variation of both surface profile and surface features. Of these methods, surface profile variation was found to be more effective. Incipient slip was observed across the width, and between the front and back edges, but the greater general distortion observed suggests that sensing incipient slip between the front and back edges of the grasper has the most virtue. Importantly, this can be achieved without compromising the overall grip stability of the grasper.

The next stage of research is to exploit this fundamental mechanism of preferential incipient slip within a sensing system that monitors local shear forces. This will inform the selection and development of transducer technology capable of detecting incipient slip with a sufficient resolution and speed that mitigating action can be taken before gross tissue slip.

References

- [1] Gregory Tholey, Jaydev P Desai, and Andres E Castellanos. Force Feedback Plays a Significant Role in Minimally Invasive Surgery. *Annals of Surgery*, 241(1):8, 2005.
- [2] B. Tang, G.B. Hanna, and A. Cuschieri. Analysis of errors enacted by surgical trainees during skills training courses. *Surgery*, 138(1):14–20, July 2005.
- [3] C.R. Wagner, N. Stylopoulos, and R.D. Howe. The role of force feedback in surgery: analysis of blunt dissection. In *Proceedings 10th Symposium on Haptic Interfaces for Virtual Environment and Teleoperator Systems. HAPTICS 2002*, pages 68–74, Orlando, FL, USA, 2002. IEEE Comput. Soc.
- [4] E.A.M. Heijnsdijk, J. Dankelman, and D.J. Gouma. Effectiveness of grasping and duration of clamping using laparoscopic graspers. *Surgical Endoscopy*, 16(9):1329–1331, September 2002.
- [5] C.-H. King, M.O. Culjat, M.L. Franco, C.E. Lewis, E.P. Dutton, W.S. Grundfest, and J.W. Bisley. Tactile Feedback Induces Reduced Grasping Force in Robot-Assisted Surgery. *IEEE Transactions on Haptics*, 2(2):103–110, April 2009.
- [6] Natalie T. Burkhard, J. Ryan Steger, and Mark R. Cutkosky. The Role of Tissue Slip Feedback in Robot-Assisted Surgery. *Journal of Medical Devices*, 13(2):021003, June 2019.
- [7] Seyed Mohsen Khadem, Saeed Behzadipour, Alireza Mirbagheri, and Farzam Farahmand. A modular force-controlled robotic instrument for minimally invasive surgery - efficacy for being used in autonomous grasping against a variable pull force: Modular force-controlled robotic instrument. *The International Journal of Medical Robotics and Computer Assisted Surgery*, 12(4):620–633, December 2016.
- [8] Natalie T. Burkhard, Mark R. Cutkosky, and J. Ryan Steger. Slip Sensing for Intelligent, Improved Grasping and Retraction in Robot-Assisted Surgery. *IEEE Robotics and Automation Letters*, 3(4):4148–4155, October 2018.

-
- [9] Yonggang Jiang, Zhiqiang Ma, Bonan Cao, Longlong Gong, Lin Feng, and Deyuan Zhang. Development of a Tactile and Slip Sensor with a Biomimetic Structure-enhanced Sensing Mechanism. *Journal of Bionic Engineering*, 16(1):47–55, January 2019.
- [10] B. Delhaye, P. Lefevre, and J.-L. Thonnard. Dynamics of fingertip contact during the onset of tangential slip. *Journal of The Royal Society Interface*, 11(100):20140698–20140698, September 2014.
- [11] Wei Chen, Heba Khamis, Ingvars Birznieks, Nathan F. Lepora, and Stephen J. Redmond. Tactile Sensors for Friction Estimation and Incipient Slip Detection – Towards Dexterous Robotic Manipulation: A Review. *IEEE Sensors Journal*, pages 1–1, 2018.
- [12] M.R. Tremblay and M.R. Cutkosky. Estimating friction using incipient slip sensing during a manipulation task. In *[1993] Proceedings IEEE International Conference on Robotics and Automation*, pages 429–434, Atlanta, GA, USA, 1993. IEEE Comput. Soc. Press.
- [13] Heba Khamis, Raquel Izquierdo Albero, Matteo Salerno, Ahmad Shah Idil, Andrew Loizou, and Stephen J. Redmond. PapillArray: An incipient slip sensor for dexterous robotic or prosthetic manipulation – design and prototype validation. *Sensors and Actuators A: Physical*, 270:195–204, February 2018.
- [14] Jeffrey Stoll and Pierre Dupont. Force Control for Grasping Soft Tissue. page 4, May 2006.
- [15] K. L. Johnson. *Contact mechanics*. Cambridge University Press, Cambridge Cambridgeshire New York, 1987.
- [16] Y. C. Fung. *Biomechanics: Mechanical Properties of Living Tissues*. Springer Science & Business Media, March 2013. Google-Books-ID: yx3aBwAAQBAJ.
- [17] Jun Wai Kow, Peter Culmer, and Ali Alazmani. Thin soft layered actuator based

- on a novel fabrication technique. In *2018 IEEE International Conference on Soft Robotics (RoboSoft)*, pages 176–181, Livorno, April 2018. IEEE.
- [18] W. Schwarz. The surface film on the mesothelium of the serous membranes of the rat. *Zeitschrift fr Zellforschung und mikroskopische Anatomie*, 147(4):595–597, 1974.
- [19] Phillip Mucksavage, David C. Kerbl, Donald L. Pick, Jason Y. Lee, Elspeth M. McDougall, and Michael K. Louie. Differences in Grip Forces Among Various Robotic Instruments and da Vinci Surgical Platforms. *Journal of Endourology*, 25(3):523–528, March 2011.
- [20] Ali Alazmani, Rupesh Roshan, David G Jayne, Anne Neville, and Peter Culmer. Friction characteristics of trocars in laparoscopic surgery. *Proceedings of the Institution of Mechanical Engineers, Part H: Journal of Engineering in Medicine*, 229(4):271–279, April 2015.
- [21] Joseph C. Norton, Jordan H. Boyle, Ali Alazmani, Pete R. Culmer, and Anne Neville. Macro-Scale Tread Patterns for Traction in the Intestine. *IEEE Transactions on Biomedical Engineering*, 67(11):3262–3273, November 2020.
- [22] Huawei Chen, Liwen Zhang, Deyuan Zhang, Pengfei Zhang, and Zhiwu Han. Bioinspired Surface for Surgical Graspers Based on the Strong Wet Friction of Tree Frog Toe Pads. *ACS Applied Materials & Interfaces*, 7(25):13987–13995, July 2015.

2.6 Appendix

Selection of grasper face pattern

The hexagonal pattern selected for the gripping surface, based on [21], is not representative of the typical saw tooth pattern that is utilised on the majority of robotics surgical graspers. However, this pattern was selected for two main reasons:

The use of the hexagonal pattern makes it possible to vary the density of the hexagonal pillars across the grasper face, as a method for varying the coefficient of friction across it. For this experiment the Centre-Hex grasper just used a combination of pillars and no pillars to vary the CoF, but for future experiments this pattern selection offered the possibility of being able to easily tune the CoF for the different grasper sections.

Traditional saw tooth graspers are significantly anisotropic, they provide a strong resistance to shear force acting along the length of the grasper, but minimal resistance to any lateral movements [22]. The hexagonal pattern instead provides an isotropic gripping surface. An area of future research will be to investigate the influence of non-parallel retractions, utilising an isotropic pattern allows the effects of the rotation and lateral slip on the sensor performance to be evaluated, without the grasper pattern design skewing the results.

This isn't the first time a hexagonal pillar array has been utilised on a surgical grasper. *Chen et al* [22] investigated the use of a variety of different shaped micro pillars, on the scale of approximately 100 microns, to try and improve the grip of surgical graspers, and reduce tissue damage, using bioinspired designs based on tree frog toe pads. They found hexagonal and diamond shaped micro pillars provided a significant improvement in the coefficient of friction for sliding in both lateral and longitudinal directions, when compared to traditional saw toothed graspers [22]. Although this work utilised micro pillar arrays, research by *Norton et al.* [21] demonstrated that larger hexagonal macro pillars of up to 750 microns still provided a very effective grip for biological tissue.

Parametric study

The following work builds on the results reported in Section 2.3 by exploring the performance and slip mechanics of the grasper faces under a wider range of grasping forces, retraction speeds, and material stiffnesses.

Method

A parametric study was performed on two of the three grasper faces to investigate how variations in force, speed, and material stiffness influence the development of tissue slip for the different grasper designs, see Section 2.2 for a complete description of the designs and test methods. The Centre Hex grasper was excluded from this study as the significant decrease in the CoF of the contact made it unsuitable for use in surgical grasping. For this study a single variable was altered whilst all other variables remained at their nominal values, see Table 2.1 for a summary of the range of variables used. The results for the local and general distortions from the parametric study are presented in Figure 2.6, 5 repeats were carried out for each test condition.

Table 2.1: Experimental Parameters.

Material (Elastic Modulus)	Compression Force	Retraction Speed
Mat A* (241 kPa)	10 N	2 mm/s
Mat B (320 kPa)	20 N*	5 mm/s*
Mat C (610 kPa)	30 N	10 mm/s

*Indicates nominal test conditions.

Results

From the parametric study it is clear that the variation of stiffness had the most significant effect on the induction of incipient slip, with increasing stiffness significantly decreasing the levels of distortion observed in both directions. As the stiffness of the simulant increases its response will tend towards that of a rigid body, at which point incipient slips will no longer be present as the whole of the surface will move simultaneously.

Variation of force also influenced the occurrence of incipient slip both across the width

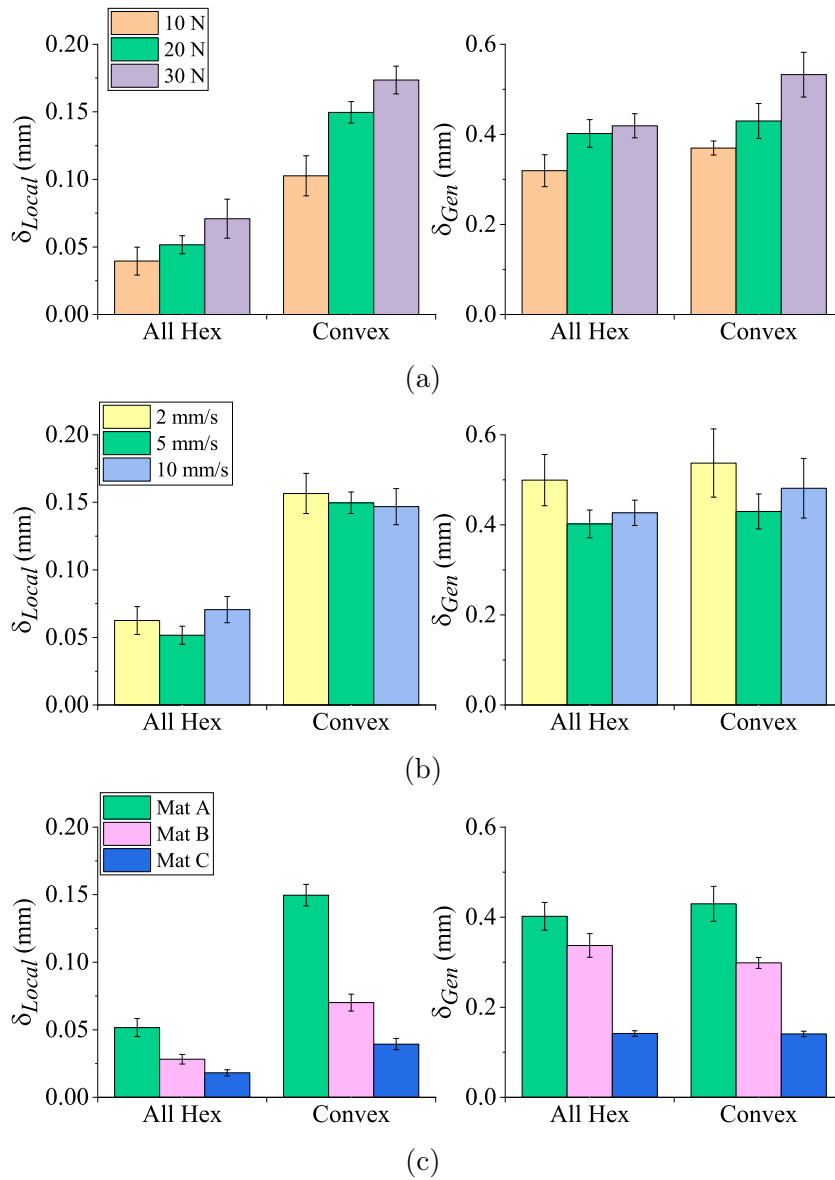


Figure 2.6: Influence of grasper design on the level of incipient slip, indicated by the magnitude of both local and general tissue distortion. Affect of: (a) Variation in force, using Mat A with a 5 mm/s retraction speed. (b) Variation in speed, using Mat A with a 20 N clamp load. (c) Variation in tissue simulant stiffness, with a 20N clamp load and 5 mm/s retraction speed.

and along the length of the grasper, with a higher normal force resulting in higher levels of both local and general distortion. This occurs as the increase in normal force results in a higher level of mechanical engagement between the grasper and tissue, increasing the friction and slowing the rate of slip propagation, whilst the retraction speed remains the same. Therefore any tissue that has already slipped will experience a greater level of displacement and distortion before macro slip does occur, as it occurs later in the retraction.

For variations in speed the incipient slip across the width appears unaffected, with minimal change in the local distortion, indicating that slip across the width is independent of the retraction speed. The general distortion however does show a decrease when the speed increases from 2 mm/s to 5 mm/s, though this then levels off by the 10 mm/s retraction. This could be because the increased retraction speed increases the relative rate of slip propagation, due to the higher momentum of the retraction movement, reducing the amount of displacement that is able to occur before macro slip occurs. However, further research is required to fully understand why this occurs between 2 mm/s and 5 mm/s but then not on the increase to 10 mm/s.

Chapter 3

Incipient Slip Sensing for Improved Grasping in Robot Assisted Surgery

Preface

This chapter was published as the journal paper:

Incipient Slip Sensing for Improved Grasping in Robot Assisted Surgery. Ian Waters, Lefan Wang, Dominic Jones, Ali Alazmani, and Peter Culmer. IEEE Sensors. 2022.

Sections 3.1 through 3.6 constitute the main body of this publication, whilst the appendix details the sensor calibration process. This paper takes one of the phenomena identified in chapter 2, that there is a slip differential between the front and rear of the grasper, as a result of a tissue's deformable properties, and utilises it to develop a slip sensor capable of detecting incipient slip.

Abstract

The limited grasping control available in Robot Assisted Surgery is considered a significant limitation of the technology. Traditionally the integration of haptic feedback has been proposed to resolve this issue but has found limited adoption. Here we investigate an alternate approach based on the concept of detecting localised slips caused by the intrinsic elastic properties of soft tissues. This method allows for the early detection of slip so that mitigating actions can be taken before gross slip can occur, allowing the grasper to minimise the force required to maintain stable grasp control. In this paper we detail the design of a sensor developed to detect incipient slip by monitoring the relative difference in tissue movement at the front and back of the grasper, caused by tissue slip. We then demonstrate the sensor's efficacy for the early detection of slip, as well as its ability to automate grasping under representative surgical conditions, with the automated case providing comparable performance to one which uses the maximum allowable grasp force. This work provides evidence that the slip detection methodology developed is consistently able to detect incipient slip before macro slip occurs, thus offering a strong basis for its use in automating surgical grasping tasks to avoid tissue trauma and slip.

3.1 Introduction

Robotic surgical devices have helped advance Minimally Invasive Surgery (MIS), with the introduction of 3D vision, tremor removal, and improved dexterity all contributing to improved surgical outcomes [1]. However the lack of haptic feedback is still highlighted as a major limitation of the technology [1; 2]. Robotic surgical devices mechanically separate the surgeon and patient, completely denuding the surgeon of their sense of touch, which is already significantly limited by the tools used in MIS procedures. This can lead to multiple issues including the over application of force, limited grasp control, tissue slip, and an inability to palpate tissue to identify abnormalities [3; 4; 5].

The use of haptic feedback during tissue grasping tasks has been demonstrated to reduce tissue trauma caused by crushing due to excessive grasping forces [6; 7; 8]. However it

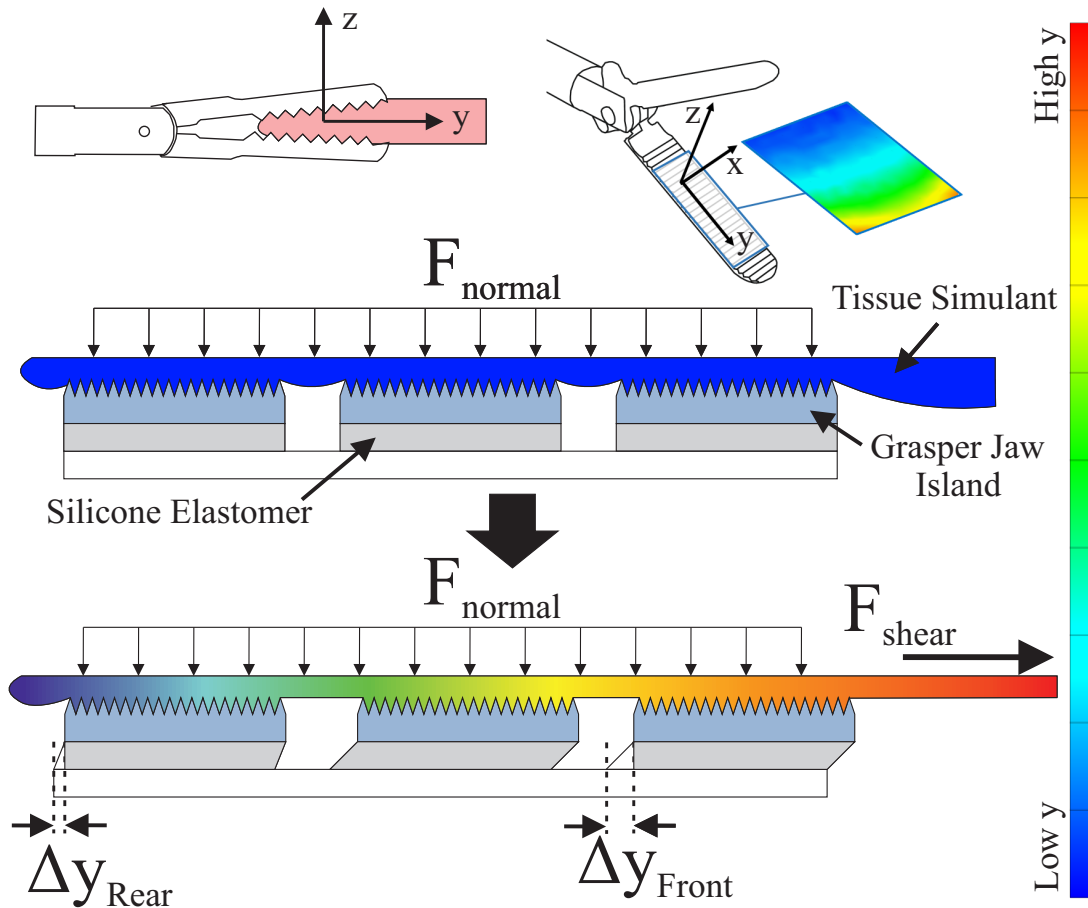


Figure 3.1: Concept of the slip sensor's mechanical operation; the grasper face is separated into movable islands that can be tracked to detect the difference in slip between the front and rear of the grasper (The scale indicates the relative displacement of the colours used in the diagram).

also increases the cognitive load on the surgeon, which could result in surgical errors [9], and there is a paucity of knowledge on its ability to prevent adverse slip events, which can delay surgery or lead to further complications [4]. We believe a more direct method of controlling the grasping force, whilst maintaining grip security, would be through slip monitoring and detection. If it is possible to detect the point in time when tissue starts to slip, then the gripping force can be adjusted to use the minimum force required to maintain stable control, reducing tissue trauma as well as the occurrence of slip events during surgery. This method of control also opens up the possibility for automation of grasping, allowing the surgeon to focus on more critical tasks [10].

Several notable examples of surgical graspers designed to detect slip have been reported. *Khadem et al.* [11] created a system that automatically adjusts the clamping load based

on the applied retraction force, aiming to remain within a predefined safe grasping zone, however this requires prior knowledge of the slip behaviour of the grasped tissue. *Burkhard et al.* [12] developed a method that aims to directly detect slip events, this uses a thermal sensing technology that monitors changes in heat flux through the tissue as it slips. This was able to detect slip after less than 2mm of gross tissue displacement in trials on porcine tissue. *Jones et al.* [13] developed a force based slip sensor, using a two axis soft inductive tactile sensor (SITS) to detect when the coefficient of friction first peaks during tissue retraction to indicate when slip has occurred. The common feature of the latter two approaches is that they aim to identify the time at which macro slip occurs, which requires the whole tissue contact area to be slipping before mitigating action can be taken, therefore risking a loss of grip stability. One possible solution to this is to focus on exploiting and sensing the occurrence of incipient slips.

Incipient slips are localised slips that occur prior to the onset of macro slip [14]. In incipient slip the total shear force is less than the total frictional force, but in localised areas of the surface contact the local shear force exceeds the local friction, causing small localised movements at the surface while the remainder of the contact remains static [14]. As more shear force is applied the number of incipient slip sites will increase, when the total shear force exceeds the total frictional force the entirety of the contact will begin to slip, otherwise termed macro slip [14].

The phenomenon of incipient slip helps human fingers detect slip before macro slips can occur [15], and has already been utilised by the wider robotics community to improve grasping [16], but currently has seen limited use in the field of surgical manipulation, or the grasping of deformable materials. *Stoll and Dupont* [17] looked to monitor changes in tissue stiffness as an indicator of incipient slip, but the method only measured global rather than local shear forces, and so would provide minimal time for mitigating actions to be taken.

The majority of incipient slip sensors developed by the wider robotics community use curved finger like surfaces to encourage incipient slip [16; 18; 19]. This curved surface

results in a variation in the normal force across the surface, creating areas of high and low friction which lead to slips occurring preferentially towards the edge of the contact, where the normal force is low [16]. Despite using similar methods to encourage incipient slip a range of different sensing methods and modalities are used to detect it (e.g. vibration, shear force, normal force distribution and optical tracking), for a detailed summary of these see the review by *Chen et al.* [16]. We have previously produced an incipient slip sensor, for use with soft tissues, that utilises the variation of the normal force to induce predictable incipient slip events, which were monitored using a localised measurement system [20].

Our aim is to develop and evaluate an instrumented grasper face for detecting incipient slips before macro slip occurs. In section 3.2 we present the sensing concept and detailed design of the sensor system, before evaluating its efficacy over a range of operating conditions in Section 3.3. A case study is then presented in Section 3.4 to demonstrate the concept's feasibility for use in grasping automation. This work can then form the basis for a grasping system capable of automating grasping and force control within surgery, through the detection of incipient slip events.

3.2 System Development

3.2.1 Concept

The concept underpinning this work aims to exploit the deformable nature of soft tissue to create detectable levels of incipient slip. Although the majority of incipient slip sensors utilise variations in normal force to encourage incipient slip, they are generally attempting to grasp rigid objects [16], whereas many tissues in the human body are typically compliant and highly deformable. Therefore as tissue is retracted by a surgical grasper it stretches, creating a tensile force which is resisted by the friction at the grasper face. When the tensile shear force exceeds the frictional force the tissue at the front of the grasper will start to slip, allowing it to stretch and deform, causing the tensile force to then propagate along the grasper face to the adjacent section of tissue [21]. This leads to

a propagation of slip, followed by tissue deformation, along the grasper face, resulting in a difference in the relative tissue displacement at the front and rear of the grasper (Fig. 3.1).

Our concept is based on monitoring the difference in local tissue displacement that occurs between the front and rear of the grasper, created by the propagation of slip along its length. To achieve this the grasper's surface is separated into multiple sections or 'islands' that can move independently of each other, similar to those we utilised previously [20]. As the tissue is retracted the tensile force applied to the front island causes it to move forward with the tissue, until the shear force acting between the tissue and island exceeds the frictional force, at which point the island's displacement will halt as the tissue slips. The tension will then propagate through to the next island, as the front island is no longer maintaining a secure grip, resulting in the occurrence of displacement and then slip at each subsequent island (Fig 3.1). Consequently by tracking the displacement of the islands it is possible to detect when the tissue first slips against the front island, whilst the other islands maintain a stable control of the tissue. The novelty of this sensor system is the way in which it harnesses the deformation inherent in soft tissues to create measurable levels of incipient slip, which can be detected before the onset of macro slip.

3.2.2 System Design and Fabrication

A scaled demonstration of a surgical grasper (Fig. 3.2) was developed to evaluate this concept. This consists of three islands distributed along the length of the grasper that can move independently of each other, with sensors positioned beneath the front and rear islands to track their displacement. Each island consists of a 3D printed rigid gripping surface (Rigid 4000 Resin, Formlabs), with a 1 mm layer of silicone elastomer (Ecoflex 00-30, Smooth-on) underneath to allow them to move freely. The grasper was scaled up from a standard surgical grasper to allow for improved characterisation and analysis of incipient slip, and its associated mechanics. A regular hexagonal pattern (0.75 mm height, width and separation) was applied to the surface of the grasper as this provides isometric frictional properties, which can easily be varied through altering the pattern

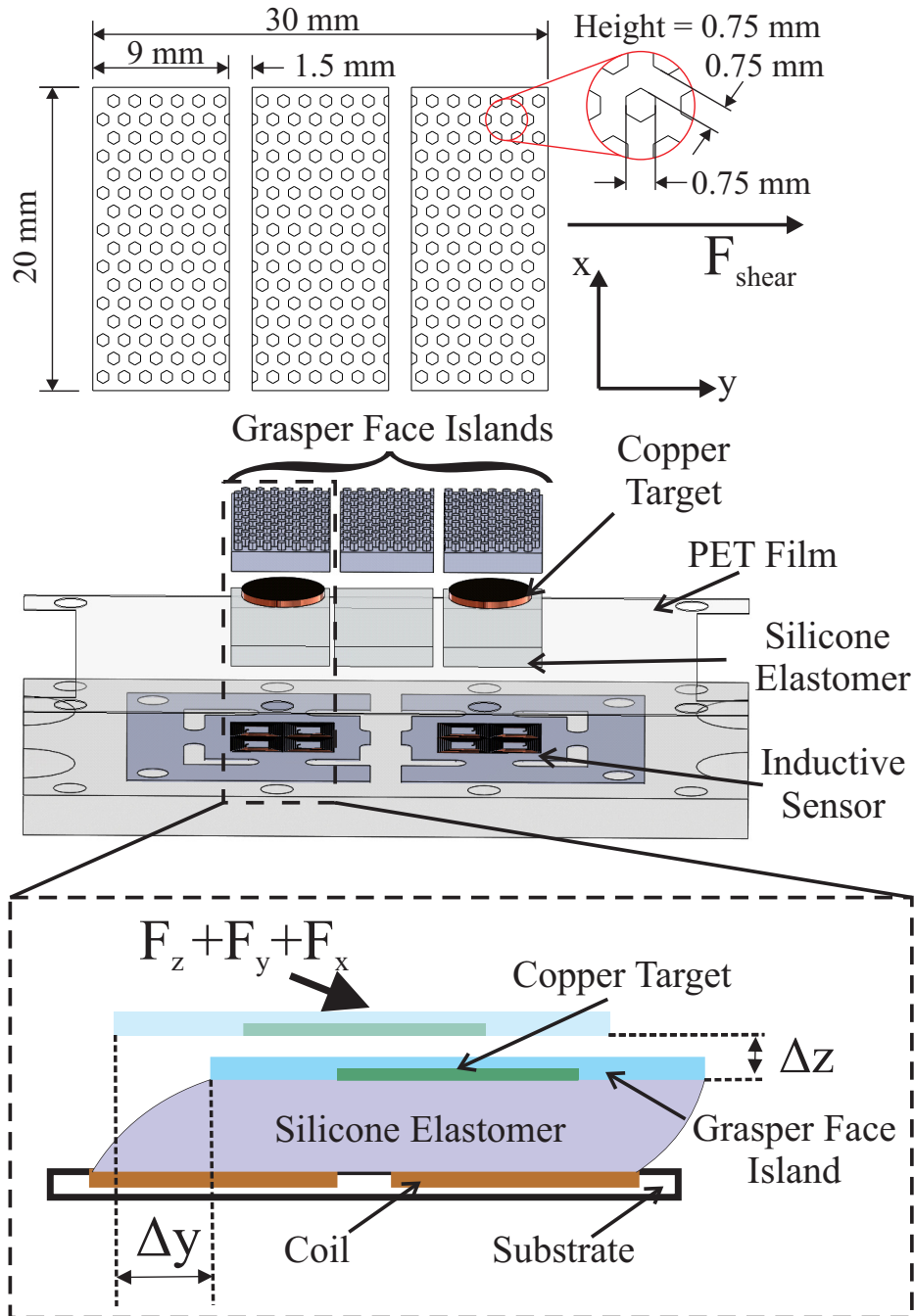


Figure 3.2: Top: Dimensioned grasper face islands. Middle: Exploded model of the different components making up the sensor system. Bottom: Illustration of the principle of operation of SITS sensors.

density [21; 22].

To monitor the relative displacement of the islands tri-axis SITS sensors were selected due to their thin form factor, and the ability to tune their resolution to suit the desired application [23; 24]. These utilise the eddy current effect to detect the movement of a conductive target over a set of sensing coils. Eddy currents are induced within the con-

ductive target by an alternating current passing through the coils, in turn this produces a magnetic field which opposes the original field of the coils, causing a change in their inductance (Fig.3.2). The variation of this inductance across a set of four coils can then be used to determine the position and movement of the target above them [23].

The SITS sensors utilised consisted of four 5mm square coils each consisting of 3 layers of coils with a 0.1 mm pitch, a 0.1 mm trace width, with 10 turns per layer, whilst a copper disc (8 mm diameter \times 0.8mm) embedded in the base of the rigid gripping surface was used as the conductive target. A 0.15 mm layer of PET film was placed above the coils to protect them from any fluid ingress (Fig. 3.2). To measure their change in inductance a four channel inductance to digital converter chip was used (LDC1614, Texas Instruments). For more information on the design and operation of these sensors see [24; 23]. The sensors were monitored and controlled via a microcontroller (Teensy 3.6, PJRC) using the I²C serial protocol.

3.2.3 Data Processing

To calibrate the SITS sensors a multi axis sensor calibration rig was employed [24], this moves the conductive target over each set of four coils using three linear stages, monitoring its displacement in x,y and z via a set of encoders. A 3D scanning operation was carried out with z stepped in 0.2 mm increments from z=-0.6:1.2 mm, and a grid scan was conducted between y=-3:3 mm and x=-1:1 mm at each z level, where {0,0,0} represents the position of the target in its unloaded 'neutral' position.

A neural network was implemented to determine the sensor displacement (D) from the inductance values (I) of the four coils,

$$D_{x,y,z} = f(I_{1,2,3,4}) \quad (3.1)$$

using the Matlab neural net fitting toolbox (Matlab, Mathworks). The neural net consisted of a two-layer feed forward neural network with 15 neurons in the hidden layer,

with the Tanh function used as the activation function, and the Levenberg-Marquardt back propagation algorithm as the training method, these were selected based on prior research [24]. Validation of this model against a separate data set showed a high correlation with the output of the neural net, with root mean squared errors of 0.043 mm, 0.050 mm and 0.064 mm, in x, y and z respectively.

3.2.4 Slip Detection

In the context of this paper incipient slip refers to the condition when at least one of the islands is found to be slipping against the tissue, while the remaining islands retain a stable grip. With the current sensor design the whole of the island's contact area must be slipping against the tissue for slip to be detectable at that island. During retraction this will always occur at the front islands first due to the way shear forces, and the resultant slip, propagate from the front to rear of the grasper, as detailed in Section 3.2.1.

To be able to identify the time at which incipient slip starts to occur at the front sensor an algorithm was developed using initial trial data (See Fig. 5), an example trace is shown in Figure 3.3. This algorithm was focused on detecting slip during grasper retraction as this is considered the most challenging case, when tissue is most likely to slip during surgery due to the higher shear forces being applied.

From Figure 3.3 it can be observed that an incipient slip event occurs at the front island around the 4 second mark, indicated by the plateauing of the displacement, suggesting the island is no longer moving with the retracting tissue. As the front sensor begins to slip the rear sensor then starts to take up tension, indicated by its rapid increase in displacement after the incipient slip event occurs at the front island, as the tension, deformation, and slip propagate from the front to the back of the grasper.

By calculating the change in the separation between the front and rear islands, as shown in Figure 3.3, a clear peak appears when the front island starts to slip against the tissue. This peak occurs because as the front island starts to slip, the rear islands start to take up tension (due to the slip propagation along the grasper), thus reducing the separation

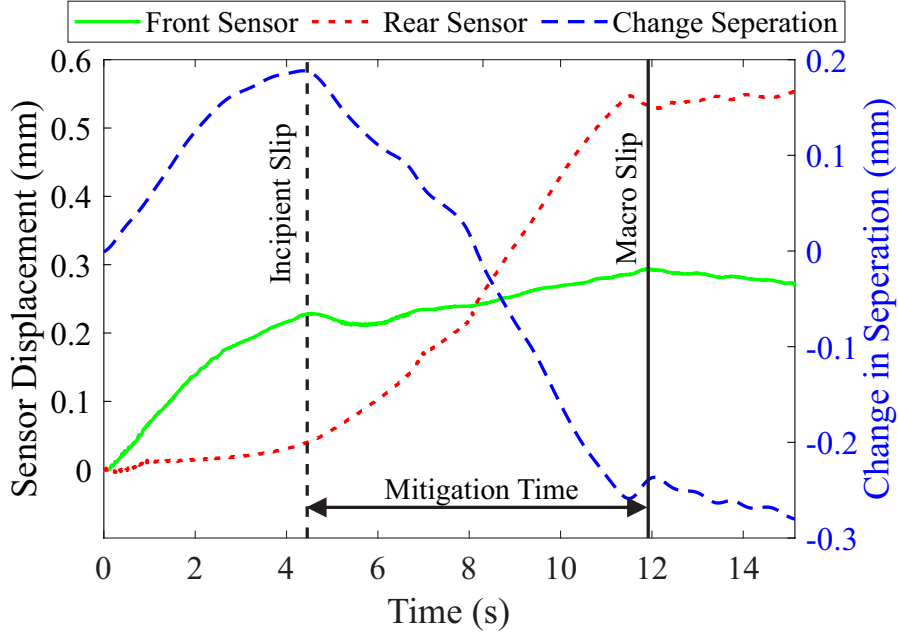


Figure 3.3: Example trace showing the displacement of the front and rear sensor islands, as well as the change in the separation between the two. Test conditions: Mat A, 20 N clamp load, and 2 mm/s retraction speed.

between the front and rear islands after this point. To automatically identify the time at which this peak occurs, and therefore incipient slip, the differential of the change in separation between the two sensors was defined as,

$$S = \frac{d(\Delta y_{Front} - \Delta y_{Rear})}{dt} \quad (3.2)$$

where S is the rate of change in separation, and y is the displacement in the direction of shear of the front and rear sensors. A third order Butterworth filter with a cut off frequency of 5 Hz was then applied to attenuate noise. When the mean value of the rate of change of separation measured over a 0.1 s period first becomes less than 0, indicating a peak, incipient slip of the front island is considered to have occurred, where $t = n$ is the current time. This algorithm was developed at a sample rate of 100 Hz.

$$\overline{[S]}_{t=n-0.1}^{t=n} < 0 \quad (3.3)$$

3.3 System Evaluation

To evaluate the performance of the sensor to identify incipient slip prior to macro slip a test rig was developed, this simulates the clamping and retraction of tissue under representative surgical conditions. A typical test involved clamping the tissue between the sensed grasper face and a flat surface, at a constant fixed load, before retracting the tissue in a direction parallel to the grasper face along its length for 30 mm, to ensure that the tissue enters the macro slip regime.

3.3.1 Experimental Set Up and Analysis

An adaption of the test rig from [21] was used to create a controlled simulation of surgical grasping and retraction (Fig. 3.4). This consists of a linear load tester (Instron 5940, Instron) for tissue retraction, and a pneumatic piston (MGPM20TF-75Z, SMC) & (ITV1030, SMC) regulator to simulate grasping under a constant load. The retraction distance and global shear force were logged via the linear load tester, whilst the SITS sensors were monitored via the microcontroller. All data logging and control was managed and synchronised between the linear load tester and the microcontroller using a real-time embedded control board (MyRIO, National Instruments), with a sample rate of 100 Hz. Tissue simulants were clamped against a clear acrylic plate with a camera (AVE2, Instron) positioned behind it, this captured images at a rate of 50 Hz for use in tracking the displacement of the tissue simulant through Digital Image Correlation (DIC).

3.3.2 Data Analysis

The time macro slip occurs can be identified by monitoring when the global shear force acting on the tissue starts to plateau, as this indicates the tissue is fully slipping against the grasper, preventing further increases in the tensile force of the tissue. To calculate the time of macro slip the differential of the global shear force (F_S), measured by the

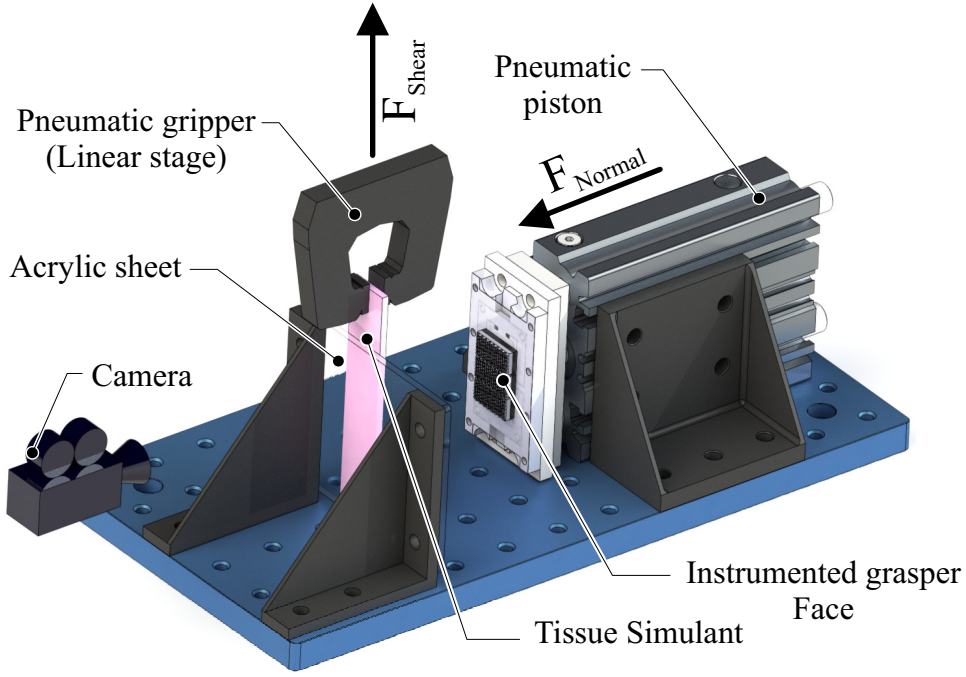


Figure 3.4: Model of the testing setup used for simulating the clamping and retraction of tissue.

linear load tester, was used to identify when the shear force starts to level off.

$$\overline{\left[\frac{dF_s}{dt} \right]_{t=n-0.1}^{t=n}} < 0.025V_s, \quad (3.4)$$

When the rate of change of force, averaged over the previous 0.1 s, is less than 0.025 times the retraction speed (V_s), macro slip is indicated to have occurred.

The time difference between the point of macro slip and the point that incipient slip is detected was then calculated, this gives an indication of the available time to take mitigating action, termed the mitigation time (Fig. 3.3).

For validation of the actual magnitude of displacement and slip that is occurring between the tissue simulant and grasper face, the displacement of the tissue simulant was tracked using images from the camera and DIC software (GOM Correlate, GOM). The average displacement of the tissue grasped by the the front, central, and rear grasper islands during the initial clamping action was tracked throughout the retraction, in the direction of shear.

3.3.3 Experimental Parameters

To analyse the sensor characteristics a set of operating parameters were defined based on those used in typical surgical practice. The major variables identified were the clamping force, retraction speed, and material stiffness.

A clamping force range of 10-30 N was selected as this approximates the applied pressure range of a standard surgical grasper [25; 26], and a retraction speed range of 1-5 mm/s was used, based on standard laparoscopic retraction speeds for tissue manipulation and grasper retraction [27].

Due to the inherent variability with using biological tissue samples a range of tissue simulants were developed to vary the material stiffness in a more repeatable manner. Three different tissue simulants were created that mimic the tensile properties of liver tissue [28]. The simulants consist of 3 layers of silicone elastomer (Ecoflex 00-30, Smooth-on) with different fabrics sandwiched between each layer of silicone to vary the elastic modulus (E), whilst maintaining similar frictional and compressive properties. Material A (Mat A - $E = 241$ kPa) and B (Mat B - $E = 320$ kPa) used 2 & 4 layers of a lightweight netted spandex respectively, whilst Material C (Mat C - $E = 610$ kPa) used 2 layers of a higher density woven spandex. These simulants were fabricated using the silicone applicator from [29] to form a 3 mm thick sample, with the fabric layers placed 0.3 mm below each surface, these were then laser cut into 20 mm x 100 mm strips. To allow tissue displacements to be tracked using DIC a speckle pattern was applied to one side using enamel spray paint, with a very thin 0.05 mm layer of silicone applied on top to prevent delamination of the pattern. A layer of surfactant lubricant was applied to the surface of the simulants before each test, simulating the serous fluid that coats most organs [30]. To calculate the elastic modulus of the three different simulants ATSM D412 Type C tensile specimens were evaluated on a linear load tester.

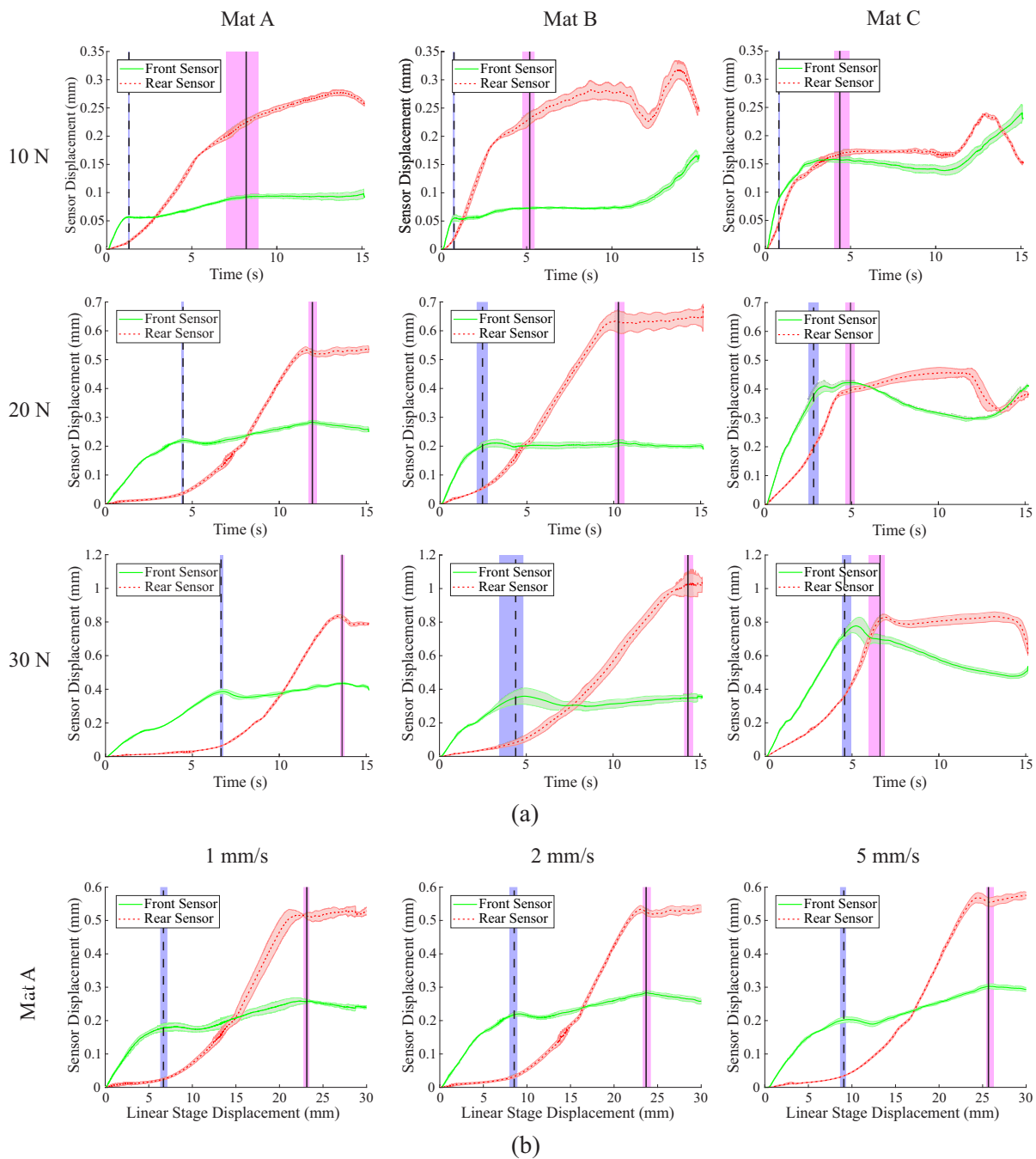


Figure 3.5: Graphs showing average sensor displacement, with the shaded area representing the standard deviation. The vertical dotted lines indicate the time incipient slip occurs, while the solid vertical line indicates the time of macro slip, the shaded areas around each show range of slip times/displacements. a) Sensor displacement vs time for changes in force and material stiffness at a retraction speed of 2 mm/s. b) Sensor displacement vs linear stage displacement (retraction distance) for variations in retractions speed for Mat A under a 20 N clamping load.

3.3.4 Results

Figure 3.5 (a) provides a summary of the average displacement measured by the sensors under the front and rear islands, for variations in the material stiffness and clamping force. Early signs of incipient slip are identifiable in the majority of cases, indicated by the plateauing of the front sensor's displacement, followed by a rapid increase in the displacement of the rear sensor island. The exception to this is the 10 N load case for the high stiffness material, Mat C, where both front and rear take up tension and then slip almost simultaneously.

The results for the influence of varying retraction speed on sensor displacements are shown in Figure 3.5 (b), these are plotted against the displacement of the linear stage to normalise the x-axis scale for the different retraction speeds. In all test cases the front island clearly slips before the rear island, allowing for reliable early detection of incipient slip. Despite large variations in the retraction speed, the retraction distance at which incipient and macro slip occur shows minimal change.

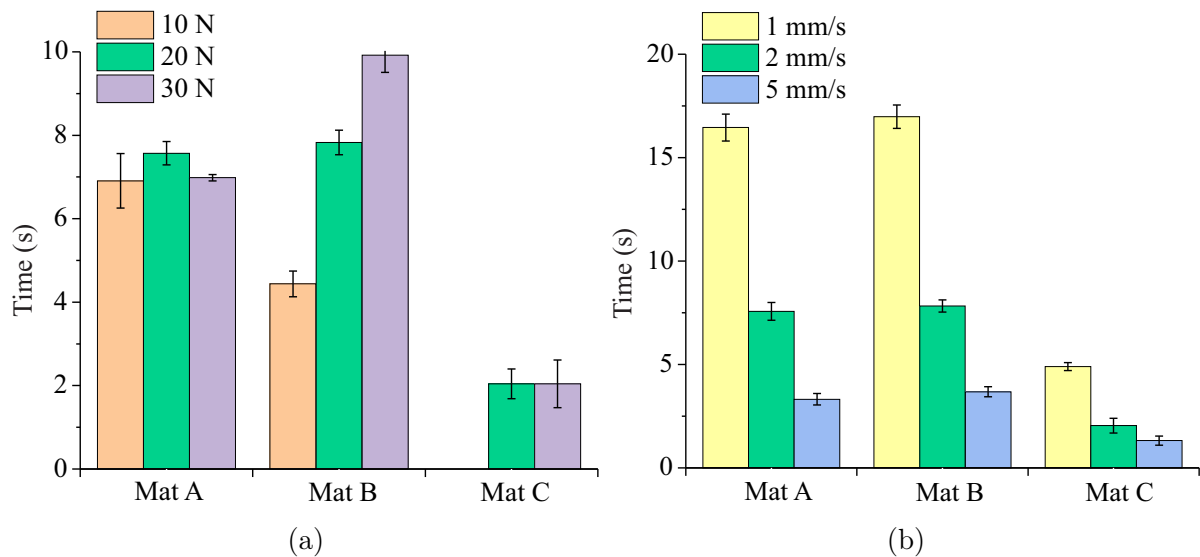


Figure 3.6: Graphs showing the mean time difference between the detection of incipient and macro slip ($N=5$), the error bars indicate the standard deviation. (a) Variation of force and material stiffness at 2 mm/s retraction speed. (b) Variation of speed and material stiffness at 20 N clamp load.

A summary of the effects of the clamp force, material stiffness and retraction speed on the available mitigation time are provided in Figure 3.6. In all cases where incipient slip

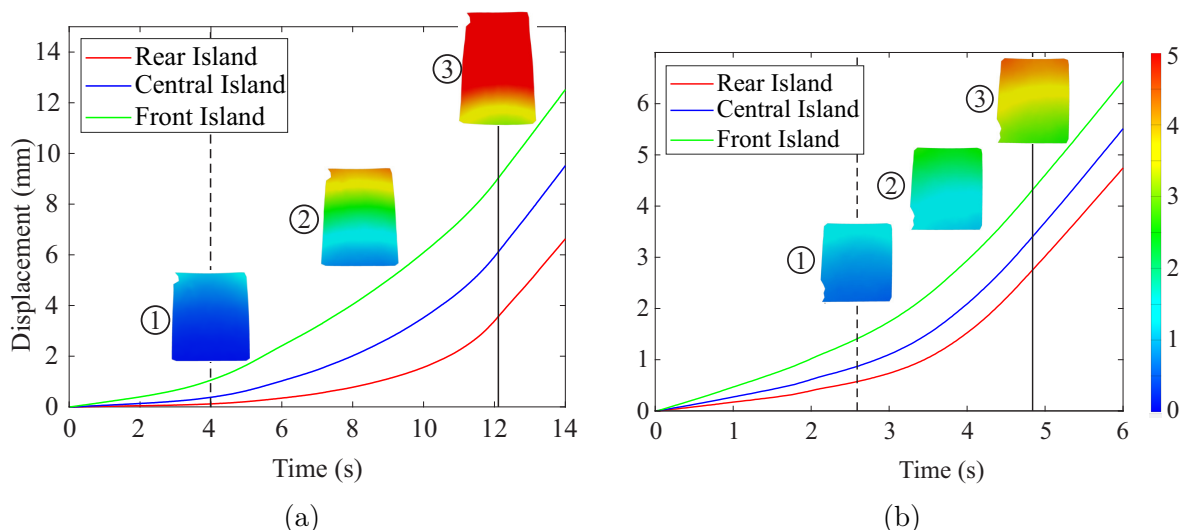


Figure 3.7: Graphs show the average tissue displacement at the front, central and rear islands measured using DIC. The dotted line indicates the point of incipient slip while the solid line indicates macro slip. Colour maps show displacement profiles, 1 is the point of incipient slip, 2 is midway between incipient and macro slip, and 3 is the point of macro slip (a) Mat A, 20 N, 2 mm/s. (b) Mat C, 20 N, 2 mm/s.

is reliably detected there is at least a 1.3 s gap between incipient slip detection and the occurrence of macro slip. Retraction speed was found to be inversely proportional to the mitigation time, with a doubling of retraction speed resulting in a 55% reduction in the available time. The variation in force appeared to have no significant effect on mitigation time (once incipient slip was detectable) for Mat A & C, however, for Mat B increases in clamp load resulted in significant increases in mitigation time. Material stiffness had the most significant effect on mitigation time, comparing Mat A and Mat C (to exclude the influence of force in Mat B), a 2.5 times increase in the material stiffness from Mat A to Mat C results in a 73% reduction in the available mitigation time for the 20 N load case and a 71% reduction in the 30 N case.

The tissue displacement characteristics measured using the DIC system are presented in Figure 3.7. These show how the average tissue displacement under the islands varies over time for both Mat A and Mat C. Data is shown from the start of retraction until macro slip has occurred. In addition, the spatial displacement distribution across the grasper face at key time points is shown as a series of colour maps.

During the early stages of retraction there is a gradual increase in tissue displacement at

the front of the grasper, whilst towards the rear the tissue motion is significantly lower. As the retraction progresses, slip propagates along the length of the grasper, leading to increases in the magnitude and rate of tissue displacement under successive grasper islands. This continues until the point of macro slip, when the full contact area of the grasper begins to slip, after which all three islands move at the speed of retraction. For the low stiffness material (Mat A) this process of slip propagation is gradual, with the front tissue showing significant displacement (and so slip) before movement is observed at the rear of the grasper. The stiffer tissue (Mat C) displays more rapid slip propagation, with tissue displacement evident at the rear of the grasper by the time that incipient slip is detected at the front island. Comparing these responses at the point of incipient slip, the tissue at the rear of the grasper has moved 0.12 mm and 0.60 mm for Mat A and C respectively, whilst the front had displaced 1.05 mm (Mat A) and 1.46 mm (Mat C), clearly highlighting how a slip differential develops along the length of the grasper face during retraction.

3.4 Case Study: Automation

To investigate the efficacy of using the presented incipient slip detection technique for automating grasping a case study was conducted. A simple algorithm was created that applies an initial clamping load of 10 N, and then scans for incipient slip event using the algorithm detailed in Section 3.2. When incipient slip is detected the clamp force is increased by 5 N, the system then pauses for 1 s to allow the clamp force to be applied, and then starts the scan operation again, it carries on stepping the force up to a maximum of 30 N. The maximum and minimum force used were based on those from the previous set of tests, while the 5 N step was selected to ensure that propagation of the slip front is prevented by the step increase, whilst still providing a range of graduations between the maximum and minimum force.

The analysis was carried out with a retraction speed of 1 mm/s using Mat A as the tissue simulant. These parameters were selected as they provide a large time window

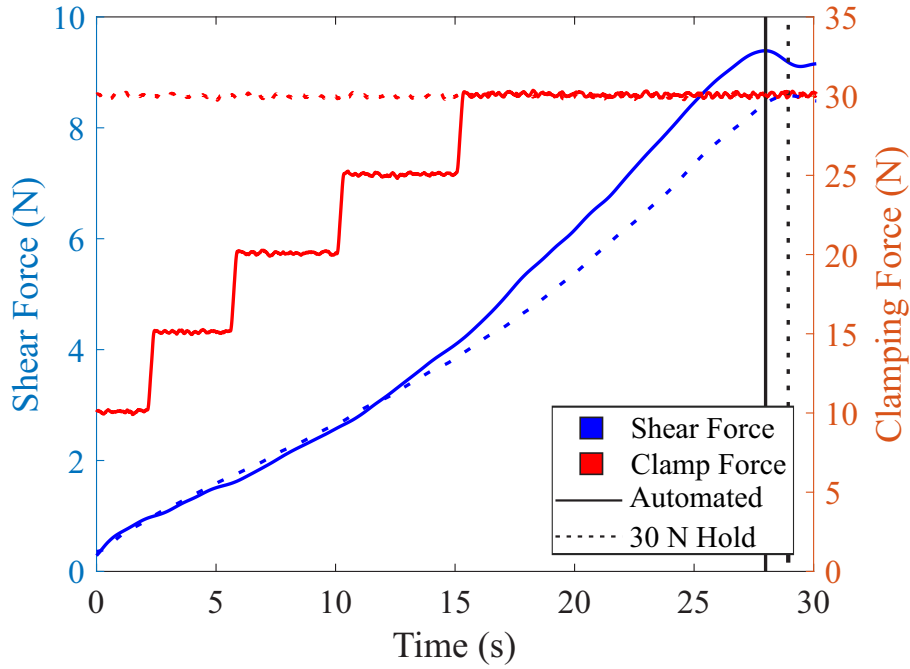


Figure 3.8: Variation in shear and clamp loads for automated and fixed load control methods. The black vertical lines indicate the times of macro slip for each case. Mat A with a 1 mm/s retraction speed.

for mitigating action to be taken, and allow for a consistent and repeatable detection of incipient slip, events even at low forces, providing optimal conditions for successful slip detection and mitigation. To assess the capability of the automated slip mitigation system it was compared to a case in which a fixed 30 N clamping load was applied throughout the retraction, to evaluate its performance against the maximum clamp load scenario.

The variation in shear force over time in the automated and 30 N load cases show a strong correlation with each other, despite the large differences in the clamping load being applied throughout the retraction (Fig. 3.8). Both control methods also produced a similar time to macro slip, with a time of 27.90 ± 0.1 s for the automated case and 29.26 ± 0.24 s for the constant 30 N load case. They also required similar shear loads to induce macro slip, with peak loads of 9.64 ± 0.15 N and 8.84 ± 0.21 N, for the automated and constant 30 N load cases respectively.

To provide an indicator of the potential for tissue damage to occur, as a result of grasping, the applied impulse was calculated, as both the magnitude of the force and the time over which it is applied have an influence on the level of tissue trauma observed [31]. The impulse was calculated by integrating the clamp force over time up to the point of macro

slip. The 30 N load case exhibited an average impulse of 879.18 ± 7.46 N.s, while the automated control method exhibited approximately 23% less impulse at 677.8 ± 3.5 N.s.

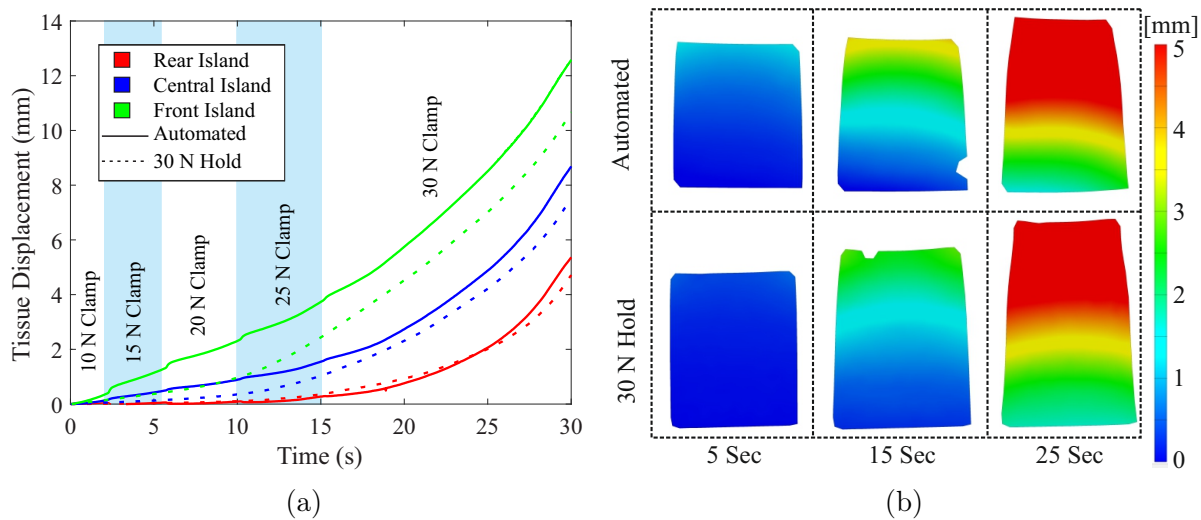


Figure 3.9: Comparison of tissue displacement for automated and fixed load control methods. Test carried out on Mat A with a 1 mm/s retraction speed. (a) Average displacement of tissue under the front, central and rear islands (b) Colour map showing tissue displacements.

The results for the tissue displacement observed using DIC (Fig. 3.9(a)) indicate that there is more tissue displacement at the front of the grasper in the automated case, as the tissue slips against the sensor, with up to 1.5 mm more displacement than in the fixed 30 N load case. However, the displacements of the central and rear islands maintain a much higher correlation between the two control methods throughout the full retraction. Some of the additional displacement observed at the front is the result of tissue compression during the step changes in clamp load, rather than the tissue slip, this is indicated by the step change in displacement at the points that the step change in clamp load occurs (Fig. 3.9(a)). The colour maps in Figure 3.9(b) show a similar pattern, with the tissue slip and subsequent displacement propagating slightly faster in the automated test case.

3.5 Discussion

This work demonstrates that by utilising the deformable nature of the grasped material, it is possible to reliably encourage detectable levels of preferential incipient slip in deformable materials, that are similar to biological tissue. The grasper and sensor system

developed were able to sense the onset and progression of incipient slip under a range of representative surgical conditions, with a sufficient time window for mitigating actions to be implemented before macro slip occurs.

The sensor technology and associated slip detection algorithm showed high reliability when grasping lower stiffness materials (Mat A & B), accurately identifying when incipient slip occurs at the front island, across the full range of clamp forces (Fig. 3.5). For the high stiffness material (Mat C) the system was able to detect incipient slip consistently in the higher clamp load cases, however for the 10 N case the algorithm produced a false positive, indicating incipient slip had occurred after approximately 1 s, even though displacement of the front sensor had not started to plateau. In this case the front and rear sensors take up tension and then slip almost simultaneously, rather than the gradual propagation from the front to rear of the grasper observed in the other cases. This is because the tissue behaviour tends towards rigid body motion as the stiffness increases, so slip propagates more rapidly from the front to rear, acting on each sensor island almost simultaneously. Similar behaviour can also be observed for the high stiffness 20 N & 30 N load cases, where there is significantly less delay between the front and rear islands taking up tension compared to the lower stiffness materials, however the slip propagation is still slow enough for incipient slip to be reliably detected (Fig 3.5).

Despite low forces making the detection of incipient slip challenging, once it becomes possible to detect incipient slip, further increases in clamp load didn't significantly affect the available mitigation time, for either Mat A or C (Fig. 3.6). This is because the increase in clamping force delayed the occurrence of both incipient and macro slip by a similar amount, maintaining a similar mitigation time (Fig. 3.5). However Mat B appears to react differently to changes in clamp load, with increases in force providing progressive increases in the available mitigation time (Fig. 3.6). The point at which incipient slip is first detected increases by a similar magnitude to Mat A for each step increase in clamp force, but the point of macro slip is much more delayed (Fig. 3.5). Further investigation is required to understand the cause of this behaviour.

Variations in the material stiffness also significantly affected the available mitigation time. This was particularly evident for the high stiffness material, Mat C, its increased stiffness caused a significant decrease in the available time (Fig 3.6). As stated earlier this is due to the transition towards more rigid behaviour, with the slip propagating through the material much quicker, significantly reducing the time at which macro slip occurs, and resulting in minimal delay between slip at the front and rear islands (Fig. 3.5).

The variation of retraction speed had minimal effect on the ability of the system to detect incipient slip (Fig. 3.5), but a significant effect on the available mitigation time (Fig. 3.6). This is because variations in the retraction speed don't affect the shape or amplitude of the sensor displacement curves, but instead scales them along the time axis, as shown when plotting them against the linear stage displacement (Fig. 3.5). The points of incipient and macro slip occur at approximately the same linear displacement for all 3 retraction speeds, whilst the mitigation time scales inversely with retraction speed, with a doubling in retraction speed resulting in approximately half the available mitigation time.

The displacement characteristics of the islands as measured by the sensors (see Fig. 3.5) correlate with those measured by the DIC system up to the point incipient slip is detected. The absolute magnitude of displacement differs between the measures because the DIC reports the average displacement of the tissue under the whole island, whereas the sensor movement is dependent on the tissue movement at the rear of the island (the last contact point to slip). However, the overall characteristics show agreement and support the premise on which this technique is based, that tissue propagation occurs progressively from the front to the rear of the grasper during retraction.

The case study into the automation of the grasping action further demonstrates the efficacy of the methodology and system developed for the early detection of tissue slip, and demonstrates that it could be an effective means of automating the grasp control, and reducing the applied gripping force, helping to reduce tissue trauma. The automated control system was able to detect the occurrence of tissue slip at the front island, and

increased the clamp load to prevent it, limiting the rate of slip propagation to a similar level observed for the max load case (Fig. 3.9). This resulted in comparable grasping performance, with similar times till macro slip, and similar peak shear forces required to induce it, whilst reducing the impulse and applied clamp forces during the earlier stages of retraction (Fig 3.8), limiting the probability of tissue trauma [31].

Several factors were identified within this laboratory-based work that require further investigation, prior to translation into surgical practice, since they may introduce uncertainties which affect the performance of this technique:

- **Size:** the current prototype is scaled-up and would need a 50-100% reduction in size to meet the size of typical robotic surgical graspers. The magnitude of this scale change is unlikely to impact on the incipient slip mechanics between tissue and grasper which are central to this sensor. However, it will be significantly more challenging to construct an instrumented multi-island grasper face at this scale, without recourse to alternative manufacturing techniques, an area of ongoing research.
- **Tissue properties:** the incipient slip sensing method presented here does not require knowledge of the mechanical properties of a grasped tissue to detect slip. However, mechanical factors that affect the rate of slip propagation across the grasper face will determine the sensitivity of the system and its ability to act as a slip 'early-warning' system. In addition, biological tissues exhibit significant heterogeneity in comparison to the simulants presented here. Accordingly, it will be important to evaluate a range of biological tissues to determine appropriate operating regimes in both mechanical terms (e.g. stiffness, lubrication regime, viscoelasticity) and the clinical focus (e.g. tissue types).
- **Surgical use:** in this study, surgical grasping was simplified as controlled uniaxial retraction between parallel grasper faces. In reality, surgical manipulation is more complex, involving additional lateral motion and rotation of the grasper, together with pivoted 'scissor action' jaws. Determining the impact of these factors on slip-sensing performance will require additional study focused on grasper kinematics.

- Automation: in this study, the algorithm used to automate grasping operates in isolation. Translation towards surgical use will require integration of these aspects into the control scheme of the surgical robot. This has the opportunity to enhance the slip detection and prevention algorithm, by providing it with additional contextual information from the robot system (e.g. grasper position, speed, and visual cues). Ultimately, while the progression of autonomy in surgical robotics must be pursued with caution, enhanced grasping control has the potential to operate transparently to the surgeon, in a similar fashion to anti-lock braking systems that are now a common and invaluable feature of the modern car.

3.6 Conclusions and Further Work

In summary, the slip detection methodology, and associated sensing system, detailed in this paper are capable of providing significant improvements in the early detection of incipient slip when grasping deformable materials, well before macro slip occurs. This allows for mitigating actions to be taken automatically to prevent slip events, and maintain stable control of the tissue, whilst reducing the applied grasping forces. However, this method of slip detection is limited to applications involving softer more deformable materials, as higher stiffness materials produce less clear slip differentials between the front and rear of the grasper, especially in low force cases due to the high rate of slip propagation.

Further work is now required to fully understand the range of biological tissues for which this method would be suitable. In addition work is required on developing the sensing technology utilised to miniaturise it so that it can be suitably integrated within a standard surgical grasper. However, this body of work provides strong evidence that the developed sensing methodology is capable of providing significant improvements towards the automation of slip detection and force control in surgical robotics, minimising the occurrence of tissue trauma and adverse tissue slip events.

References

- [1] Daniel M Herron and Michael Marohn. Prepared by the SAGES-MIRA Robotic Surgery Consensus Group. page 24, 2006.
- [2] O. A. J. van der Meijden and M. P. Schijven. The value of haptic feedback in conventional and robot-assisted minimal invasive surgery and virtual reality training: a current review. *Surgical Endoscopy*, 23(6):1180–1190, June 2009.
- [3] Gregory Tholey, Jaydev P Desai, and Andres E Castellanos. Force Feedback Plays a Significant Role in Minimally Invasive Surgery. *Annals of Surgery*, 241(1):8, 2005.
- [4] B. Tang, G.B. Hanna, and A. Cuschieri. Analysis of errors enacted by surgical trainees during skills training courses. *Surgery*, 138(1):14–20, July 2005.
- [5] E.A.M. Heijnsdijk, J. Dankelman, and D.J. Gouma. Effectiveness of grasping and duration of clamping using laparoscopic graspers. *Surgical Endoscopy*, 16(9):1329–1331, September 2002.
- [6] C.-H. King, M.O. Culjat, M.L. Franco, C.E. Lewis, E.P. Dutson, W.S. Grundfest, and J.W. Bisley. Tactile Feedback Induces Reduced Grasping Force in Robot-Assisted Surgery. *IEEE Transactions on Haptics*, 2(2):103–110, April 2009.
- [7] C.-H. King, M.O. Culjat, M.L. Franco, J.W. Bisley, G.P. Carman, E.P. Dutson, and W.S. Grundfest. A Multielement Tactile Feedback System for Robot-Assisted Minimally Invasive Surgery. *IEEE Transactions on Haptics*, 2(1):52–56, January 2009.
- [8] Verena Nitsch and Berthold Farber. A Meta-Analysis of the Effects of Haptic Interfaces on Task Performance with Teleoperation Systems. *IEEE Transactions on Haptics*, 6(4):387–398, October 2013.
- [9] Natalie T. Burkhard, J. Ryan Steger, and Mark R. Cutkosky. The Role of Tissue Slip Feedback in Robot-Assisted Surgery. *Journal of Medical Devices*, 13(2):021003, June 2019.

-
- [10] Guang-Zhong Yang, James Cambias, Kevin Cleary, Eric Daimler, James Drake, Pierre E. Dupont, Nobuhiko Hata, Peter Kazanzides, Sylvain Martel, Rajni V. Patel, Veronica J. Santos, and Russell H. Taylor. Medical robotics—Regulatory, ethical, and legal considerations for increasing levels of autonomy. *Science Robotics*, 2(4):eaam8638, March 2017.
- [11] Seyed Mohsen Khadem, Saeed Behzadipour, Alireza Mirbagheri, and Farzam Farahmand. A modular force-controlled robotic instrument for minimally invasive surgery - efficacy for being used in autonomous grasping against a variable pull force: Modular force-controlled robotic instrument. *The International Journal of Medical Robotics and Computer Assisted Surgery*, 12(4):620–633, December 2016.
- [12] Natalie T. Burkhard, Mark R. Cutkosky, and J. Ryan Steger. Slip Sensing for Intelligent, Improved Grasping and Retraction in Robot-Assisted Surgery. *IEEE Robotics and Automation Letters*, 3(4):4148–4155, October 2018.
- [13] D Jones, A Alazmani, and P Culmer. A Soft Inductive Tactile Sensor for Slip Detection Within a Surgical Grasper Jaw. page 4, 2019.
- [14] K. L. Johnson. *Contact mechanics*. Cambridge University Press, Cambridge Cambridgeshire New York, 1987.
- [15] B. Delhaye, P. Lefevre, and J.-L. Thonnard. Dynamics of fingertip contact during the onset of tangential slip. *Journal of The Royal Society Interface*, 11(100):20140698–20140698, September 2014.
- [16] Wei Chen, Heba Khamis, Ingvars Birznieks, Nathan F. Lepora, and Stephen J. Redmond. Tactile Sensors for Friction Estimation and Incipient Slip Detection – Towards Dexterous Robotic Manipulation: A Review. *IEEE Sensors Journal*, pages 1–1, 2018.
- [17] Jeffrey Stoll and Pierre Dupont. Force Control for Grasping Soft Tissue. page 4, May 2006.
- [18] M.R. Tremblay and M.R. Cutkosky. Estimating friction using incipient slip sensing

- during a manipulation task. In [1993] *Proceedings IEEE International Conference on Robotics and Automation*, pages 429–434, Atlanta, GA, USA, 1993. IEEE Comput. Soc. Press.
- [19] Filipe Veiga, Jan Peters, and Tucker Hermans. Grip Stabilization of Novel Objects using Slip Prediction. *IEEE Transactions on Haptics*, pages 1–1, 2018.
- [20] Ian Waters, Dominic Jones, Ali Alazmani, and Peter Robert Culmer. Utilising Incipient Slip for Grasping Automation in Robot Assisted Surgery. *IEEE Robotics and Automation Letters*, 7(2):1071–1078, April 2022.
- [21] Ian Waters, Ali Alazmani, and Peter Culmer. Engineering incipient slip into surgical graspers to enhance grasp performance. *IEEE Transactions on Medical Robotics and Bionics*, pages 1–1, 2020.
- [22] Joseph C. Norton, Jordan H. Boyle, Ali Alazmani, Pete R. Culmer, and Anne Neville. Macro-Scale Tread Patterns for Traction in the Intestine. *IEEE Transactions on Biomedical Engineering*, 67(11):3262–3273, November 2020.
- [23] Hongbo Wang, Dominic Jones, Gregory de Boer, Junwai Kow, Lucia Beccai, Ali Alazmani, and Peter Culmer. Design and Characterization of Tri-Axis Soft Inductive Tactile Sensors. *IEEE Sensors Journal*, 18(19):7793–7801, October 2018.
- [24] Lefan Wang, Dominic Jones, Graham J Chapman, Heidi J Siddle, David A Russell, Ali Alazmani, and Peter Culmer. An Inductive Force Sensor for In-Shoe Plantar Normal and Shear Load Measurement. *IEEE Sensors Journal*, pages 1–1, 2020.
- [25] Andrew W. Brown, Stuart I. Brown, Donald Mclean, Zhigang Wang, and Alfred Cuschieri. Impact of fenestrations and surface profiling on the holding of tissue by parallel occlusion laparoscopic graspers. *Surgical Endoscopy*, 28(4):1277–1283, April 2014.
- [26] Phillip Mucksavage, David C. Kerbl, Donald L. Pick, Jason Y. Lee, Elspeth M. McDougall, and Michael K. Louie. Differences in Grip Forces Among Various Robotic

-
- Instruments and da Vinci Surgical Platforms. *Journal of Endourology*, 25(3):523–528, March 2011.
- [27] Ali Alazmani, Rupesh Roshan, David G Jayne, Anne Neville, and Peter Culmer. Friction characteristics of trocars in laparoscopic surgery. *Proceedings of the Institution of Mechanical Engineers, Part H: Journal of Engineering in Medicine*, 229(4):271–279, April 2015.
- [28] Andrew R Kemper, Anthony C Santago, Joel D Stitzel, Jessica L Sparks, and Stefan M Duma. Biomechanical Response of Human Liver in Tensile Loading. page 12, January 2010.
- [29] Jun Wai Kow, Peter Culmer, and Ali Alazmani. Thin soft layered actuator based on a novel fabrication technique. In *2018 IEEE International Conference on Soft Robotics (RoboSoft)*, pages 176–181, Livorno, April 2018. IEEE.
- [30] W. Schwarz. The surface film on the mesothelium of the serous membranes of the rat. *Zeitschrift fr Zellforschung und mikroskopische Anatomie*, 147(4):595–597, 1974.
- [31] A. I. Margovsky, R. S. A. Lord, and A. J. Chambers. The effect of arterial clamp duration on endothelial injury: An experimental study. *ANZ Journal of Surgery*, 67(7):448–451, July 1997.

3.7 Appendix

Sensor calibration method

This appendix expands on the information provided in Section 3.2.3, to provide more detail on the calibration of the SITS sensors utilised in the sensed grasper for detecting incipient slip. The sensors were calibrated using a multi axis calibration rig (Fig. 3.10) that consisted of three linear translation stages (MTS50-Z8, Thorlabs Inc.), each controlled by a DC servo motor controller (KDC101, Thorlabs Inc.), providing a travel range of 50mm along each motor axis, with a minimum repeatable increment of $0.8 \mu\text{m}$, and maximum speed of 2.4 mm/s .

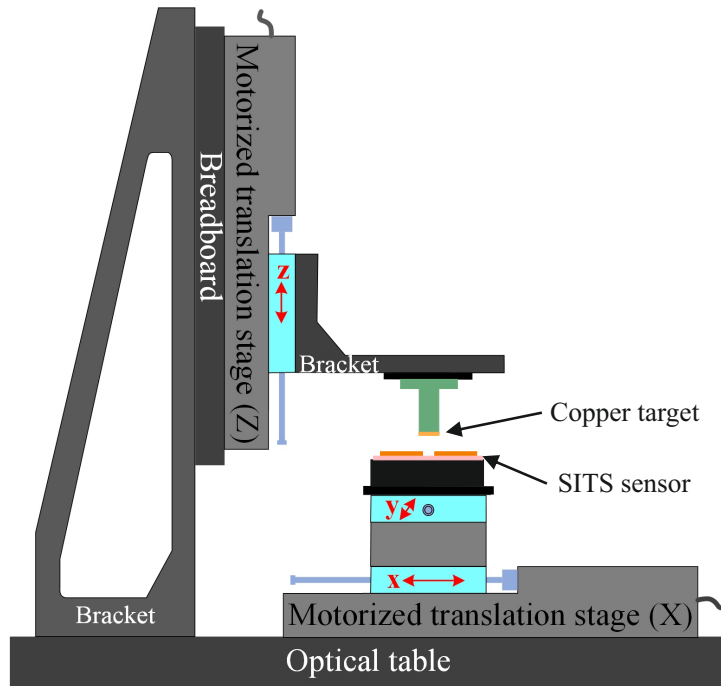


Figure 3.10: Configuration of the multi-axis sensor calibration system. Adapted from [24]

The copper target of the SITS sensor was then attached to the end effector, as shown in Figure 3.10, positioned centrally over the four coils of the sensor. Calibration data was then gathered by carrying out a 3D sweep of the target above the sensor, with z stepped in 0.2 mm increments from $z=-0.6:1.2 \text{ mm}$, and a grid scan conducted between $y=-3:3 \text{ mm}$ and $x=-1:1 \text{ mm}$ at each z level, where $\{0,0,0\}$ represents the position of the target in its unloaded 'neutral' position. A neural network was implemented to determine the

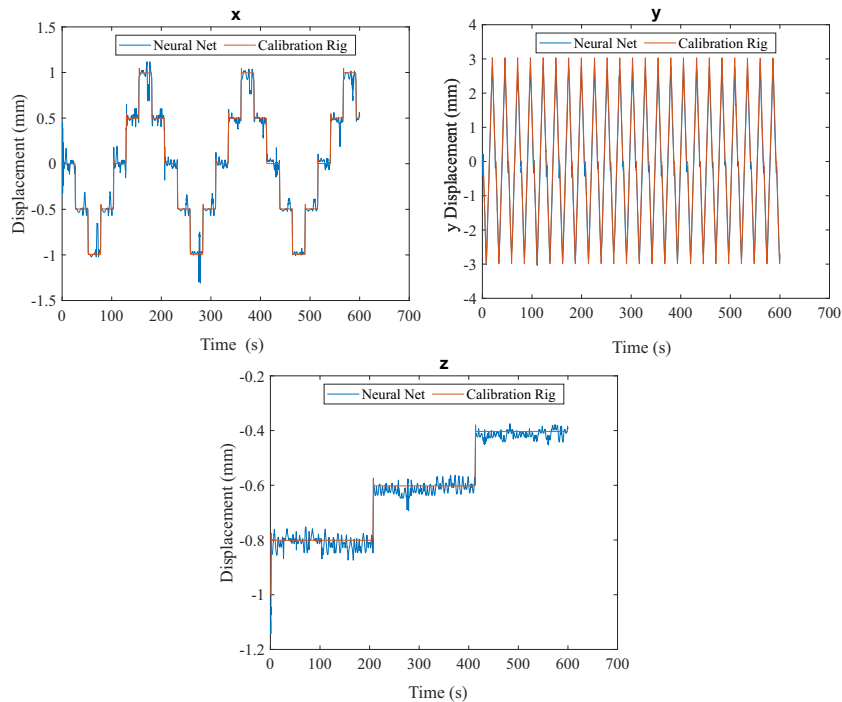


Figure 3.11: Graphs showing comparison between the output of the trained neural network and the displacement measured by the calibration rig in x,y and z for the validation data set for the SITS sensor.

sensor displacement (D) from the inductance values (I) of the four coils, by comparing them to the position data gathered from the three stages of the calibration rig.

$$D_{x,y,z} = f(I_{1,2,3,4}) \quad (3.5)$$

The Matlab neural net fitting toolbox (Matlab, Mathworks) was used to train the neural network, with the inductance values as the input and the calibration rig measurements as the target outputs. The neural net consisted of a two-layer feed forward neural network with 15 neurons in the hidden layer, with the Tanh function used as the activation function, and the Levenberg-Marquardt back propagation algorithm as the training method, these were selected based on prior research [24].

Another sweep was then conducted to gather a set of validation data to ensure that the neural network was capable of producing accurate and reliable results for data sets it had not previously been trained on, but that were within the same measurement scope as the training data. A comparison between the neural networks output and the displacement

measured by the calibration rig is presented in Figure 3.11, the neural net and calibration rig data showed a high correlation with each other, with root mean squared errors of 0.043 mm, 0.050 mm and 0.064 mm, in x, y and z respectively. The x data does show an occasional significant spike, and variation from the calibration rig value, this occurs when there is a change in the direction of the y stage, where the sensor is towards the limits of its working area. Further investigation is required though to understand if this is the result of backlash in the motor causing a shift in position, an error with the neural net, or the result of the sensor design. However, the y data, which is most critical for this application as this is the direction of shear, and therefore slip, shows a much smoother correlation between the neural network and calibration rig.

Chapter 4

Encouraging and Detecting Preferential Incipient Slip for Use in Slip Prevention in Robot-Assisted Surgery

Preface

This chapter was published as the journal paper:

Encouraging and Detecting Preferential Incipient Slip for Use in Slip Prevention in Robot-Assisted Surgery. Ian Waters, Dominic Jones, Ali Alazmani, and Peter Robert Culmer. MDPI Sensors. 2022.

Sections 4.1 through 4.6 constitute the main body of this publication, whilst the appendix details the sensor calibration process. This paper details the development, and evaluation, of a sensor based on one of the phenomena identified in chapter 2. The sensor employs the fact that through varying the normal, and thus frictional, force across the grasper it is possible to encourage incipient slip to occur towards the outer edge, which can then be detected by monitoring the displacement of separate movable sensor islands.

Abstract

Robotic surgical platforms have helped to improve minimally invasive surgery, however limitations in their force feedback and force control can result in undesirable tissue trauma or tissue slip events. In this paper we investigate a sensing method for the early detection of slip events when grasping soft tissues, which would allow surgical robots to take mitigating action to prevent tissue slip and maintain stable grasp control, whilst minimising the applied gripping force, reducing the probability of trauma. The developed sensing concept utilises a curved grasper face to create areas of high and low normal, and thus frictional, force. In the areas of low normal force there is a higher probability that the grasper face will slip against the tissue. If the grasper face is separated into a series of independent moveable islands, then by tracking their displacement it will be possible to identify when the areas of low normal force first start to slip, whilst the remainder of the tissue is still held securely. The system was evaluated through the simulated grasping and retraction of tissue under conditions representative of surgical practice, using silicone tissue simulants and porcine liver samples. It was able to successfully detect slip before gross slip occurs with a 100% and 77% success rate for the tissue simulant and porcine liver samples respectively. This research demonstrates the efficacy of this sensing method, and the associated sensor system, for detecting the occurrence of tissue slip events during surgical grasping and retraction.

4.1 Introduction

Although robotic surgical devices have helped improve surgical outcomes in Minimally Invasive Surgery [1], their limited force control still remains an issue, especially when manipulating soft biological tissues [1; 2]. The lack of haptic feedback, due to a physical separation between surgeon and patient, can result in tissue trauma due to the over application of gripping forces, or result in tissue slip due to insufficient grasping [3; 4].

One of the main solutions identified in literature to limit tissue trauma, caused by excessive grasping forces, is the inclusion of force sensors and haptic or visual feedback of

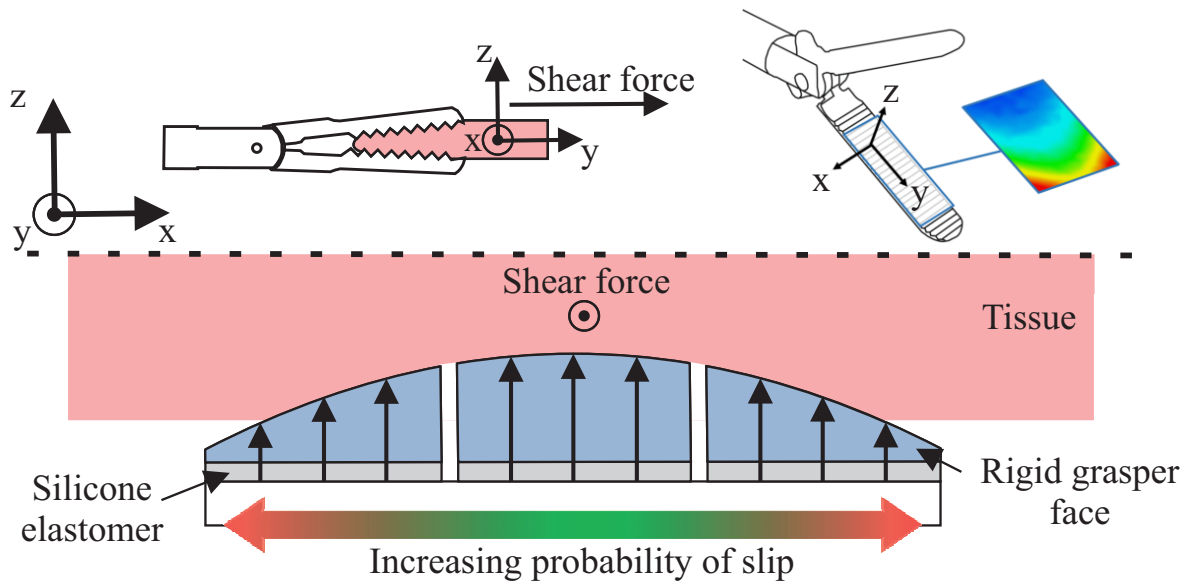


Figure 4.1: Diagram demonstrating the concept of encouraging incipient slip across grasper face through the variation of normal force using a curved surface.

the grasping force information to the surgeon. Although this method has been shown to reduce tissue trauma [5; 6; 7], it requires constant monitoring by the surgeon, increasing their cognitive load [8]. Furthermore, it only provides information on the forces that are being applied, not whether the tissue is being held securely. A more direct method for controlling grasping forces is through the identification, and early detection, of slip events. If the onset, or precursor phenomena, to slip can be identified, then the clamp force can be adjusted automatically to prevent further slip. This could allow the surgical robot's grasper to use the minimal force to maintain a stable grasp of the tissue, helping to reduce tissue trauma, whilst still allowing for reliable and controlled manipulation of the tissue.

Research into grasper systems has identified several that aim to detect or predict the occurrence of tissue slip as the basis for an automated surgical grasper. *Khadem et al.* [9] developed an automated surgical grasper which aimed to predict when slip was going to occur based on prior experimentation, adjusting the clamping force relative to the current retraction force to stay within a pre-defined safe grasping zone, limiting its application to known and quantified tissues. Other systems have been developed to detect when slip is occurring, rather than attempting to predict it. The most mature of these is

that developed by *Burkhard et al.* [10], this sensor uses a technique based on hot wire anemometry to monitor the variation in heat flux as an indicator of slip. This method has been demonstrated to successfully detect slip for a range of biological tissues [10], and has been utilised for the grasping automation of surgical instruments [8]. Another instrumented grasper employed force sensors to detect the onset of slip by monitoring the normal and shear force at the face of the grasper, and using these to calculate when the coefficient of friction first peaks to indicate that slip is occurring [11].

Both of the slip detection sensors described above utilise a single sensing node, and thus cannot identify localised slip behaviour across the grasper. As a result they are better suited to detection of larger macro slips. Macro slips occur when the global shear force exceeds the global frictional force across the contact, leading to the entirety of the contact slipping [12]. The use of more localised sensing methods would allow for the detection of *incipient slips* [13]; small localised slip phenomena which occur when shear forces in a localised region exceed the corresponding frictional forces, causing local slip while the remainder of the contact remains held securely [12]. As shear force increases the number of these incipient slip events will increase until the global shear force exceeds the global frictional force, at which point the surface enters a state of macro slip where the whole of the contact area is slipping freely.

A key aspect of being able to detect incipient slip is being able to preferentially encourage it to occur in a predictable and repeatable manner [13]. This strategy is utilised by the human finger, which employs a curved surface to create a normal force distribution, resulting in a frictional force distribution, leading to incipient slips occurring towards the outer edge of the finger pad, whilst the middle is still gripping securely [14]. This method of utilising the variation in normal, and thus frictional force distribution to encourage preferential incipient slip, has been utilised significantly by the wider robotics community [13; 15; 16], but has not yet been applied in the field of surgical grasping. An in depth review of incipient slip sensors can be found in this recent review [13].

Other than our prior work, the only reported example of a sensor designed to detect

incipient slip in surgery employs an approach that exploits the deformable nature of human tissue, and monitors the change in material stiffness to estimate the first stages of macro slip [17]. However this system only monitors the global shear forces rather than trying to identify localised slips, resulting in only a short time window for mitigating actions to be taken [17].

The aim of our research is to produce an instrumented surgical grasper capable of inducing, and then detecting, preferential incipient slips before macro slip occurs, that is applicable for a range of soft biological tissues, and would be compatible with current surgical grasper designs. This sensor has already been demonstrated for the successful automation of surgical grasping using tissue simulants [18]. In this paper we present the sensor concept and design, before analysing its ability to reliably detect incipient slip over a wide range of test conditions, representative of those used in surgery. Initial experiments were conducted using a range of tissue simulants to define the slip detection algorithm that was utilised in [18], and to evaluate it on a repeatable substrate. The complete system was then applied to the grasping of porcine liver tissue to demonstrate its efficacy for real world application in surgical grasping for the early detection of slip when manipulating soft biological tissues.

This work builds on our prior work in the area [19; 18; 20], here our contribution is to rigorously evaluate the ability of the system to detect slip under a wider range of clearly defined test conditions for force, retraction speed and material stiffness. In this paper we also extend testing to evaluate the system using porcine liver samples, providing a more representative test of the system for use in the grasping of soft biological tissues.

4.2 System Development

4.2.1 Concept and Requirements

The foundation of this sensing approach is to induce localised incipient slip in a predictable and repeatable manner so that it can then be detected. To achieve this we have

utilised biomimicry of the human finger [14], similar to other robotic graspers [13; 15; 16]. A convex curved grasper face is used to create areas of high normal, and thus frictional, force in the middle of the grasper, with these forces gradually decreasing toward the edges of the curved face, promoting tissue to slip first at the outer sections of the grasper [19; 18] (Fig. 4.1). By separating the grasper into a series of independently moveable 'islands', then tracking the displacement of these islands during tissue retraction, it is possible to detect when the edge sections start to slip relative to the middle of the grasper. In the initial phase of a typical tissue retraction process, the shear forces will initially be low, therefore friction forces are dominant across the grasper face and all of the islands will grip the tissue securely. As retraction progresses, the shear force increases, and in the areas of low normal and frictional force (towards the outer edge of the grasper) the local shear force will exceed the local frictional force resulting in localised (incipient) slip, whilst the middle will continue to maintain a stable grip of the tissue and move with it (Fig. 4.1). This results in a differential in the relative displacement between the islands at the edge and middle of the grasper, which can then be used as an indicator to the presence of incipient slip of the outer islands.

4.2.2 System Design and Fabrication

A scaled model of a surgical grasper was created to evaluate the sensor concept. A curved grasper face ($r=100.25$ mm) was separated into a 5×3 grid of moveable islands across the width and length of the grasper (Fig. 4.2). The separation along the length, axial to the curvature of the face, was to try and isolate the slip effects across the width, due to the normal force variation, from those along the length of the grasper, caused by the deformable properties of the tissue [19; 20].

Each island consists of a 3D printed rigid upper gripping surface (Rigid 4000 Resin, Formlabs) to securely hold the tissue, with a 1 mm thick layer of silicone elastomer (Ecoflex 00-30, Smooth-on) placed below to allow each island to move freely, allowing for displacement differentials to occur between them (Fig. 4.2). The upper gripping surface was patterned with hexagonal features (0.75 mm width, height and separation),

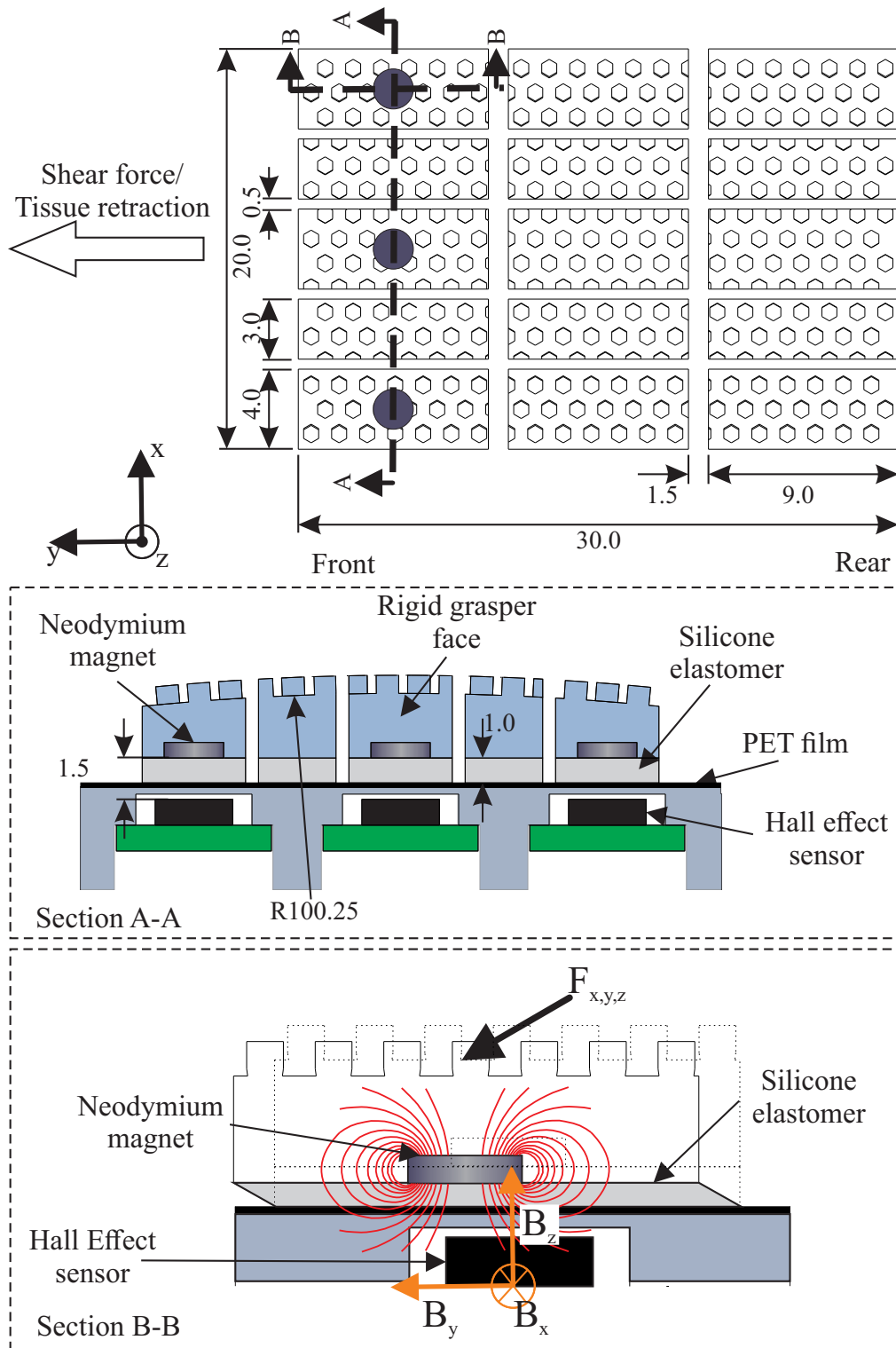


Figure 4.2: Detailed drawing of grasper design showing independently movable islands, the grey circles indicate the positions of the magnetic sensing nodes (All dimensions are in mm). Section A-A: Cross section displaying the design of the sensed and passive islands. Section B-B: Cross section showing how the magnetic field moves through the Hall effect sensor as force is applied to the island.

to provide an isometric frictional performance that is suitable for the gripping of soft lubricated biological tissues [19; 21].

To monitor the displacement differential between the outer and middle islands, neodymium disc magnets (2 mm diameter \times 0.5 mm thick) were embedded in the base of the rigid upper gripping surface of the front left, middle, and right islands (Fig. 4.2). A tri-axis Hall effect sensor (MLX90393, Melexis) was then placed below each of these islands to track their displacement, through monitoring the movement of the magnetic field ($B_{x,y,z}$) that occurs as the magnet moves above the sensor chip when a force ($F_{x,y,z}$) is applied to the upper gripping surface, and the elastomer layer below deforms (Fig. 4.2). The magnetic fields ($B_{x,y,z}$) can then be converted into a corresponding displacement based on previously calculated sensor calibrations. These sensors were selected based on prior work, that indicated they provide sufficient sensitivity for the detection of the slip differentials that occur between the outer edge and middle of the grasper, with a sufficiently compact footprint to fit three nodes across the width of the grasper face [19; 22], thermal effects were considered negligible due to the minimal temperature variation within the human body. These sensors were configured to sample the magnetic field at a frequency of 408 Hz.

4.2.3 Signal Processing

To determine the relationship between the magnetic field and island displacement for each sensor node, a custom three-axis sensor calibration system was constructed. This was used to sweep a magnet in a 3D volume (covering x,y and z axes) above the Hall effect sensor, with the magnet connected directly to the linear stage assembly to ensure there is no slip, thus ensuring that the stage displacement corresponds to the resultant magnetic flux. Full details of the instrumentation and process are detailed in [22]). The sweep in the x-y plane was conducted from -2 to 2 mm at 0.2 mm/s for each step in z (-0.65:1.25 mm in 0.1 mm increments), where $\{0,0,0\}$ is the position of the neodymium magnet centre when the island is unloaded and centred over the hall effect sensor. A neural network (Matlab, Mathworks) was then trained to fit the magnetic field reading of

the sensor to the displacements measured by the calibration system. This neural network utilised a two-layer feed forward network [22], with 40 neurons in the hidden layer, and was trained using a Bayesian regularization backpropagation algorithm, due to non-linear relationship between displacement and magnetic field [22]. This neural network provided a strong correlation with the validation data, with root mean squared errors of 0.029 mm, 0.025 mm and 0.018 mm, in x, y and z respectively. The output of the neural network was post-processed using a third-order Butterworth filter with a cut off frequency of 10 Hz to attenuate high frequency noise.

4.2.4 Slip Detection

In the context of this sensing system, incipient slip is defined as the occurrence of slip between the grasped tissue and at least one of the grasper islands, whilst the other islands retain a stable grasp of the tissue. When using a convex curved grasper, as shown in (see

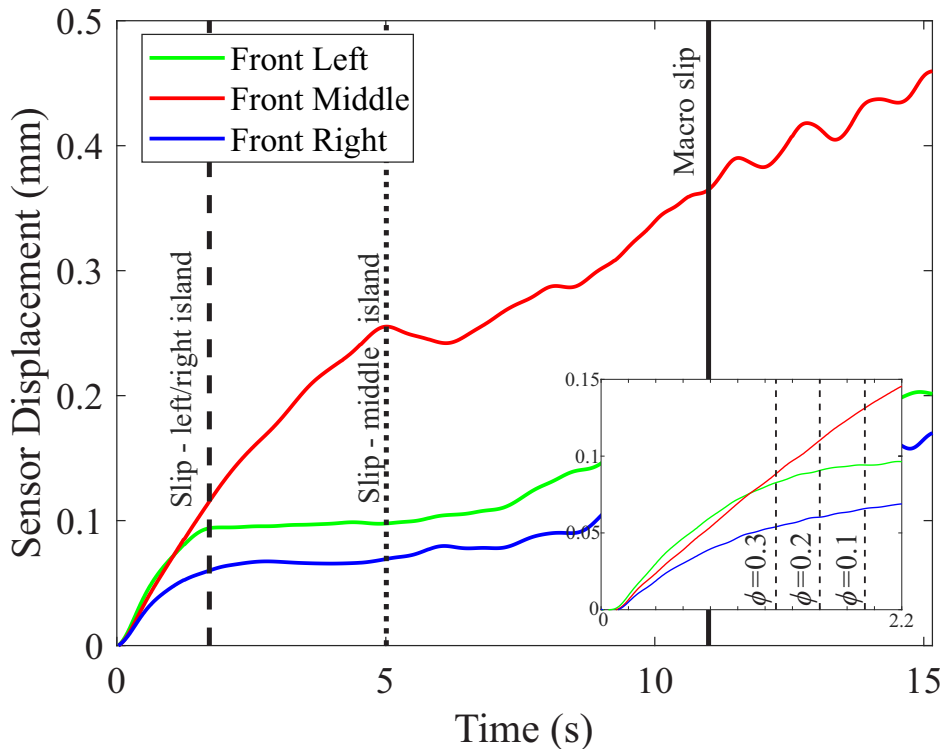


Figure 4.3: Example of typical displacement characteristics for the front left, middle, and right islands of the grasper, under a 20N clamp load with a retraction speed of 2 mm/s (using Mat A). The inset shows how the variation of the slip ratio changes the time at which incipient slip of the edge islands is detected.

Fig. 4.1) is used the incipient slip is expected to occur first at the outer islands of the grasper. Accordingly, tracking island displacement and considering the differential between outer and inner islands provides a means to identify when incipient slip starts to occur at the grasper face. An algorithm was developed based on the results gathered using three different tissue simulants, over the wide range of applied clamping loads and retraction speeds (Fig. 4.5), to automatically identify the onset of incipient slip.

A typical response from this sensor system retracting a tissue simulant is presented in Figure 4.3. This shows the variation of the displacement of the front left, middle, and right islands throughout the full retraction. A similar response was observed across the full range of test conditions investigated for the tissue simulants. During the initial stages of the retraction, when the shear forces are low, the outer and middle islands move together with the retracting tissue at the same velocity. However, as the shear force increases with further retraction, the outer islands start to slip against the tissue due to the lower normal and frictional forces at these points. This results in a decreasing velocity of these islands as they slip more and more against the tissue, indicated by the plateauing of the island's displacement, whilst the middle island continues to grip the tissue securely and move with it. Therefore by comparing the velocity of the left (V_l) and right (V_r) outer islands to that of the middle island (V_m), it is possible to define the magnitude of the relative slip differential between them. The ratio between the velocity of the middle and outer islands is termed the slip ratio (ϕ), this algorithm has been used previously by us for the automation of the force control during the grasping and retraction of tissue simulants [18].

$$\phi = \mathbf{min} \left[\frac{V_l}{V_m}, \frac{V_r}{V_m} \right] \quad (4.1)$$

If the velocity of the middle islands is positive, then a slip ratio (ϕ) = 1 indicates that the outer and middle islands are moving at the same velocity, therefore there is no slip occurring at the outer islands relative to the middle. However as the slip ratio (ϕ) decreases the relative velocity of the outer islands is decreasing, due to an increasing

amount of slip occurring between these islands and the tissue simulant. When the slip ratio reaches 0 the outer islands are no longer moving with the tissue simulant as it retracts, indicating the tissue is freely slipping against the outer island(s). Over the full range of parameters investigated (3 tissue simulants, 3 clamp loads, 3 retraction speeds) (Fig. 4.5), a ϕ value of 0.2 or less was found to be a reliable and robust indicator that the outer islands were encountering a significant amount of slip relative to the middle, without producing a false early indicator of slip, or resulting in slip being detected too late for any mitigating actions to be taken. This algorithm is activate only once the middle island has moved 0.02 mm in the direction of shear, to avoid false detection due to signal noise (i.e. the retraction process must have started).

4.3 Materials and Methods

4.3.1 Experimental Set Up

A test rig was developed which simulates the grasping and retraction of tissue that occur during robotic surgery, as shown in Figure 4.4, to evaluate the efficacy of the sensor in detecting incipient slip events. The instrumented grasper face was attached to a pneumatic piston (MGPM20TF-75Z, SMC) to grasp the tissue. The grasping force was controlled via a pneumatic regulator (ITV1030, SMC) which had been pre-calibrated against a ref-

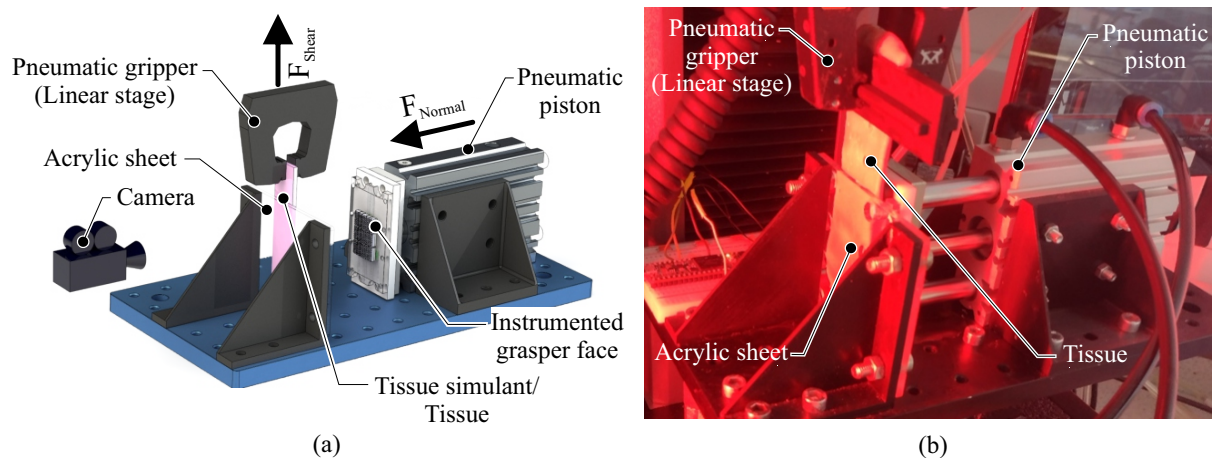


Figure 4.4: (a) A schematic showing key components of the experimental system. (b) An image of the experimental system used for simulating surgical grasping and retraction.

erence load cell. A linear load tester (Instron 5940, Instron) with a pneumatic jaw was employed to simulate the retraction motion of the grasper. The global shear force and retraction speed were monitored via the linear load tester, whilst the array of Hall effect sensors in the grasper were read via a microcontroller (Teensy 3.6, PJRC). A real-time embedded controller (MyRIO, National Instruments) was then used to synchronise and interface these systems to control the clamping and retraction motions, and record the data at a frequency of 100 Hz. In addition, a camera (AVE2, Instron) was positioned behind the clear acrylic counter face to record tissue movement at a frequency of 50 Hz.

4.3.2 Experiment I: Silicone Tissue Simulants

An initial assessment of the sensor system and slip detection method was conducted to understand the sensor’s response to slip events and the underlying slip mechanics. This was conducted using silicone tissue simulant to emulate the properties of soft tissues and enable controlled and repeatable testing.

Three tissue simulants with different material tensile stiffness were used: Mat A ($E = 241$ kPa), Mat B ($E = 320$ kPa) and Mat C ($E = 610$ kPa). Each tissue simulant comprises three layers of silicone elastomer (Ecoflex 00-30, Smooth-on) encapsulating internal layers of strain-limiting deformable spandex fabric, located 0.3 mm below the upper and lower tissue surfaces. The fabric layers were altered to vary tensile stiffness (as detailed above) whilst maintaining consistent frictional and compressive characteristics (1051 ± 60 kPa). After fabrication, the simulants were laser cut into $100 \times 20 \times 3$ mm test samples. A speckle pattern was applied on one face using enamel spray paint, to allow the displacement to be tracked using Digital Image Correlation (DIC) (GoM Correlate, GoM). A layer of surfactant lubricant was applied immediately prior to the test to mimic the serous fluid coating commonly exhibited on soft tissues [23]. The material stiffness of each sample was measured using the ASTM D412 Type C tensile method, their response found to be similar to that of liver tissue [24].

Testing consisted of a simulated grasp process exploring factors of grasp load and retrac-

tion speed. In each test, a fixed grasping load was applied to the tissue simulant and it was then retracted at a constant speed for 30 mm. Grasping loads of 10 N, 20 N and 30 N were evaluated, these were identified as representative of the grasping pressures observed during surgical practice [25; 26]. Retraction speeds of 1, 2 and 5 mm/s were selected based on those typically used for tissue manipulation [27]. 5 repeats were conducted for each test case.

4.3.3 Experiment II: Porcine Liver

To evaluate the performance and characteristics of the sensor system in a more surgically realistic configuration, a series of tests were conducted using ex vivo porcine liver samples.

To evaluate the performance and characteristics of the sensor system in a more surgically realistic configuration, a series of tests were conducted using ex vivo porcine liver samples.

In these tests the same sensor and grasper design, as well as the slip detection algorithm developed for the tissue simulants, was used to allow direct comparison with the tissue simulants. The tests explored variation of clamp force, using the same configuration of 10, 20 and 30 N with a fixed retraction speed of 2 mm/s for all tests, as this is the average speed used during manipulation tasks [27], and experiments with the tissue simulants indicated speed had a very predictable and quantifiable influence on tissue slip, and the rate of slip propagation. For each load condition two separate porcine livers were analysed, with 5 test samples taken from each liver for a total of 10 tests at each load condition. To prepare the samples the livers were sliced into thin strips with a nominal thickness varying from 4-12 mm. The variability is the result of the soft and deformable nature of the liver tissue making sample preparation challenging (in contrast to the high tolerances achieved with fabricating simulants), however this provides a representative reflection of the conditions expected in a surgical environment. A nominal 100 x 20 mm rectangle was cut from each slice using a stencil and a scalpel, and was then immersed in a saline solution to prevent drying providing a more representative sample [10]. For characterisation of the material properties of each liver, three ASTM D412 Type C tensile

specimens and one 100 mm x 20 mm compression specimen were cut from each liver. The tensile moduli ranged from 482-1304 kPa with an average of 718 ± 223 kPa, comparable to results seen in literature [24]. Some test pieces were excluded due to artefacts in the sample (e.g.tears/holes in the tissue, material inhomogeneities) causing anomalous results. The average compressive stiffness was 875 ± 159 kPa, however during the first 10% of compressive strain it was significantly less than this, in the range of 100-300 kPa, similar to prior literature [28].

Each liver was retracted in the same manner as the tissue simulants; the specified clamp force was applied followed by a 30 mm retraction of the tissue at 2 mm/s. Only a single repeat was conducted on each liver sample to mitigate the effects of tissue damage caused during the grasping and retraction process impacting on the response.

4.4 Results

4.4.1 Experiment I: Silicone Tissue Simulants

A summary of representative results for the tissue simulant testing is provided in Figure 4.5(a), showing the change in displacement of the sensor islands at the front left, middle and right of the grasper throughout the retraction, as a function of the material stiffness and applied clamping force. In all test cases, movement of the left and right sensor islands plateaus in advance of the middle islands, indicating the left and right islands are preferentially slipping as anticipated despite the significant variations in both clamp load and material stiffness. The horizontal arrows on the graphs indicate the time difference between the detection of incipient slip and the occurrence macro slip, termed the mitigation time ($\Delta t_{mitigation}$), and the time differential between the detection of incipient slip at one of the front outer islands and of the front middle island (Δt_{front}). Changes in material stiffness had a significant influence on the available mitigation time, as did load, though these effects are better summarised in Figure 4.6.

Figure 4.5(b) displays the effect of retraction speed on sensor performance, showing move-

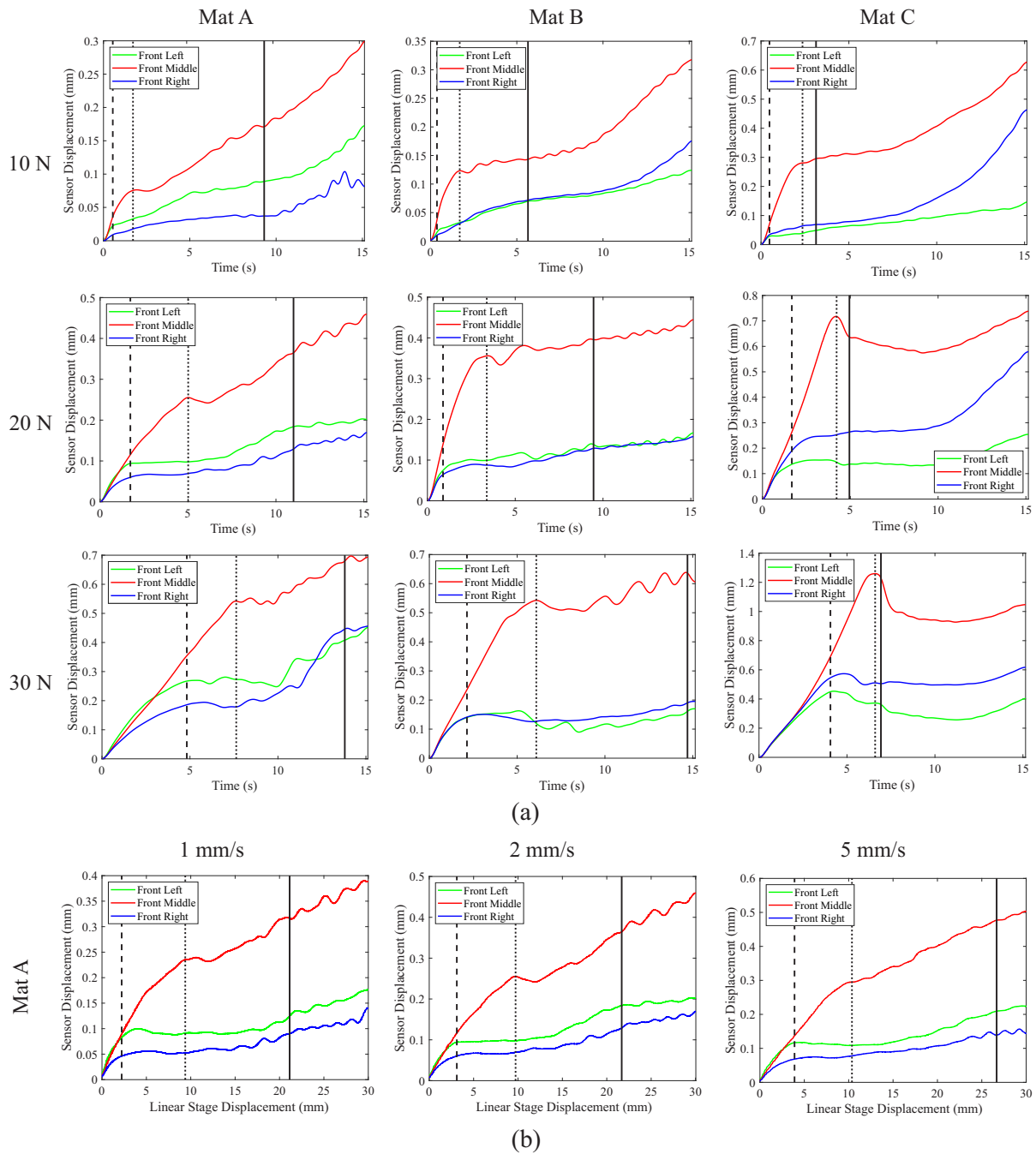


Figure 4.5: Graphs showing typical sensor displacements. The vertical dashed and dotted lines indicate the time slip is first detected at the outer and middle islands respectively, while the solid vertical line indicates the time of macro slip. The horizontal arrows indicate the time difference between the detection of incipient slip and the occurrence macro slip ($\Delta t_{mitigation}$), and the time between the detection of incipient slip of one of the front outer islands and the front middle island (Δt_{front}). (a) Sensor displacement vs time for changes in force and material stiffness at a retraction speed of 2 mm/s. (b) Sensor displacement vs linear stage displacement (retraction distance) for variations in retractions speed for Mat A under a 20 N clamping load.

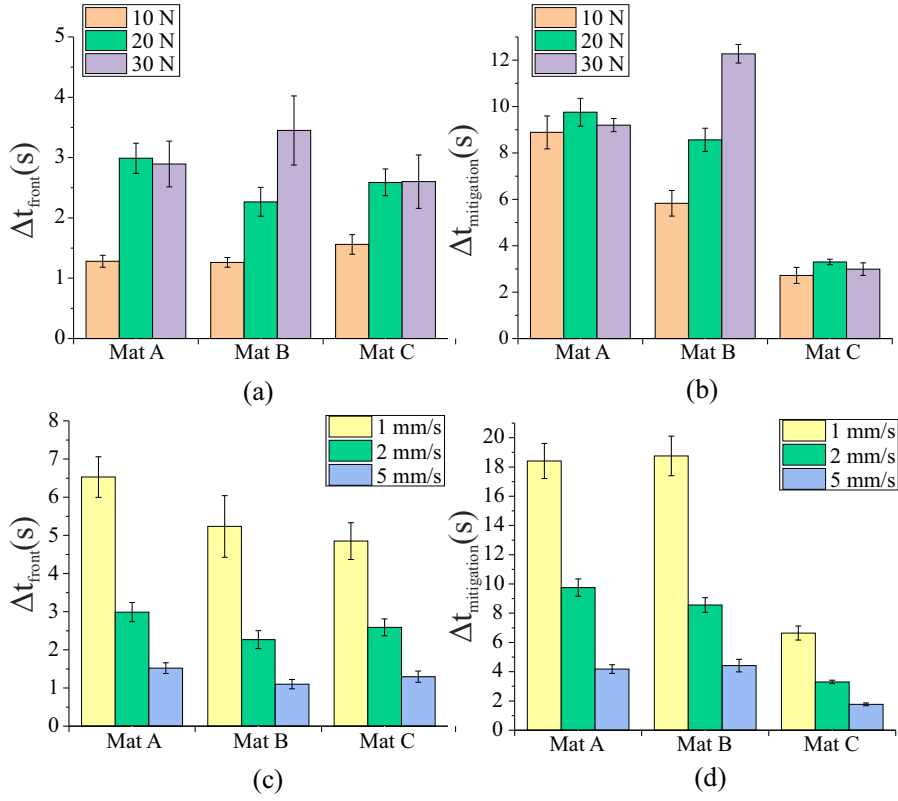


Figure 4.6: Graphs showing the mean time difference ($N=5$) between: (a) Detection of slip at the outer and middle grasper islands (Δt_{front}) for variation of force and material stiffness with a 2 mm/s retraction speed. (b) Available mitigation time ($\Delta t_{mitigation}$) for variation of force and material stiffness with a 2 mm/s retraction speed. (c) Δt_{front} for variation of retraction speed and material stiffness with a 20 N clamp load. (d) $\Delta t_{mitigation}$ for variations of retraction speed and material stiffness with a 20 N clamp load. The error bars indicate the standard deviation

ment of the respective islands with respect to the displacement of the linear stage retracting the tissue in order to normalise the results along the x axis for the different retraction speeds. From these results it is evident that the various stages of slip occur at similar levels of retraction (e.g. movement of the linear stage), despite changes in the retraction speed.

A summary of the effects of the variation in the material stiffness, clamping force, and retraction speed is provided in Figure 4.6. These graphs compare how the different variables affect Δt_{front} , and $\Delta t_{mitigation}$. For tissue simulants Mat A and Mat C the variation in clamping force results in no significant change to the mitigation time. However, the increase in clamp force from 10 N to 20 N did produce a significant increase in Δt_{front} for

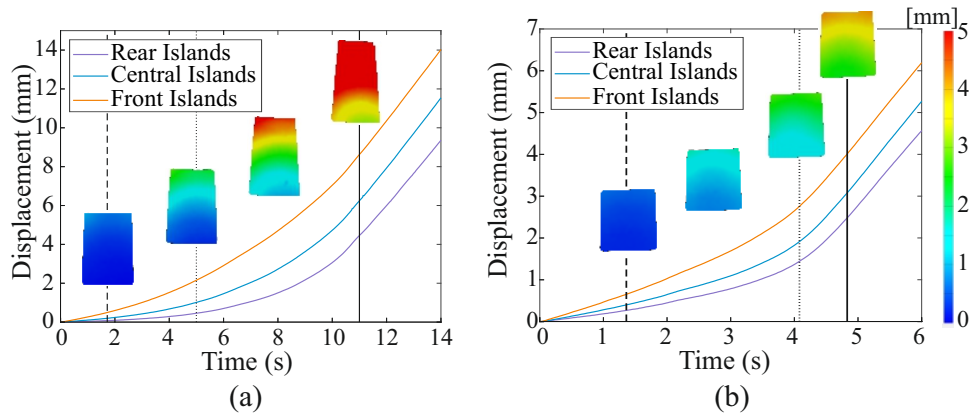


Figure 4.7: Typical results for average tissue displacement at the front, middle and rear of the grasper face measured using DIC. The vertical dashed and dotted lines indicate the time slip is first detected at the outer and middle islands respectively, while the solid vertical line indicates the time of macro slip. The colour maps show the change in displacement profiles over time. (a) Mat A, 20 N, 2 mm/s. (b) Mat C, 20 N, 2 mm/s.

these two materials (Fig. 4.6(a)). For Mat B an increase in the clamping force resulted in an increase in both Δt_{front} and $\Delta t_{mitigation}$. The effects of retraction speed appear to be inversely proportional to Δt_{front} and $\Delta t_{mitigation}$, with a doubling in retraction speed resulting in a 49% and 47% reduction in the time difference respectively.

Figure 4.7 shows representative results of tissue simulant displacement and deformation during testing, as measured using DIC, for the 20 N, 2 mm/s retraction cases for Mat A and C. This data shows how the displacement of the simulant varies between the front and rear of the grasper during the retraction, providing an indication of the magnitude of displacement that has occurred when incipient slip is first detected. For Mat A, when incipient slip is first detected at the outer front islands, the simulant at the rear of the grasper has moved only ca. 0.07 mm in comparison to ca. 0.49 mm at the front. For the stiffer material, Mat C, slip is detected when there is approximately 0.27 mm and 0.65 mm of displacement at the front and rear respectively. It should be noted that these measurements are taken from the face of the tissue simulant contacting the smooth acrylic counter face, at which there will be lower friction than at the grasper face. While this will result in more slip than occurs at the grasper contact, it provides a valuable indication of the overall characteristics of tissue deformation.

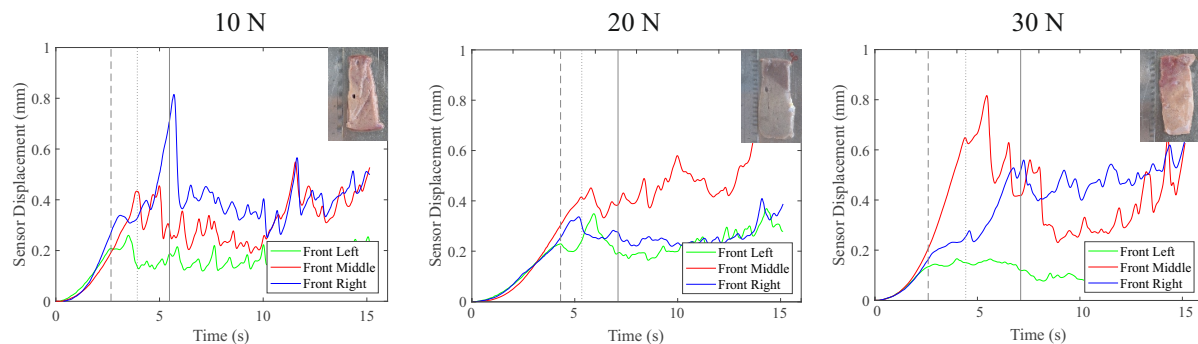


Figure 4.8: Graphs showing example sensor displacement for cases in which the early detection of slip was successful for porcine liver samples for various load cases. The vertical dashed and dotted lines indicate the time slip is first detected at the outer and middle islands respectively, while the solid vertical line indicates the time of macro slip.

4.4.2 Experiment II: Porcine Liver

The ex vivo testing with liver tissue was completed successfully, with no occurrence of tissue failure prior to gross slip occurring. Figure 4.8 provides a representative summary of the results for tests in which incipient slip of the outer islands was successfully detected for the three different clamp force conditions investigated. Across the full set of tests, incipient slip was reliably identified in 77% of cases, with detection rates of 80%, 80% and 70% for the 10 N, 20 N, and 30 N test conditions respectively.

As expected, in comparison to the tissue simulant experiment, there was significant variation between results in the ex vivo testing across the different liver samples. This is due to the magnitude of variation between the samples in terms of thickness, material properties and the presence of anomalies (e.g. non homogenous tissue containing features such as blood vessels). This variability was responsible for a range of phenomena causing unsuccessful attempts to detect incipient slip, as illustrated in Figure 4.9. 71.4% of unsuccessful deflections were the result of an uneven compression, or load application, across the width of the grasper, whilst the simultaneous slip of all 3 islands (14.3%), and the lag of one of the sensors causing the premature detection of slip (14.3%), were responsible for the remaining failed detections. The occurrence of mechanical snagging, where tissue catches on the islands and then releases rapidly, was seen in two cases, but the manner in which it occurred didn't affect the sensor's ability to reliably detect slip.

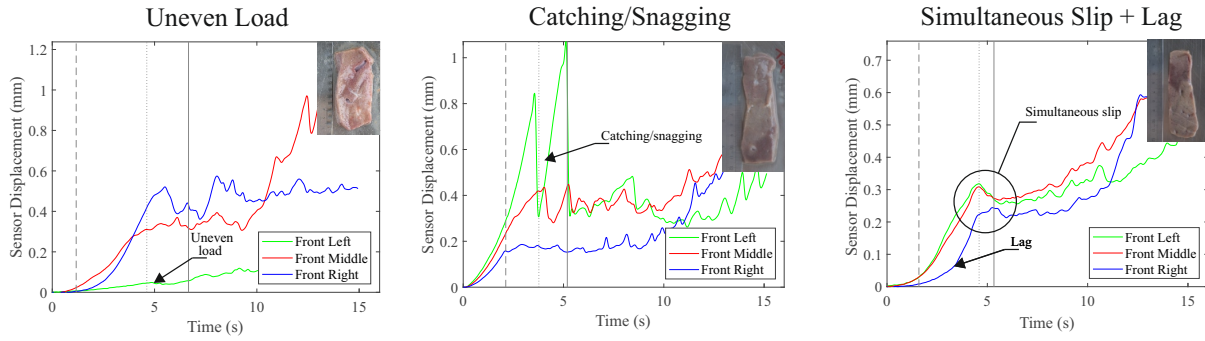


Figure 4.9: Graphs showing sensors displacements for cases in which early slip detection was unsuccessful, or there was abnormal sensor responses for liver tissue retractions.

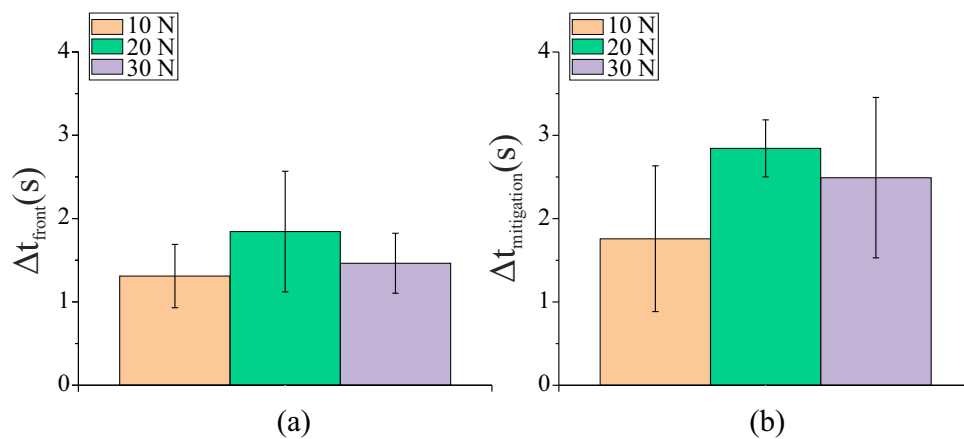


Figure 4.10: Graphs showing the mean time difference ($N=10$) between: (a) Detection of slip at the outer and middle grasper islands (Δt_{front}). (b) Available mitigation time ($\Delta t_{mitigation}$). For variation of the clamp force with a 2 mm/s retraction speed. The error bars indicate the standard deviation.

A summary of how the variation in clamp force affects the time between the detection of incipient slip at the front outer and middle grasper islands, Δt_{front} , as well as the available mitigation time, $\Delta t_{mitigation}$, is shown in Figure 4.10. These values were only calculated for the tests in which slip detection was considered successful. There is no significant difference ($p < 0.05$) between any of the load conditions investigated, this is likely due to the high level of variability between liver samples masking any potential trends.

4.5 Discussion

The results presented in this work demonstrate that measuring preferentially-induced incipient slip as a means to detect and prevent gross slip is an effective approach with relevance to surgery. When grasping tissue simulants it was able to successfully detect slip in 100% of cases, despite the large variations in test conditions (Fig. 4.5). For the more challenging case of ex vivo porcine liver samples, slip was accurately detected in 77% of cases, despite still using the same algorithm and sensor developed for the silicone tissue simulants. The decrease in successful detection was due to the variability in the liver tissue samples compared to the silicone simulants.

The majority of slip detection failures that occurred when grasping the porcine liver samples were the result of unevenness in the magnitude of tissue compression across the width of the grasper, which led to poor mechanical engagement with at least one of the outer sensor islands. This was usually due to either variation of the liver sample thickness across the width of the grasper, or was the result of anomalies within the tissue, e.g. holes, pits or tissue variation (Fat/liver tissue), which caused unexpected variations in the normal force. In some cases this resulted in an asymmetrical slip that didn't affect the performance of the sensor significantly, but in others there was almost no engagement between one of the outer sensor islands and the liver tissue (Fig. 4.9), resulting in these islands slipping instantly when the retraction starts. However it may be possible to mitigate this issue by monitoring the normal force exerted on each island during the initial grasping, and using this to determine the level of mechanical engagement of the different islands. The system could then determine which islands should be monitored for the detection of incipient slip events. It is also possible that a smaller grasper face would be less susceptible to anomalies and thickness variations in the tissue, though further investigation is required to confirm this.

In addition to the uneven load distribution there were three further abnormal results presented in Figure 4.9. The 'snagging' issue occurred as a result of tissue artefacts, like holes or tears in the tissue, catching on the sensor islands, leading to a catch and

release of the tissue, and associated spikes in sensor displacement in contrast to the more gradual changes that occur during a grip dominated by friction. For the other two issues identified 4.9, the occurrence of simultaneous slip, and the lag in the displacement of one of the sensor islands, based on the video footage of the slip it is clear that the sensor is reporting the same motions that are occurring at the tissue-grasper interface, though the root cause of this behaviour has not yet been identified.

Although the sensor system was able to successfully detect slip for the tissue simulants in 100% of cases, across the full range of clamp forces, retraction speeds, and material stiffnesses, there are still indications of potential limitations to the approach. Evaluation of the effects of variation in clamp force for the tissue simulants (Fig. 4.5(a)) indicate that at a low clamping force (10 N) there is little displacement of the left and right sensor islands before they start to slip. This suggests that there is low mechanical engagement between these outer islands and the tissue simulant due to the lower normal force. As the clamping force increases the mechanical engagement also increases, this can be observed by analysing Δt_{front} , the time between slip at the front outer and middle grasper islands, for Mat A and C (Fig. 4.6). When moving from 10-20 N Δt_{front} increases, but then there is no further increase when the load increase to 30 N, suggesting that there is a minimum clamp force, and level of mechanical engagement, required to ensure that the sensor islands can reliably engage with the tissue. The grasper design could be modified to improve performance by altering the curvature of the grasper, and/or the stiffness of the movable silicone below the upper gripping surface, to suite the desired application and operating range. Mat B didn't present the same behaviour to variations in the clamp load, this is suspected to be due to the different manner in which the restraining fabrics in this simulant are layered compared to Mat A and C, this differing performance of Mat B was also observed in previous experiments [20].

For the porcine liver tissue, variation in clamp force didn't appear to significantly affect the Δt_{front} (Fig. 4.10), this is likely due the higher tissue thickness and low compressive stiffness which allowed for significant mechanical engagement between the liver sample and the grasper islands over all three force conditions.

There is significant variation in the available mitigation time, $\Delta t_{mitigation}$, for the different tissue simulants. This is due to variations in the rate of slip propagation between the front and rear of the grasper, with stiffer materials having a higher rate of slip propagation, resulting in a shorter time available for mitigating actions to be taken before macro slip occurs [20]. However, variations in material stiffness of the tissue simulants appeared to have no significant effect on the sensor's ability to detect slip of the edge islands relative to the middle (Fig. 4.5(a)), or on Δt_{front} for Mat A and C, across the full range of forces and retraction speeds investigated (Fig. 4.6). This indicates that this slip detection method is at least partly independent of the tensile material properties of the grasped tissue, a highly desirable property for future deployment in surgical environments.

The long term aim of this work is the application of the sensing system within a surgical robot. To make this viable requires addressing a number of challenges, recognised as limitations in the current system:

- Grasper size: The instrumented grasper presented within this paper is approximately a factor of 2.5 times the size of a standard robotic surgical grasper. This difference in scale is not expected to affect the fundamental slip mechanics which form the basis for this sensing method. The variation of normal force to induce incipient slip has previously been utilised for a range of conventional robotic grippers [13], and the effect has even been observed to occur at the nanoscale asperity level of contacts [12], indicating this phenomenon can be considered independent of the scale of the contact in this application. However, scale remains an issue with respect to manufacture. Recent advances in Hall-Effect sensor development will aid development of more compact systems in the future [29].
- Tissue properties: The current sensor system and method have been demonstrated to be effective at detecting incipient slip of porcine liver samples, despite the lack of optimisation of the sensor design or detection algorithm for this target. This indicates that the sensor system has some robustness to the material properties of the grasped tissue. However further evaluation is now required to investigate the full

range of tissues, and mechanical properties, for which this technique is applicable, including variations in the size and shape of the tissue being manipulated.

- **Surgical application:** The grasping and retraction actions reported within this paper are necessarily simplified in comparison to the manipulation movements which occur during actual robotic surgery. In a surgical environment, retraction can include aspects of lateral and rotational movement. Standard surgical graspers also utilise a scissor-like mechanism to grasp tissue, rather than the parallel action utilised here. Further experimentation using a simulated surgical system is planned to evaluate how these aspects may affect the performance and robustness of this sensing approach.

4.6 Conclusions and Further Work

In summary the slip sensing approach presented in this work has been demonstrated as an effective way to detect the occurrence of incipient slip events for a variety of deformable tissue-like materials, including porcine liver. The sensor shows robustness to variation in the tensile stiffness of the material, though there are indications that tissue compressibility and clamp load are factors that will affect the working range. A significant challenge to address in future translation towards surgical use is the variability and anomalies present within biological tissue which resulted in some detection failures. Solutions have been identified to resolve these and in general this work shows the potential to use this method to automate the surgical grasping of soft biological tissue. The focus of future work is to scale down the sensor such that it can be integrated within a standard robotic surgical system, and to optimise the detection algorithm to identify and mitigate for tissue anomalies and variability.

References

- [1] Daniel M Herron and Michael Marohn. Prepared by the SAGES-MIRA Robotic Surgery Consensus Group. page 24, 2006.
- [2] O. A. J. van der Meijden and M. P. Schijven. The value of haptic feedback in conventional and robot-assisted minimal invasive surgery and virtual reality training: a current review. *Surgical Endoscopy*, 23(6):1180–1190, June 2009.
- [3] B. Tang, G.B. Hanna, and A. Cuschieri. Analysis of errors enacted by surgical trainees during skills training courses. *Surgery*, 138(1):14–20, July 2005.
- [4] E.A.M. Heijnsdijk, J. Dankelman, and D.J. Gouma. Effectiveness of grasping and duration of clamping using laparoscopic graspers. *Surgical Endoscopy*, 16(9):1329–1331, September 2002.
- [5] C.-H. King, M.O. Culjat, M.L. Franco, C.E. Lewis, E.P. Dutson, W.S. Grundfest, and J.W. Bisley. Tactile Feedback Induces Reduced Grasping Force in Robot-Assisted Surgery. *IEEE Transactions on Haptics*, 2(2):103–110, April 2009.
- [6] C.-H. King, M.O. Culjat, M.L. Franco, J.W. Bisley, G.P. Carman, E.P. Dutson, and W.S. Grundfest. A Multielement Tactile Feedback System for Robot-Assisted Minimally Invasive Surgery. *IEEE Transactions on Haptics*, 2(1):52–56, January 2009.
- [7] Verena Nitsch and Berthold Farber. A Meta-Analysis of the Effects of Haptic Interfaces on Task Performance with Teleoperation Systems. *IEEE Transactions on Haptics*, 6(4):387–398, October 2013.
- [8] Natalie T. Burkhard, J. Ryan Steger, and Mark R. Cutkosky. The Role of Tissue Slip Feedback in Robot-Assisted Surgery. *Journal of Medical Devices*, 13(2):021003, June 2019.
- [9] Seyed Mohsen Khadem, Saeed Behzadipour, Alireza Mirbagheri, and Farzam Farahmand. A modular force-controlled robotic instrument for minimally invasive surgery -

- efficacy for being used in autonomous grasping against a variable pull force: Modular force-controlled robotic instrument. *The International Journal of Medical Robotics and Computer Assisted Surgery*, 12(4):620–633, December 2016.
- [10] Natalie T. Burkhard, Mark R. Cutkosky, and J. Ryan Steger. Slip Sensing for Intelligent, Improved Grasping and Retraction in Robot-Assisted Surgery. *IEEE Robotics and Automation Letters*, 3(4):4148–4155, October 2018.
- [11] D Jones, A Alazmani, and P Culmer. A Soft Inductive Tactile Sensor for Slip Detection Within a Surgical Grasper Jaw. page 4, 2019.
- [12] K. L. Johnson. *Contact mechanics*. Cambridge University Press, Cambridge Cambridgeshire New York, 1987.
- [13] Wei Chen, Heba Khamis, Ingvars Birznieks, Nathan F. Lepora, and Stephen J. Redmond. Tactile Sensors for Friction Estimation and Incipient Slip Detection – Towards Dexterous Robotic Manipulation: A Review. *IEEE Sensors Journal*, pages 1–1, 2018.
- [14] B. Delhaye, P. Lefevre, and J.-L. Thonnard. Dynamics of fingertip contact during the onset of tangential slip. *Journal of The Royal Society Interface*, 11(100):20140698–20140698, September 2014.
- [15] M.R. Tremblay and M.R. Cutkosky. Estimating friction using incipient slip sensing during a manipulation task. In *[1993] Proceedings IEEE International Conference on Robotics and Automation*, pages 429–434, Atlanta, GA, USA, 1993. IEEE Comput. Soc. Press.
- [16] Filipe Veiga, Jan Peters, and Tucker Hermans. Grip Stabilization of Novel Objects using Slip Prediction. *IEEE Transactions on Haptics*, pages 1–1, 2018.
- [17] Jeffrey Stoll and Pierre Dupont. Force Control for Grasping Soft Tissue. page 4, May 2006.
- [18] Ian Waters, Dominic Jones, Ali Alazmani, and Peter Robert Culmer. Utilising

- Incipient Slip for Grasping Automation in Robot Assisted Surgery. *IEEE Robotics and Automation Letters*, 7(2):1071–1078, April 2022.
- [19] Ian Waters, Ali Alazmani, and Peter Culmer. Engineering incipient slip into surgical graspers to enhance grasp performance. *IEEE Transactions on Medical Robotics and Bionics*, pages 1–1, 2020.
- [20] Ian Waters, Lefan Wang, Dominic Jones, Ali Alazmani, and Peter Culmer. Incipient Slip Sensing for Improved Grasping in Robot Assisted Surgery. *IEEE Sensors Journal*, pages 1–1, 2022.
- [21] Joseph C. Norton, Jordan H. Boyle, Ali Alazmani, Pete R. Culmer, and Anne Neville. Macro-Scale Tread Patterns for Traction in the Intestine. *IEEE Transactions on Biomedical Engineering*, 67(11):3262–3273, November 2020.
- [22] Dominic Jones, Lefan Wang, Ali Ghanbari, Vasiliki Vardakastani, Angela E. Kedgley, Matthew D. Gardiner, Tonia L. Vincent, Peter R. Culmer, and Ali Alazmani. Design and Evaluation of Magnetic Hall Effect Tactile Sensors for Use in Sensorized Splints. *Sensors*, 20(4):1123, February 2020.
- [23] W. Schwarz. The surface film on the mesothelium of the serous membranes of the rat. *Zeitschrift fr Zellforschung und mikroskopische Anatomie*, 147(4):595–597, 1974.
- [24] Andrew R Kemper, Anthony C Santago, Joel D Stitzel, Jessica L Sparks, and Stefan M Duma. Biomechanical Response of Human Liver in Tensile Loading. page 12, January 2010.
- [25] Andrew W. Brown, Stuart I. Brown, Donald Mclean, Zhigang Wang, and Alfred Cuschieri. Impact of fenestrations and surface profiling on the holding of tissue by parallel occlusion laparoscopic graspers. *Surgical Endoscopy*, 28(4):1277–1283, April 2014.
- [26] Phillip Mucksavage, David C. Kerbl, Donald L. Pick, Jason Y. Lee, Elspeth M. McDougall, and Michael K. Louie. Differences in Grip Forces Among Various Robotic

- Instruments and da Vinci Surgical Platforms. *Journal of Endourology*, 25(3):523–528, March 2011.
- [27] Ali Alazmani, Rupesh Roshan, David G Jayne, Anne Neville, and Peter Culmer. Friction characteristics of trocars in laparoscopic surgery. *Proceedings of the Institution of Mechanical Engineers, Part H: Journal of Engineering in Medicine*, 229(4):271–279, April 2015.
- [28] Blake Johnson, Scott Campbell, and Naira Campbell-Kyureghyan. Characterizing the Material Properties of the Kidney and Liver in Unconfined Compression and Probing Protocols with Special Reference to Varying Strain Rate. *Biomechanics*, 1(2):264–280, September 2021.
- [29] Theo Le Signor, Nicolas Dupre, and Gael F. Close. A Gradiometric Magnetic Force Sensor Immune to Stray Magnetic Fields for Robotic Hands and Grippers. *IEEE Robotics and Automation Letters*, 7(2):3070–3076, April 2022.

4.7 Appendix

Sensor calibration method

This appendix expands on the information provided in Section 4.2.3, to provide more detail on the calibration of the Magnetic sensors utilised in the sensed grasper for detecting incipient slip. The calibration rig set up was the same as described in the Appendix in Section 3.7 (See Fig.3.11), except the copper target is replaced by a neodymium disc magnet (2 mm diameter \times 0.5 mm thick), and the SITS sensor coils by a tri-axis Hall effect sensor (MLX90393, Melexis).

A set of data was gathered to help calibrate the measurement of the hall effect sensor to the displacement of the magnetic target. This was done using the three linear stages of the calibration rig to conduct a 3D sweep, the magnetic target was moved in the x-y plane from -2 to 2 mm at 0.2 mm/s for each step in z (-0.65:1.25 mm in 0.1 mm increments), where $\{0,0,0\}$ represent the position of the neodymium magnet centre in its centred unloaded position.

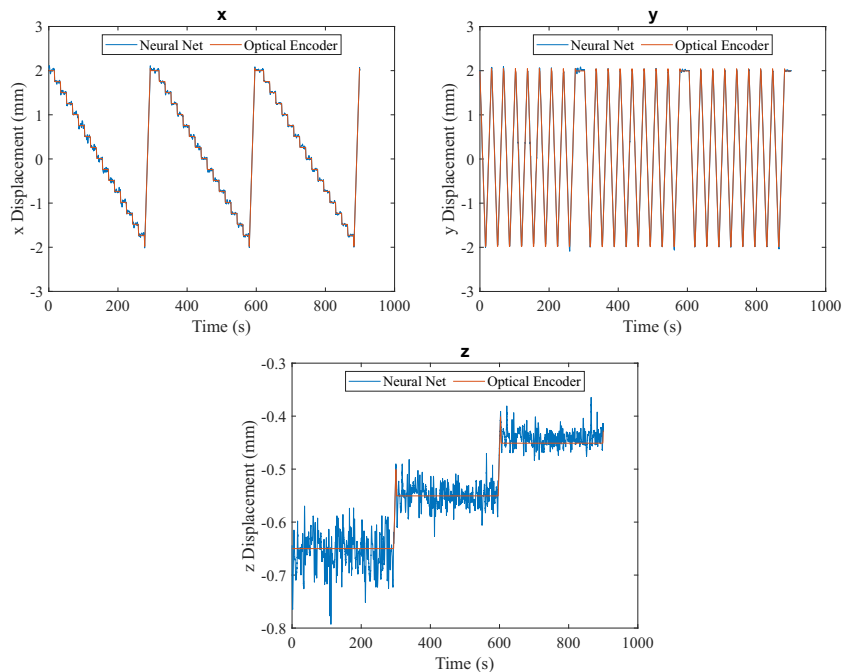


Figure 4.11: Graphs showing comparison between the output of the trained neural network and the displacement measured by the calibration rig in x,y and z for the validation data set for the magnetic sensor.

This data set was used to train a neural network (Matlab, Mathworks) to fit the magnetic field reading of the sensor to the displacements measured by the calibration system. This neural network utilised a two-layer feed forward network [22], with 40 neurons in the hidden layer, and was trained using a Bayesian regularization backpropagation algorithm, due to non-linear relationship between displacement and magnetic field [22].

To validate this neural network a separate data set was then gathered using the calibration rig to ensure that the neural network was accurate and repeatable with a data set that it had not been trained on. A comparison between the output of the neural network and the displacement measurements taken by the calibration rig are presented in Figure 4.11. This neural network provided a strong correlation with the validation data, with root mean squared errors of 0.029 mm, 0.025 mm and 0.018 mm, in x, y and z respectively.

Chapter 5

Utilising Incipient Slip for Grasping Automation in Robot Assisted Surgery

Preface

This chapter was published as the journal paper:

Utilising Incipient Slip for Grasping Automation in Robot Assisted Surgery. Ian Waters, Dominic Jones, Ali Alazmani, and Peter Robert Culmer. IEEE Robotics and Automation Letters. 2022.

Sections 5.1 through 5.5 constitute the main body of this publication, whilst the appendix provides additional results for the DIC measurements. This paper continues the work from chapter 4, on the development of a slip sensor that utilises variations in normal force to induce incipient slip, to produce a closed loop control system, utilising this sensor, that automatically adjusts clamping loads to prevent tissue slip, aiming to reduce the force used to maintain stable grasp control.

Abstract

Despite recent advances in modern surgical robotic systems, an ongoing challenge remains their limited ability to control grasp force. This can impair surgical performance as a result of either tissue slippage or trauma from excessive grasp force. In this work we investigate a force control strategy to address this challenge based on the detection of incipient slip. Our approach employs a grasper face whose shape is engineered to encourage preferential localised slips that can be sensed using embedded displacement sensors prior to gross slip occurring. This novel approach enables closed loop control of the grasping force to prevent gross slip whilst applying minimal force. In this paper we first demonstrate the efficacy of sensing incipient slip and then demonstrate how this can form a robust closed loop grasping system to maintain stable control of tissue. Results demonstrate that this approach can achieve equivalent grasping performance to a scheme employing a fixed maximal grasping force while reducing tissue loading, and thus risk of trauma. This provides the foundation for the development of automated surgical robots with adaptive grasp force control.

5.1 Introduction

The introduction of robotic surgical devices has helped advance Minimally Invasive Surgery (MIS) and has led to improved surgical outcomes [1]. However their limited grasping force control while handling soft tissue remains an issue and is the cause of a significant number of surgical errors [2; 3]. This can be due to either the over application of force, leading to tissue trauma [2], or a lack of clamping load resulting in adverse slip events during surgical procedures [3].

Haptic feedback of grasping forces has been demonstrated as a viable technique to minimise the occurrence of tissue trauma due to excessive clamping loads [4; 5; 6]. However this requires the surgeon to continually monitor and maintain an appropriate applied grasping load (neither too high nor too low), a task which is both challenging and can incur an increased cognitive load [7]. An alternative strategy can be formed through in-

spection of tissue movement at the grasper face, rather than the applied load. Specifically, through the detection and monitoring of tissue slip, the clamping force can be adjusted to use the minimum force required to prevent slip events from occurring, whilst minimising the occurrence of tissue trauma. This control method also provides the opportunity for a grasping automation method which is independent of tissue properties, helping to reduce surgeon fatigue and allowing a focus on more critical higher-level tasks [8].

A range of approaches have been proposed for using slip as the basis for automated surgical grasping. Using a predefined '*safe grasping zone*' allows regulation of grasping force as a function of detected shear, aiming to use the minimum force required to prevent slip [9]. However this requires tissue-specific safe zones to be prescribed, limiting clinical utility. More adaptive approaches have utilised sensors embedded within the grasper face to monitor tissue shear against it. Jones *et al.* [10] used a two-axis soft inductive tactile sensor to monitor normal and shear forces at the grasper face, determining slip as the point when the coefficient of friction first peaks. Burkhard *et al.* [11] developed a novel slip sensing method using hot wire anemometer techniques to monitor changes in heat flux through the tissue. The system was able to effectively detect slip during small movements in tests on porcine tissue.

Slip events during grasping can be broken down into two stages; first *incipient slip* followed by *macro slip* [12]. During incipient slip the total shear force across the contact is less than the total friction force, thus overall the contact is held securely [12]. However the friction force may vary in localised areas across the contact surface and where this is exceeded by the shear friction then localised movement will occur, these are termed 'incipient slips' [12]. As the total shear force increases these incipient slip events will increasingly occur. When the total shear force exceeds the total friction the contact will enter a macro slip regime and grip stability is lost [12].

The slip sensing approaches described above detect the occurrence of macro slip, and so require a loss of grip control to occur before mitigating actions can be taken. An alternative approach is to focus on the detection of incipient slip, allowing slip events to

be identified early and grip control to be maintained throughout the retraction process. Detection of incipient slip has been utilised by the wider robotics community for grasping control, but has seen limited application in the field of surgical robotics or in the grasping of deformable materials. The only example is reported by Stoll *et al.* [13] who developed a system based on monitoring the global shear force to determine material stiffness, and thus the early onset of macro slip. The technique was found to be effective but only provides a limited time window in which to prevent macro slip.

In developing a sensor to detect incipient slip a key aspect is to encourage these local slip events to occur in a consistent and repeatable manner [14]. Biomimicry of the human finger has been used by many as inspiration; typically employing a curved finger-like surface to create a normal force distribution, and thus the corresponding variation of frictional force, across the contact surface [14; 15; 16]. This approach has been demonstrated as a viable method for encouraging the incipient slip of lubricated and deformable materials similar to soft biological tissues [17]. Khamis *et al.* [18] investigated an alternative to using a continuous curved surface to control friction forces, instead using an array of stepped pillars to create discrete variations in height and thus normal force. Overall, incipient slip sensors typically use similar methods for varying frictional forces across the contact surface to encourage incipient slip, but they employ a range of sensing modalities to detect the occurrence of these slips, including measurement of vibration, normal force distribution, shear force magnitude, contact area or optical imaging, a detailed evaluation of these is provided in a recent review by Chen *et al.* [14].

Our research aim is to build on the incipient slip sensing methods developed across the wider robotics community for use within a surgical robotic system. This paper reports the design of an incipient slip sensor system that employs a curved grasper profile to encourage and detect the occurrence of incipient slip in deformable and lubricated tissue-like materials. We then propose a method for the automated detection of incipient slip events using this sensor and evaluate its ability to prevent the occurrence of gross slip events under representative surgical conditions. The novelty of this work is the use of incipient slip mechanics, in a physical sensing system, for early prediction (and thus

avoidance) of gross slip during the grasping and manipulation of soft-tissue like materials. This has particular relevance in the automation of surgical grasping.

5.2 System Development

5.2.1 Concept and Requirements

The core requirement of this sensing system was to induce measurable levels of incipient slip in tissue during surgical grasping conditions. We approached this using a concept which employs a curved grasping surface that is segmented into independently mobile sections. The curved surface causes higher frictional forces to occur in the middle of the grasper in comparison to the edges, thus encouraging slip to occur in the outer sections of the grasper prior to the middle [17] as illustrated in (Fig. 5.1). Using this approach, it is possible to detect incipient slip by measuring the relative displacement of the independent 'island' sections. Consider a typical retraction movement; during the initial stages the shear force is low and friction forces dominate, such that the outer and middle islands will move together with the tissue. As retraction continues, shear forces will increase (e.g. by pulling tissue), beginning to exceed frictional forces at the outer edges, thus tissue slip will occur and the outermost islands will move less than the middle island. Consequently, monitoring the differential relationship between the outer and middle island's movement provides the means to detect incipient slip.

5.2.2 System Design and Fabrication

To evaluate this sensor concept, a scaled prototype was developed and realised. Based on preliminary work [17], a curved grasper face with a radius of 100.25 mm was separated into a 5×3 grid of islands as shown in Figure 5.2, providing islands spanning the width and length of the grasper face. Islands were separated along the length of the grasper to isolate them from the effect of slip propagation between the front and back of the grasper caused by the elastic properties of the tissue [17].

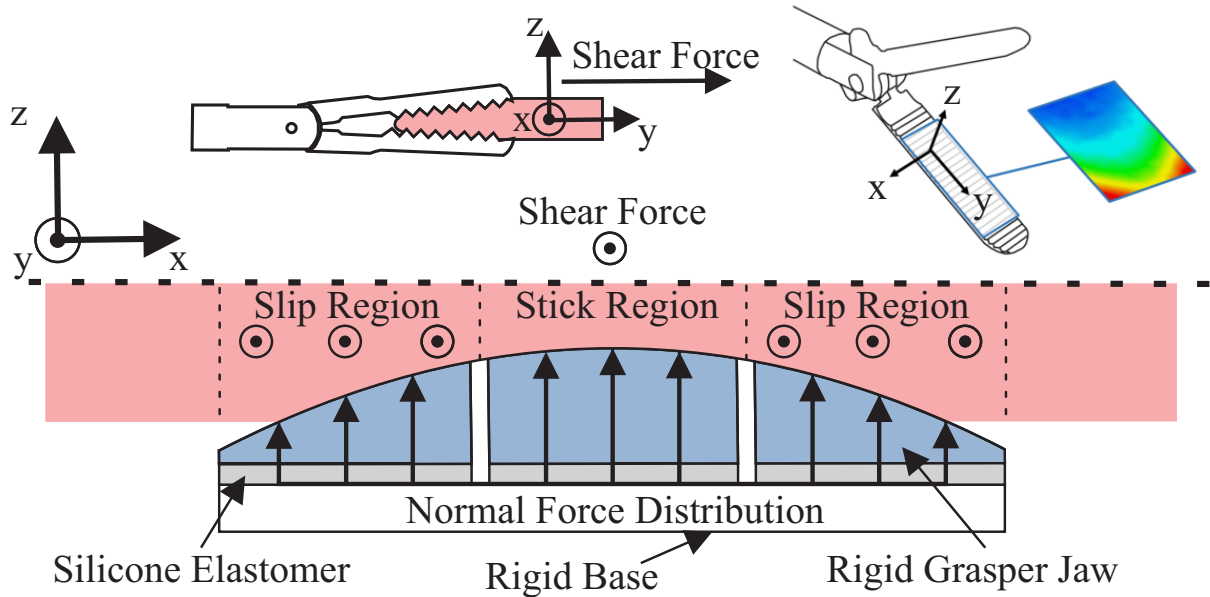


Figure 5.1: Diagram demonstrating the concept of encouraging incipient slip across independently moveable sections of the grasper face through the variation of normal force using a curved surface.

Each island comprises a 3D printed upper rigid face (Rigid 4000 Resin, Formlabs) to provide the gripping surface, and a 1 mm thick silicone elastomer base (Ecoflex 00-30, Smooth-on) to allow independent movement of the rigid face. The islands were then attached to a PET film on a rigid base. The grasper faces featured a regular hexagonal pattern (0.75 mm width, height and separation) to provide an isometric gripping surface suited to soft deformable materials [17; 19].

Prior work characterised the mechanical behaviour of the system under representative loading conditions and thus define the underlying sensor requirements [17]. The relative difference in tissue displacement at the point of incipient slip between the outer and middle of the curved grasper was found to lie within a range of 0.1-0.2 mm [17]. The sensing elements also need to be sufficiently compact to fit across the width of the grasper. To meet these requirements, a Hall effect based tactile sensing method was used. Each element consists of a three-axis Hall effect sensor chip (MLX90393, Melexis) coupled with a neodymium disc magnet (2 mm diameter \times 0.5 mm thick) embedded in the base of the grasper islands (see Fig. 5.2). When a force ($F_{x,y,z}$) is applied to the grasper face the elastomer layer deforms such that the island's gripping surface and magnet change

position relative to the Hall effect sensor. The magnetic field at the sensor ($B_{x,y,z}$) can then be calibrated and converted into a corresponding displacement. For more details on the development of these tactile sensing elements see [20]. The array of sensing elements in the grasper was interfaced to a microcontroller (Teensy 3.6, PJRC) using the I²C protocol and recorded at a sample rate of 100 Hz.

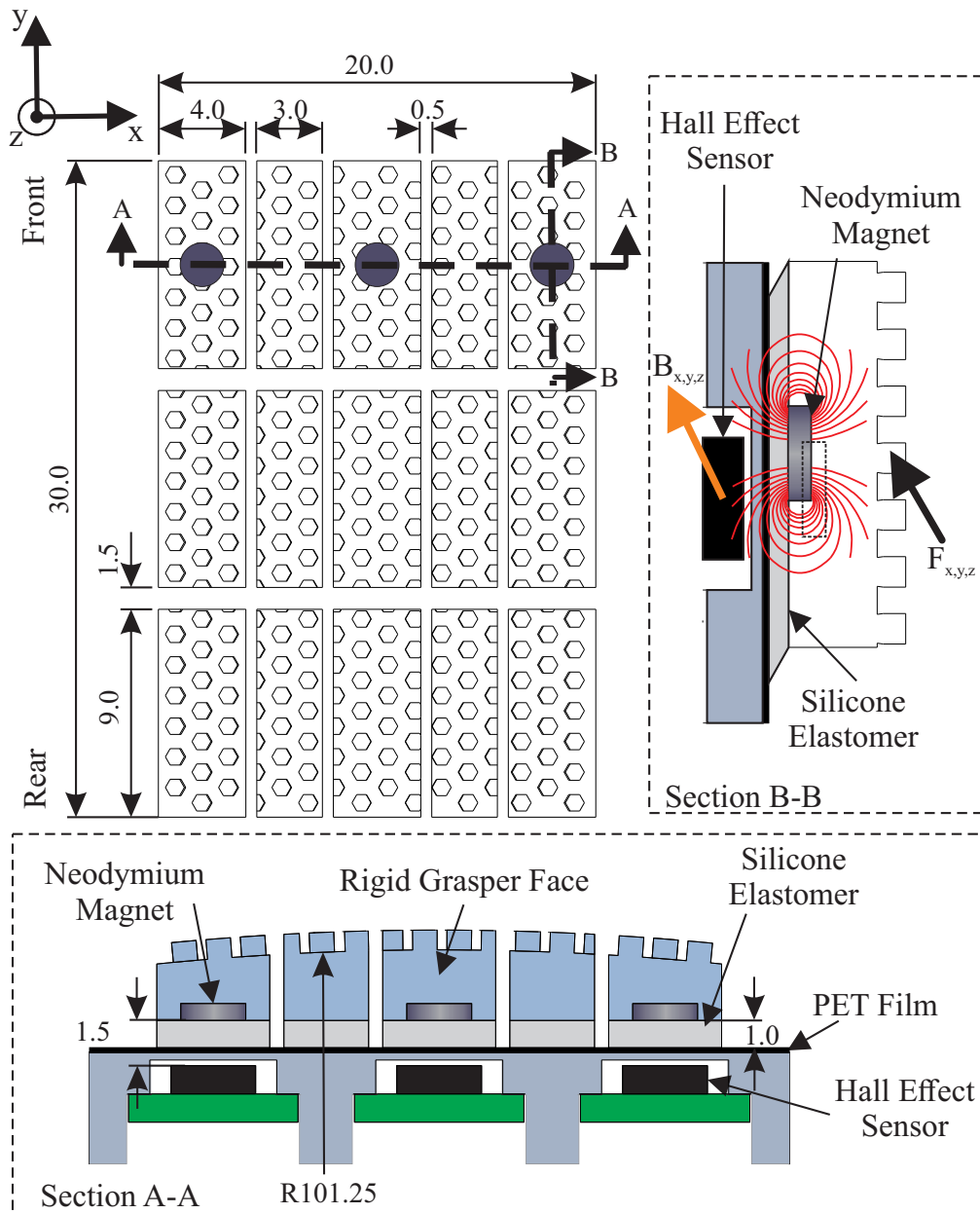


Figure 5.2: Dimensioned drawing of the grasper separated into 5×3 grid of independently moveable islands, the grey circles indicate the positions of the sensing nodes (All dimensions in mm). Section A-A: cross section across the width displaying the design of the sensed and passive islands. Section B-B: Principle of operation of the sensing system, displaying how the magnetic field moves through the Hall effect sensor as force is applied to the island.

5.2.3 Signal Processing

The sensors were calibrated using a custom three-axis sensor calibration system (detailed in [20]), to conduct a volumetric positioning sweep, moving in the x-y plane (-2 to 2 mm at 0.2 mm/s) for each z axis step (-0.65:1.25 mm in 0.1 mm increments) where $\{0,0,0\}$ represents the island in an unloaded 'neutral' position. The measured magnetic field was calibrated to displacement using a neural network implemented using the Matlab neural net fitting toolbox (Matlab, Mathworks). A two-layer feed forward network configuration was selected as appropriate to represent the system based on prior work using a similar Hall effect sensor [20]. The overall network consisted of 40 neurons in the hidden layer and used a Bayesian regularization backpropagation algorithm as the training method to accommodate the non-linear relationship between magnetic field and displacement [20]. The trained neural network showed close correlation with validation data, with root mean squared errors of 0.029 mm, 0.025 mm and 0.018 mm, in x, y and z respectively. A third order Butterworth filter with a cut off frequency of 10 Hz was applied to the output of the neural network to attenuate high frequency noise in the displacement data.

5.2.4 Slip Detection & Mitigation

In the context of this work, incipient slip is defined as the event when one or more islands start to slip against the grasped tissue, whilst the majority maintain a stable grip. This manifests as a movement differential between these islands which can be detected by monitoring the displacement of the individual islands.

Applying these general criteria to the specific form of the instrumented grasper, detection of incipient slip relates to the outer (left and right) islands slipping relative to the central islands. This phenomenon is preferentially promoted through the curved design of the islands across the grasper face (see Fig. 5.1) such that tissue at the outside of the grasper has a higher probability of slipping compared to central regions (due to differing normal loads) as increasing shear force is applied during retraction.

To automatically detect the presence of these incipient slips an algorithm was developed

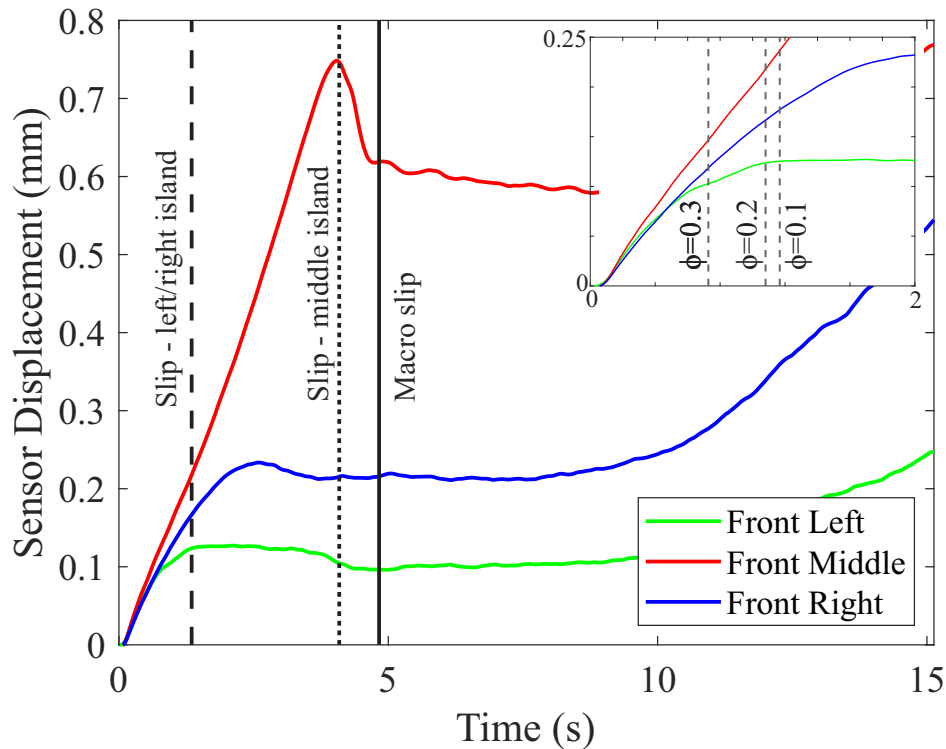


Figure 5.3: Example of typical displacement characteristics for the front left, middle and right islands of the grasper under a 20N clamp load with a retraction speed of 2 mm/s (using Mat C). The inset shows how variation of the slip ratio changes when incipient slip of the edge islands is detected.

that is focused on the detection of slip during tissue retraction, when shear force is increasing, as this represents a 'worst-case' when slip is most likely to occur. Exploratory testing was conducted to investigate the parameter space and understand the sensor characteristics. Tests consisted of retracting a tissue simulant held by the sensor (with a configuration as shown in Fig. 6) up to the point of macro slip across a range of configurations consisting of: three clamp forces (10 N, 20 N, 30 N), three retraction speeds (1 mm/s, 2 mm/s, 5 mm/s), and three levels of tissue stiffness (Mat A - 241 kPa, Mat B - 320 kPa and Mat C - 610 kPa).

Figure 5.3 shows a typical example of the sensor response from these tests, revealing the differing displacement of the three instrumented islands over the course of a tissue retraction in which a simulant, Mat C, was grasped with a constant load of 20 N, and retracted at a constant speed of 2 mm/s. Across the parameter space, the sensor system showed this consistent general response: during the early stages of retraction (low shear loading), the middle and side islands move together with the same velocity. As retraction

continues, the shear force increases and the left and right outer islands (where normal and thus frictional forces are lower) begin to slip against the tissue and their velocity decreases. This continues until movement of the outer islands stops, indicating complete slip against the tissue simulant in this region. Therefore, calculating the velocity (in the direction of shear) of the left (V_l) and right islands (V_r) as a ratio of the velocity of the middle island (V_m) defines their magnitude of slip with respect to the middle island. This ratio was thus termed the slip ratio (ϕ).

$$\phi = \mathbf{min} \left[\frac{V_l}{V_m}, \frac{V_r}{V_m} \right] \quad (5.1)$$

The physical embodiment of the slip ratio (ϕ) is presented in Figure 5.4. A slip ratio (ϕ) at or approaching 1 indicates the side and middle islands are moving together and there is no incipient slip. As ϕ decreases an increasing amount of relative slip is occurring between the tissue and the outer islands with respect to the middle. When ϕ reaches 0 there is no longer any motion of the outer island in the direction of shear, indicating that this region is slipping freely against the tissue as it is retracted. Informed by these preliminary investigations, $\phi < 0.2$ was identified as a reliable threshold to signify incipient slip of that island had occurred that was applicable across the full parameter space. This allows for robustness to noise (e.g. due to measurement or environmental factors), together with variability in the grasping conditions explored here.

A slip mitigation algorithm was developed based on the ϕ ratio, to adjust the grasping force as a function of the actual slip ratio, termed ' ϕ_a ', and the retraction speed (a variable available in surgical robotic systems). The algorithm is based on maintaining ϕ_a within a desirable envelope in which the grip is 'stable'. The target slip ratio ϕ_T varies dependent on the current state of the system, as shown in Figure 5.4 and defined in Equation 5.2, where operating regions are defined around the incipient slip onset point of $\phi=0.2$ with a safety factor of 2. Thus, for $\phi_a < 0.4$ the system should increase the grasping 'clamping' force to prevent slip occurring, but when $\phi_a > 0.8$ the system should reduce the grasp force to minimise tissue trauma as at this slip ratio there is only minimal relative slip

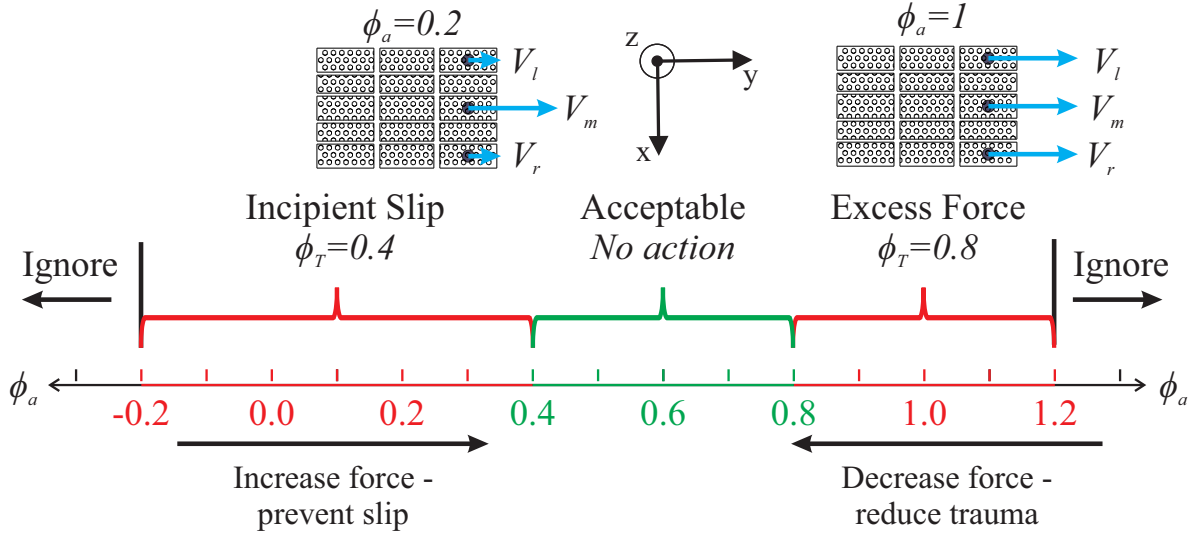


Figure 5.4: A schematic showing the grasping and slip regimes defined by ϕ slip ratios and the associated response of the automated system. Uppermost, the diagrams show how the relative velocity of the islands, in the direction of retraction, differ in these regimes.

occurring (no relative slip at $\phi_a = 1$). Between these two regimes ($0.4 \leq \phi_a \leq 0.8$) the grasp force should remain constant. Slip ratios which occur outside this range (e.g. due to low speeds as the island velocities approach zero) are considered anomalous and ignored.

$$\begin{aligned} \text{If } \phi_a < 0.4, \phi_T &= 0.4 \\ \text{ElseIf } \phi_a > 0.8, \phi_T &= 0.8 \end{aligned} \quad (5.2)$$

The grasping force to be applied $F_{c_{i+1}}$ during retraction is then determined using the equation:

$$F_{c_{i+1}} = F_{c_i} + K(\phi_T - \phi_a) \quad (5.3)$$

where the value of ϕ_T is determined based on the current value of ϕ_a as shown in Figure 5.4 and Equation 5.2, and the gain (K) varies as a linear function of the retraction speed of the linear stage (V_s).

$$K = 0.1V_s + 0.2 \quad (5.4)$$

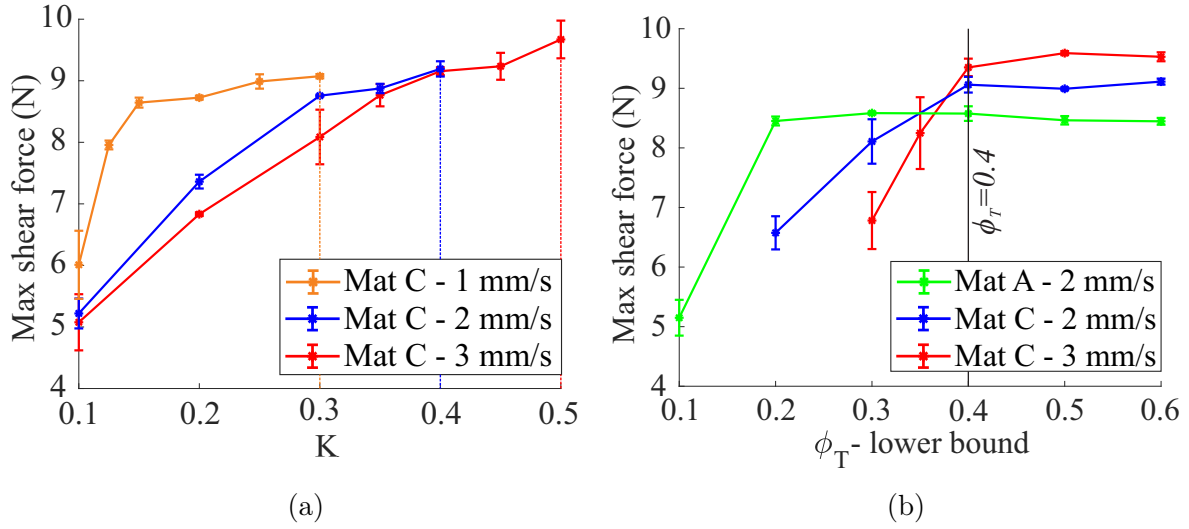


Figure 5.5: Graphs showing the effect on the shear force required to induce macro slip for the automated grasper during surgical retraction for: (a) Variation in gain. The dashed vertical lines indicate the gains identified for each retraction speed. (b) Variation of ϕ_T lower bound.

Equation 5.4 was derived experimentally through inspection of the system response across three separate retraction speeds using Mat C (the stiffest material and thus most challenging case). A gain was identified for each retraction speed by progressively increasing K until it provided comparable grasping performance (i.e. the peak shear force occurring before macro slip) to a system operating at maximum clamp load, as shown in Fig. 5.5(a). These gains were then used to fit the linear function defined in Equation 5.4. The system operates at a sampling frequency of 100 Hz.

N.B. This algorithm is only applied whilst $V_m > 0$ as this indicates firstly that there is tissue retraction occurring and secondly that the middle island is still securely gripping the tissue. If the middle island slips against the tissue ($V_m \leq 0$) the current algorithm is no longer applicable and so the grasp force remains constant.

Validation testing was conducted to ensure the slip onset threshold $\phi_T = 0.4$ was appropriate for a range of conditions. The automated grasping system described above was used at extremes of the parameter space (varying material and retraction speed) to find the resultant peak grasping load achieved. As shown in Fig. 5.5(b), increasing ϕ_T leads to initial increases in the peak shear force before the trend plateaus, a trend seen across the parameter space. From these data, using a fixed value of $\phi_T = 0.4$ for the slip threshold

provides consistent performance across the parameter space which minimises dependence on material properties (information that is difficult to ascertain in advance).

5.3 System Evaluation

The system was tested to evaluate the efficacy of using an incipient slip sensor as the basis of an automated grasping control method. The performance of this system can be evaluated through its ability to prevent the occurrence of global slip events whilst minimising the grasping force applied to the target specimen (to minimise trauma) under conditions representative of those used in surgical practice.

5.3.1 Experimental Set Up and Analysis

An experimental apparatus was configured to simulate the movements of surgical grasping and retraction, as shown in Figure 5.6. Tissue simulant samples were fixed to the

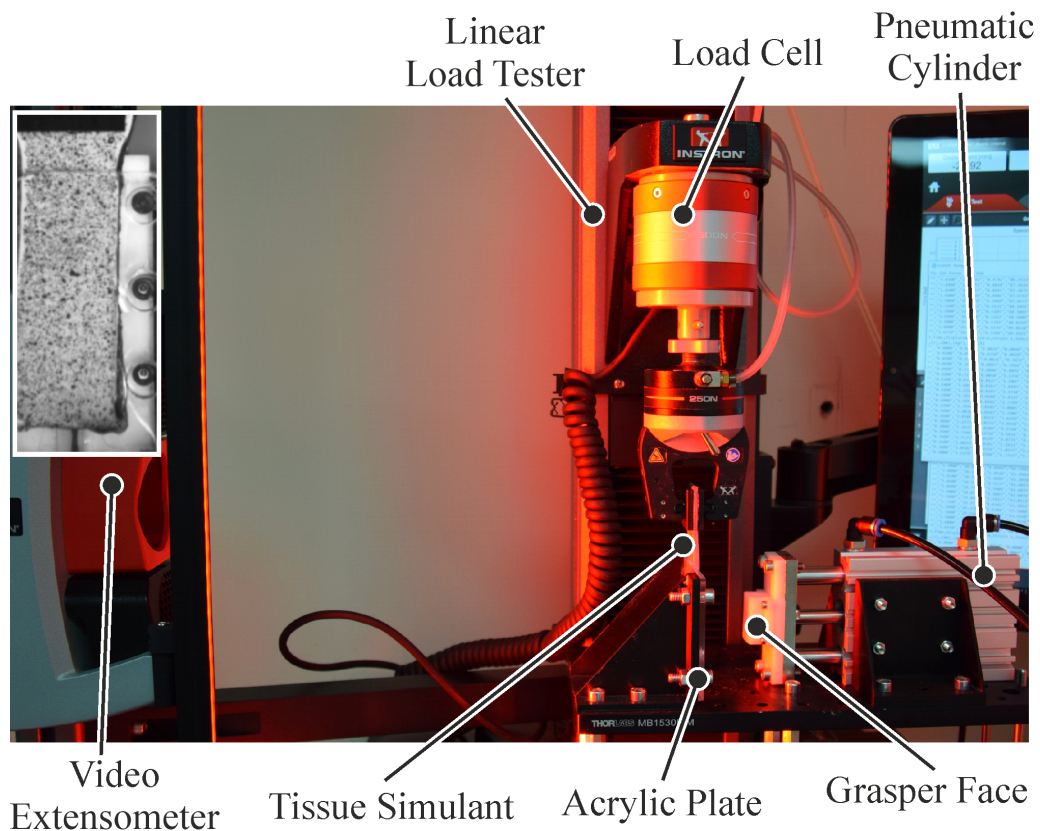


Figure 5.6: Image of the experimental set up used for simulating surgical grasping. Inset shows view of tissue simulant from video extensometer.

endpoint of a linear load tester (Instron 5940, Instron) which was then used to control retraction movements. The grasping face with integrated sensing elements was mounted onto a pneumatic piston controlled via a pressure regulator (MGPM20TF-75Z, SMC, & ITV1030, SMC) to apply controlled grasp force. The grasp force was pre-calibrated using a reference load cell with the regulator. Shear force and retraction speed were measured by the linear load tester and recorded using a real-time embedded controller (MyRIO, National Instruments). This controller also interfaced with the grasping sensor through the microcontroller, and implemented the control algorithm to vary the clamp force via the pneumatic regulator with a loop rate of 100 Hz. A clear acrylic sheet was used as the counter face of the sensed grasper to enable optical tracking of the tissue simulant deformation using a video extensometer (AVE2, Instron), which was analysed using Digital Image Correlation (DIC) software (GoM Correlate, GoM), images were captured at 50 Hz.

5.3.2 Experimental Parameters

Test parameters were defined to emulate regimes used in surgical practice and thus analyse the system over a range of representative conditions exploring the effects of retraction speed, tissue (mechanical) properties and grasping force. Retraction speeds of 1, 2 and 3 mm/s were selected based on those used for tissue manipulation [21], and two different stiffness tissue simulants Mat A (241 kPa) and Mat C (610 kPa) were analysed which had similar tensile elastic properties to liver tissue [22]. These tissue simulants consisted of three layers of silicone elastomer (Ecoflex 00-30, Smooth-on) reinforced with two layers of stretchable spandex fabric between them, 0.3 mm below the upper and lower surfaces. Samples were laser cut to form a $100 \times 20 \times 3$ mm sample. The tensile stiffness of different sample types was controlled through the choice of reinforcement fabric while the elastomer remained the same to provide comparable frictional and compressive properties. A speckle pattern was applied to one side of the simulant using enamel spray paint for tracking the displacement via DIC, and a layer of surfactant lubricant was used to emulate the serous fluid coating many soft tissues [23]. Grasping loads were varied between 10 N

and 30 N based on typical pressures reported for surgical grasping of soft tissues [24; 25]. The automated grasping system was compared to a baseline case using a fixed 30 N grasping force. The automated grasping system used an initial grasp force of 10 N to hold the tissue at the start of retraction with a 30 N upper limit (to match the baseline case). Tests were conducted to explore this experimental matrix in which 5 repeats were conducted for each unique configuration (2 control methods, 3 retraction speeds, 2 tissue simulants).

A secondary test was employed to assess the ability of the automated system to retract and then hold tissue. The tissue simulant was grasped, then two cycles of retraction (by 1.5 mm) followed by a hold were performed before a final retraction to the point of macro slip. 5 repeats were conducted for each test condition (2 control methods, 2 tissue simulants).

5.3.3 Data Processing

To compare the performance of the automated and fixed grasp methods, metrics were defined to capture the peak shear force achieved (i.e. representing the grasp holding performance) and the grasping energy used to achieve this outcome. For the latter, the impulse applied to the tissue simulant during grasping was calculated as a good indicator which relates to the probability of causing tissue trauma [26]. The Impulse (I) was calculated as follows,

$$I = \int_{t=0}^{t=M} F_c dt \quad (5.5)$$

where $t = 0$ is the start of retraction and $t = M$ is the time at which macro slip occurs as determined from the shear force (F_s).

$$\mathbf{if} \frac{dF_s}{dt} < 0.025V_s, t = M \quad (5.6)$$

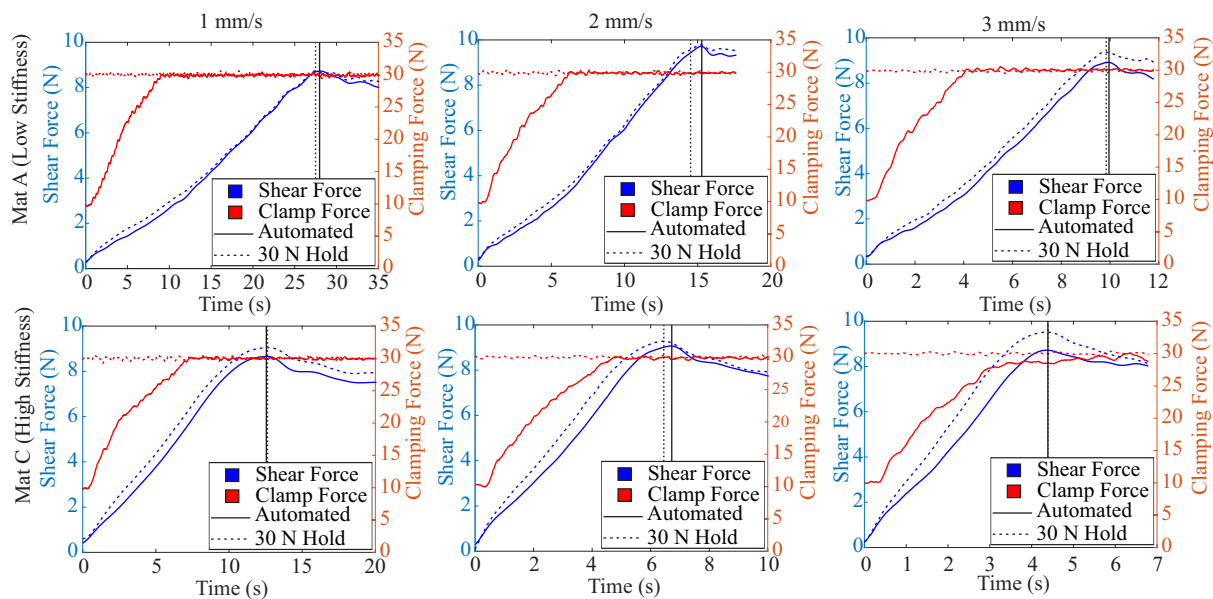


Figure 5.7: Typical grasping characteristics recorded for the automated and fixed test cases for variations in tissue simulant material stiffness and grasper retraction speed. Vertical lines indicated the point of macro slip.

5.3.4 Results

Figure 5.7 displays representative examples of the applied grasping forces and resultant shear forces for the automated and fixed grasper control methods for all the test conditions investigated.

Both control methods showed a similar pattern for the variation in shear force during the retraction process across all test cases, in which shear gradually increases as the tissue simulant is stretched until the point of global slip, as indicated on the graph. The automated system applies increasing grasp force as the shear force increases to maintain grip stability. This results in similar levels of maximum shear achieved for both methods as well as similar times of macro slip. These aspects are summarised in Figure 5.8 which shows the peak shear force and grasping impulse, up to the onset of macro slip.

Statistically significant differences ($P < 0.05$) were observed for the outcome measures when comparing the two control methods (excluding peak shear for Mat A at 2 mm/s). However, the maximum shear force observed using the automated control method was only marginally lower than for the fixed 30 N grasp case, but this was achieved with a substantial decrease in the Impulse applied to the tissue simulant. These differences were

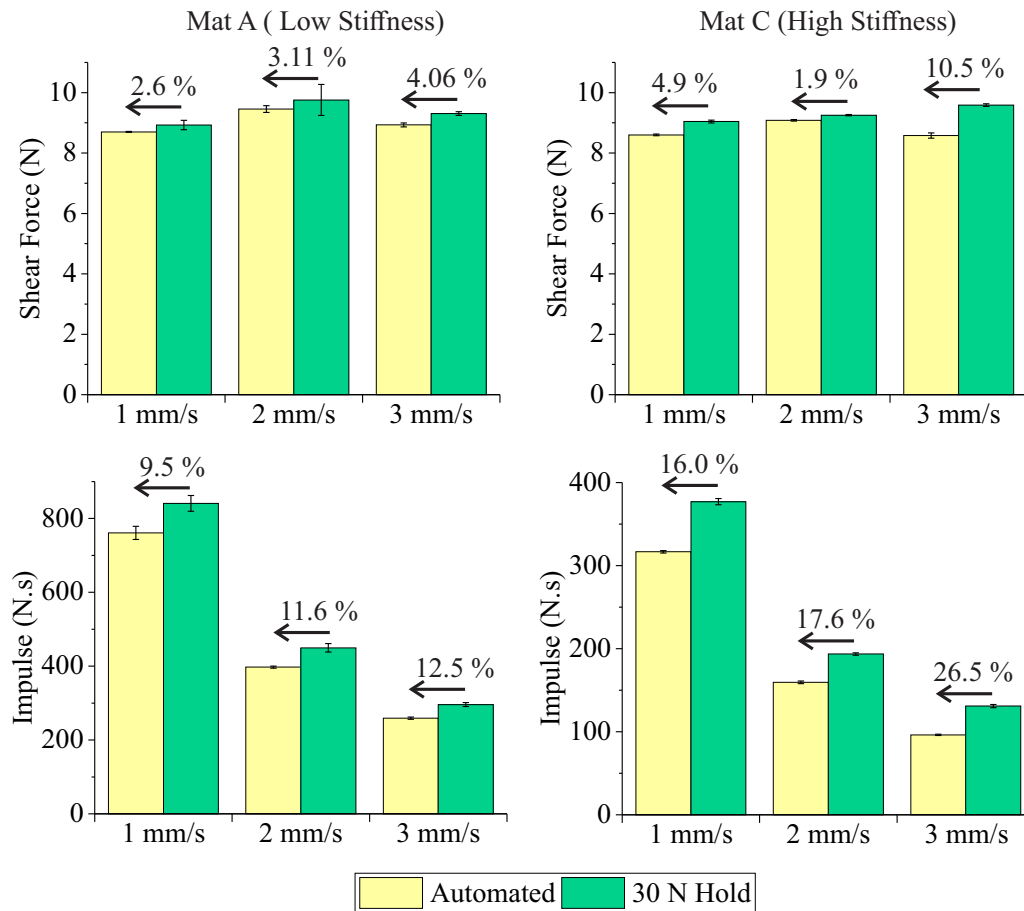


Figure 5.8: Summary of the results for the average maximum shear force and average impulse, between $t=0$ and the point of macro slip, across all test conditions. The percentages indicate the relative decrease in metrics between the 30N hold and automated test cases.

more profound for the higher stiffness material (Mat C).

Figure 5.9 examines the mechanics underlying this process, showing the deformation of the tissue simulant at the front, centre and rear of the grasper (see Fig. 5.2 for reference) as determined by the video extensometer and DIC analysis. For both the high and low stiffness tissue simulants, the automated control method shows similar behaviour to the fixed load grasp case, particularly at the centre and rear of the grasper. The tissue at the front islands slips slightly more in the automated case, with a peak difference of approximately 0.9 mm occurring during the early stages of retraction, reducing as the system increases towards maximum grasping load.

For 'retract and hold' procedures Figure 5.10 shows a typical response produced by the system in automated and fixed hold cases. While similar grasp forces are observed

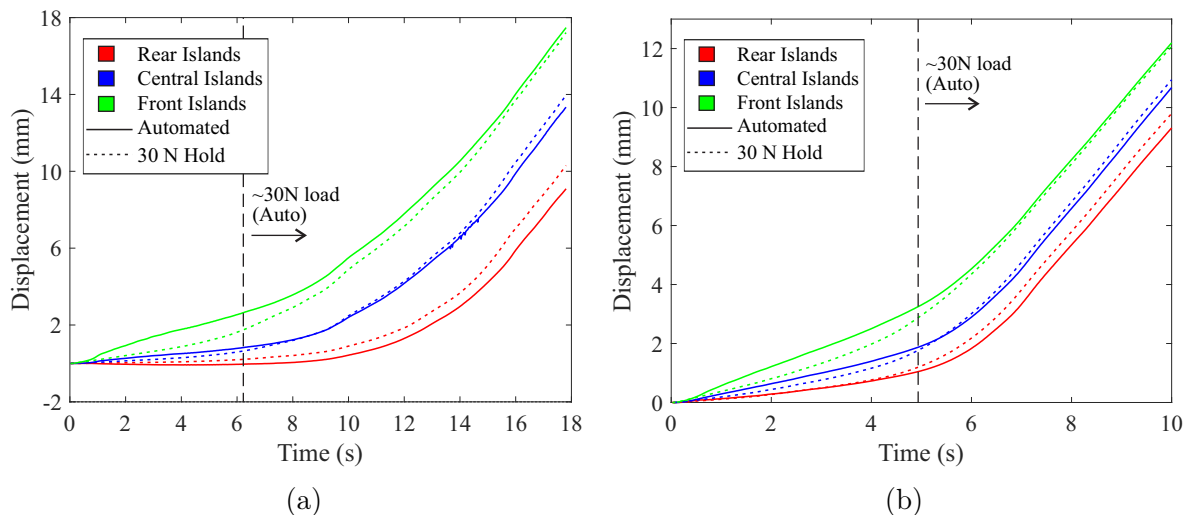


Figure 5.9: Representative displacement data for the tissue over the front, central and rear sections of the grasper, for the automated and non-automated control methods. The dashed vertical line indicates the point at which the automated system reaches the maximum 30N clamp force. (a) Low stiffness simulant (Mat A) with a 2mm/s retraction speed. (b) High stiffness simulant (Mat C) with a 2mm/s retraction speed.

throughout the process, the automated case achieves this using significantly lower clamp forces for the majority of the retraction.

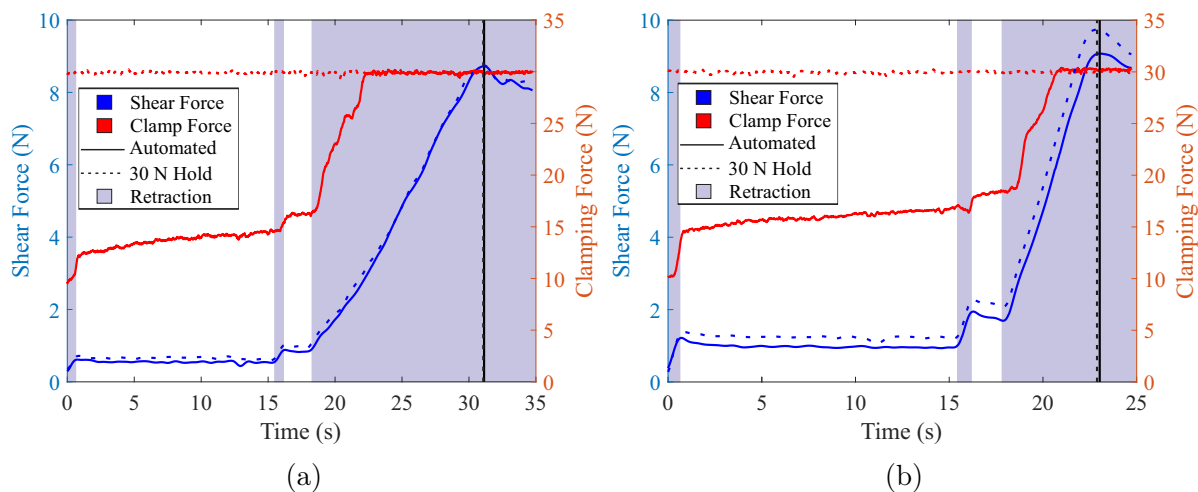


Figure 5.10: Typical force characteristics during a retract and hold of tissue simulant for: (a) Low stiffness simulant (Mat A). (b) High stiffness simulant (Mat C). The black vertical lines indicate the point of macro slip, whilst the purple shaded areas indicate when the tissue is being retracted at 2 mm/s.

5.4 Discussion

From the results gathered in this investigation it is evident that engineering a grasper to promote and detect incipient slips provides an effective basis for a system which conservatively regulates grasping force to prevent macro slip of tissue whilst minimising the applied grasp force during retraction.

Comparison of the shear forces required to induce macro slip in the automated and non-automated cases show less than 5% difference for the majority of cases despite significant variations in the material properties of the tissue simulant and the retraction speed applied (Fig. 5.8). The exception to this is the condition using a high stiffness material under a high retraction speed, where the automated system slips at 10.5% less shear load. This occurs when the grasp force plateaus before reaching the maximum load of 30 N because slip propagates rapidly through the material, such that slip occurs before mitigating action can be taken. This could be addressed by tuning either the automated controller gain (K) or the target slip ratio (ϕ_T), which requires a balance to be made between how rapidly the system responds versus its ability to minimise clamping force. Stiffer materials generally need higher gain and/or ϕ_T (lower bound) values to prevent slip occurring as they need either a faster (K) or earlier (ϕ_T (lower bound)) response to incipient slip events (Fig. 5.5), however after a certain point further increases in these values provides no further benefit to the system in preventing slip but will result in higher clamp forces being applied prematurely.

Using impulse as an indicator of the energy applied to the tissue simulant demonstrates that the automated control method brings a significant reduction in potential tissue trauma, especially in cases using the high stiffness tissue simulant. The sensor islands are positioned at the front edge of the grasper so they detect when slip occurs at that front edge and initiate a mitigating reaction. For high stiffness tissue, the front and rear of the grasper slip almost simultaneously [17], so the grasper reaches the maximum clamp load shortly before macro slip occurs, minimising the force applied over the retraction (Fig. 5.7). For the low stiffness material the slip propagation from front to back occurs more

gradually, so there is a significant amount of time before the tissue at the rear slips and the automated system remains at maximum load for longer resulting in less improvement in the impulse applied.

The differing performance (in terms of both grasp and input energy) for the automated system across the test cases suggests that there will be limitations in the operating conditions and tissue properties for which it is suitable. However, the current results do demonstrate a wide operating range which does not require tissue-specific thresholding methods for effective operation, a key to making these techniques more broadly applicable in surgical settings. The sensor's performance could also be improved by utilising an additional row of sensors at the rear of the grasper, enabling comparison of island movements between the grasper's front and rear, enabling an estimation of material stiffness and the speed of slip propagation. Both of these attributes could then be fed into the control system to optimise grasp force accordingly.

The tissue deformation under grasping observed using DIC techniques further validates the efficacy of the incipient sensing approach and the automated control method, as for both materials there is a high correlation between the automated and fixed grasp results. During the initial retraction period there is slightly more displacement at the front islands when using the automated case as less clamp force is being applied. However the adjustment made by the automated system prevents the slip propagating any faster than in the fixed hold case, resulting in near identical grasping performance, despite significantly reduced load being applied to the tissue simulant during this manoeuvre.

The system has also been demonstrated to perform effectively when conducting a 'retract and hold' of the tissue simulant, resulting in similar holding performance with significantly lower clamping forces compared to a fixed load approach (see Fig 5.10). A gradual increase is evident in the clamping force during the hold phase, a result of sensor noise on the velocity measurements causing small incremental increases in force, though further refinement of the current algorithm is being developed to mitigate these effects. However, the results presented here for short grasp and retract procedures represent those in which

the system could provide the most benefit; in shorter retractions only a fraction of the maximum possible clamp force is required to prevent slip, therefore the automated grasping system presented here could enable a significant reduction in the overall clamp forces applied, reducing the probability of causing tissue damage due to the over application of force [2; 26].

5.5 Conclusions and Further Work

This study demonstrates the efficacy of using a segmented incipient slip sensor as the basis for improving the automated grasping of soft tissues in surgery during tissue retraction. Results from the evaluation of the system show this method provides the possibility for improving surgical outcomes by reducing the forces applied to tissues during retraction whilst still maintaining a similar gripping performance to using a maximal grasping force. The system proved capable over a range of materials and retraction speeds representative of surgical conditions, though the results indicate there will be limitations to the range of materials for which the system will provide a performance benefit. Analysis of the system's performance highlighted how the system can be further developed to broaden its operating range. Further work will consider evaluation of the system performance in ex-vivo tissue samples and working to miniaturise the sensing technology for future integration into a surgical grasper.

References

- [1] Daniel M Herron and Michael Marohn. Prepared by the SAGES-MIRA Robotic Surgery Consensus Group. page 24, 2006.
- [2] B. Tang, G.B. Hanna, and A. Cuschieri. Analysis of errors enacted by surgical trainees during skills training courses. *Surgery*, 138(1):14–20, July 2005.
- [3] E.A.M. Heijnsdijk, J. Dankelman, and D.J. Gouma. Effectiveness of grasping and duration of clamping using laparoscopic graspers. *Surgical Endoscopy*, 16(9):1329–1331, September 2002.
- [4] C.-H. King, M.O. Culjat, M.L. Franco, C.E. Lewis, E.P. Dutson, W.S. Grundfest, and J.W. Bisley. Tactile Feedback Induces Reduced Grasping Force in Robot-Assisted Surgery. *IEEE Transactions on Haptics*, 2(2):103–110, April 2009.
- [5] C.-H. King, M.O. Culjat, M.L. Franco, J.W. Bisley, G.P. Carman, E.P. Dutson, and W.S. Grundfest. A Multielement Tactile Feedback System for Robot-Assisted Minimally Invasive Surgery. *IEEE Transactions on Haptics*, 2(1):52–56, January 2009.
- [6] Verena Nitsch and Berthold Farber. A Meta-Analysis of the Effects of Haptic Interfaces on Task Performance with Teleoperation Systems. *IEEE Transactions on Haptics*, 6(4):387–398, October 2013.
- [7] Natalie T. Burkhard, J. Ryan Steger, and Mark R. Cutkosky. The Role of Tissue Slip Feedback in Robot-Assisted Surgery. *Journal of Medical Devices*, 13(2):021003, June 2019.
- [8] Guang-Zhong Yang, James Cambias, Kevin Cleary, Eric Daimler, James Drake, Pierre E. Dupont, Nobuhiko Hata, Peter Kazanzides, Sylvain Martel, Rajni V. Patel, Veronica J. Santos, and Russell H. Taylor. Medical robotics—Regulatory, ethical, and legal considerations for increasing levels of autonomy. *Science Robotics*, 2(4):eaam8638, March 2017.

-
- [9] Seyed Mohsen Khadem, Saeed Behzadipour, Alireza Mirbagheri, and Farzam Farahmand. A modular force-controlled robotic instrument for minimally invasive surgery - efficacy for being used in autonomous grasping against a variable pull force: Modular force-controlled robotic instrument. *The International Journal of Medical Robotics and Computer Assisted Surgery*, 12(4):620–633, December 2016.
- [10] D Jones, A Alazmani, and P Culmer. A Soft Inductive Tactile Sensor for Slip Detection Within a Surgical Grasper Jaw. page 4, 2019.
- [11] Natalie T. Burkhard, Mark R. Cutkosky, and J. Ryan Steger. Slip Sensing for Intelligent, Improved Grasping and Retraction in Robot-Assisted Surgery. *IEEE Robotics and Automation Letters*, 3(4):4148–4155, October 2018.
- [12] K. L. Johnson. *Contact mechanics*. Cambridge University Press, Cambridge Cambridgeshire New York, 1987.
- [13] Jeffrey Stoll and Pierre Dupont. Force Control for Grasping Soft Tissue. page 4, May 2006.
- [14] Wei Chen, Heba Khamis, Ingvars Birznieks, Nathan F. Lepora, and Stephen J. Redmond. Tactile Sensors for Friction Estimation and Incipient Slip Detection – Towards Dexterous Robotic Manipulation: A Review. *IEEE Sensors Journal*, pages 1–1, 2018.
- [15] M.R. Tremblay and M.R. Cutkosky. Estimating friction using incipient slip sensing during a manipulation task. In *[1993] Proceedings IEEE International Conference on Robotics and Automation*, pages 429–434, Atlanta, GA, USA, 1993. IEEE Comput. Soc. Press.
- [16] Filipe Veiga, Jan Peters, and Tucker Hermans. Grip Stabilization of Novel Objects using Slip Prediction. *IEEE Transactions on Haptics*, pages 1–1, 2018.
- [17] Ian Waters, Ali Alazmani, and Peter Culmer. Engineering incipient slip into surgical graspers to enhance grasp performance. *IEEE Transactions on Medical Robotics and Bionics*, pages 1–1, 2020.

- [18] Heba Khamis, Raquel Izquierdo Albero, Matteo Salerno, Ahmad Shah Idil, Andrew Loizou, and Stephen J. Redmond. PapillArray: An incipient slip sensor for dexterous robotic or prosthetic manipulation – design and prototype validation. *Sensors and Actuators A: Physical*, 270:195–204, February 2018.
- [19] Joseph C. Norton, Jordan H. Boyle, Ali Alazmani, Pete R. Culmer, and Anne Neville. Macro-Scale Tread Patterns for Traction in the Intestine. *IEEE Transactions on Biomedical Engineering*, 67(11):3262–3273, November 2020.
- [20] Dominic Jones, Lefan Wang, Ali Ghanbari, Vasiliki Vardakastani, Angela E. Kedgley, Matthew D. Gardiner, Tonia L. Vincent, Peter R. Culmer, and Ali Alazmani. Design and Evaluation of Magnetic Hall Effect Tactile Sensors for Use in Sensorized Splints. *Sensors*, 20(4):1123, February 2020.
- [21] Ali Alazmani, Rupesh Roshan, David G Jayne, Anne Neville, and Peter Culmer. Friction characteristics of trocars in laparoscopic surgery. *Proceedings of the Institution of Mechanical Engineers, Part H: Journal of Engineering in Medicine*, 229(4):271–279, April 2015.
- [22] Andrew R Kemper, Anthony C Santago, Joel D Stitzel, Jessica L Sparks, and Stefan M Duma. Biomechanical Response of Human Liver in Tensile Loading. page 12, January 2010.
- [23] W. Schwarz. The surface film on the mesothelium of the serous membranes of the rat. *Zeitschrift fr Zellforschung und mikroskopische Anatomie*, 147(4):595–597, 1974.
- [24] Andrew W. Brown, Stuart I. Brown, Donald Mclean, Zhigang Wang, and Alfred Cuschieri. Impact of fenestrations and surface profiling on the holding of tissue by parallel occlusion laparoscopic graspers. *Surgical Endoscopy*, 28(4):1277–1283, April 2014.
- [25] Phillip Mucksavage, David C. Kerbl, Donald L. Pick, Jason Y. Lee, Elspeth M. McDougall, and Michael K. Louie. Differences in Grip Forces Among Various Robotic

- Instruments and da Vinci Surgical Platforms. *Journal of Endourology*, 25(3):523–528, March 2011.
- [26] A. I. Margovsky, R. S. A. Lord, and A. J. Chambers. The effect of arterial clamp duration on endothelial injury: An experimental study. *ANZ Journal of Surgery*, 67(7):448–451, July 1997.

5.6 Appendix

Additional DIC Results

To allow comparison between the automation results for the front to back method, presented in chapter 3, and the side to side method presented in chapter 5, this appendix provides additional DIC results to allow for direct comparison under the same loading and retraction conditions.

Figure 5.11 presents results for the tissue displacement measured using DIC, comparing the effect of different materials and retraction speeds for the automated and fixed load control methods, for a full explanation of the system design and test methods see Sections 5.2 and 5.3. For all cases the central and rear islands maintain almost identical displacements for the fixed load and automated control methods throughout the full retraction, indicating that they have a similar grasp performance in terms of slip prevention, and that the automated method is maintaining similar control whilst utilising less force over the full range of test conditions investigated.

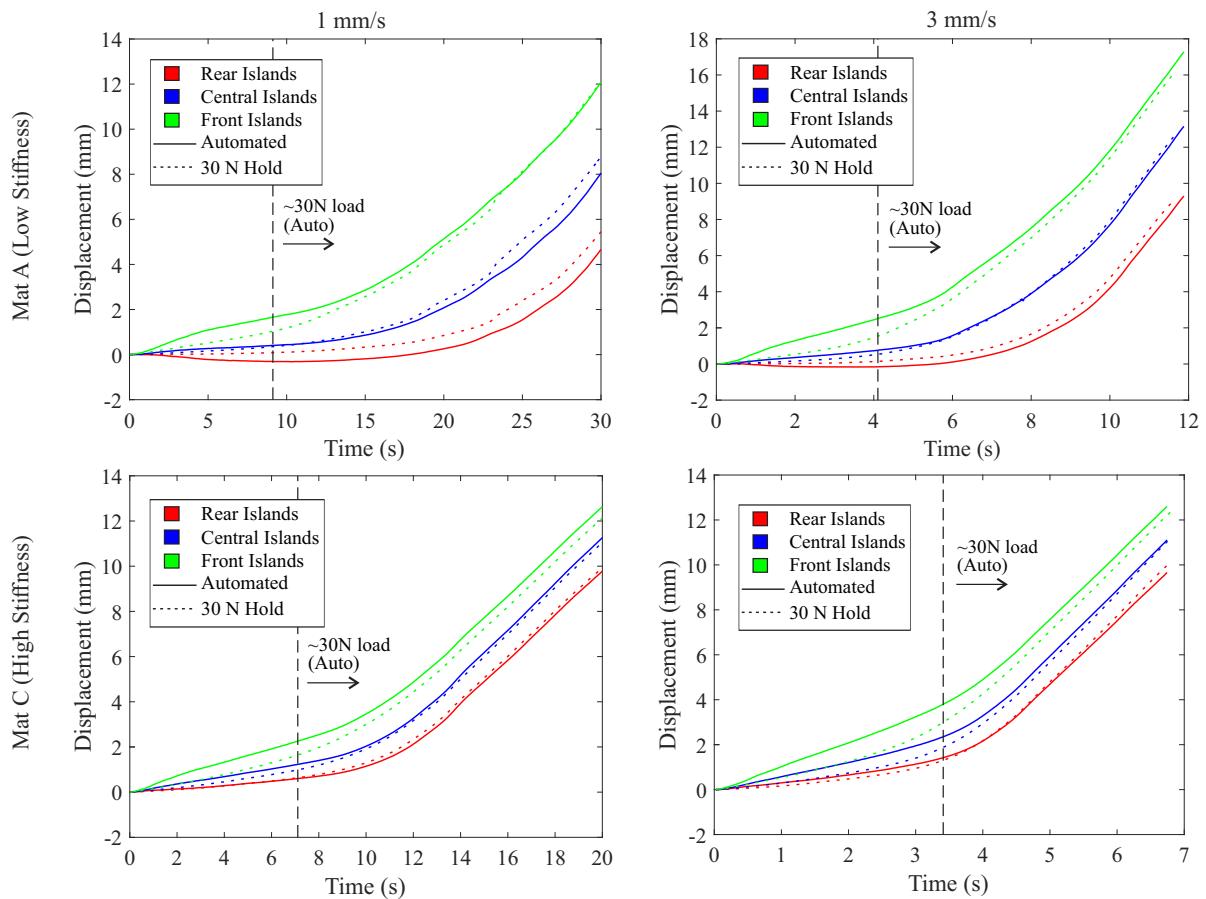


Figure 5.11: Representative displacement data for the tissue over the front, central and rear sections of the grasper, for the automated and non-automated control methods, for variations in material stiffness and retraction speed. The dashed vertical line indicates the point at which the automated system reaches the maximum 30N clamp force.

Chapter 6

Discussion and Conclusions

6.1 Introduction

The work in this thesis explores two approaches for the creation and detection of preferential incipient slips during surgical manipulation of soft tissue, with the aim of preventing tissue slip, whilst also reducing the clamp forces to try and minimise tissue trauma. Each approach utilises a different phenomenon to generate these slips:

- **Front to back method** - This method utilises the deformable behaviour of the grasped tissue to create a slip differential between the front and rear of the grasper face, due to the propagation of slip along the grasper length, as the material towards the front of the grasper has to slip and displace, before that behind can move.
- **Side to side method** - This method creates a distribution in the normal force across the width of the grasper, via a curved grasper face, thus creating a variation in the frictional forces, leading to preferential incipient slips occurring towards the outer edge of the grasper first.

Both of these approaches have been demonstrated to be successful at preferentially inducing, and detecting, incipient slip events before the occurrence of macro slip, when grasping soft, lubricated, deformable materials, similar to biological tissues encountered during surgical procedures. In addition they have been employed to automate the force control during the grasping action, providing similar grasp performance, in terms of slip prevention, to a grasper utilising the maximum grasping load throughout, whilst reducing the clamping forces applied during the retraction. The results gathered indicate these sensing approaches could be an effective way to avoid tissue slip, and reduce tissue trauma caused by excessive grasping loads. The side to side method, based on varying the normal force across the surface, has also been demonstrated to be effective at detecting incipient slip events when manipulating porcine liver tissue, despite no additional optimisation of the system for this material.

It should be noted that the slip detection approaches developed within this thesis are not limited to the sensor technologies that have been utilised to demonstrate them. Although

magnetic and SITS sensors were selected for these particular instrumented graspers there are possibly more optimal solutions. However, the methodologies of how incipient slip can be induced, either using the tissues deformable properties, or through varying the distribution of normal force, are transferable to a variety of sensing technologies that could then be employed for the automatic detection and mitigation of tissue slip events.

This chapter will compare the two slip sensing approaches developed in terms of their efficacy for the early detection of slip events, as well as their feasibility for transfer towards application within surgical practice. They will then be evaluated against alternative slip sensors developed for the detection of tissue slip during robotic surgery, and linked back to the theory of slip mechanics. The research objectives will then be reviewed, before detailing the future work now required to progress the presented methodologies towards their application in actual surgical practice.

6.2 Comparison of Developed Slip Sensing Methods

The key metric for comparing the ability of the two sensor systems to detect slip early is the available mitigation time (See Fig. 3.6 & 4.6), which gives an indication of how early the system can identify a slip event. As the retraction speed influences both sensors in a similar and predictable manner, with the retraction speed and mitigation time being inversely proportional to each other, only the results for variation of the material stiffness and clamping force will be compared during this evaluation.

Analysis of the data presented indicates that the side to side method, based on varying the normal force distribution to induce incipient slips, is more robust and reliable, accurately detecting incipient slip in all test cases investigated before the occurrence of macro slip. In comparison, the system based on utilising the deformable nature of the tissue to produce incipient slips was unable to detect slip reliably in one test case, when grasping the high stiffness tissue simulant (Mat C), under a low clamping load (10 N). This is because the normal force based method is significantly less reliant on the tissue's tensile properties to create a slip differential. The side to side method also creates higher available mitigation

times in all cases, ranging from, on average, an additional 0.74 s in the worst case, and up to 2.35 s in the best case (for a retraction speed of 2 mm/s). This is because the slip propagation rate for both methods is similar (See Fig. 2.4), but the curved surface forces the outer edges to slip preferentially, approximately 1-3 seconds before the front middle island slips (Fig. 4.6).

Comparison of the ability of both systems to automate the grasping action is only possible for the low stiffness test case (Mat A), using the slowest retraction speed (1 mm/s), as limited tests were conducted for the front to back method. Both methods produced comparable performance in terms of slip prevention, with similar times of macro slip, and similar shear forces required to induce it (See Fig.3.8 & 5.7). However, the front to back method, which utilises the tissue's deformable properties to create slip differentials, produced a more significant reduction in the applied impulse (23.0%), compared to the normal force variation based method (9.5%). This indicates that this system is using less force in the earlier stages of retraction to maintain control, thus reducing the probability of tissue damage [1]. This is because the normal force based method is detecting incipient slips earlier, thus increasing grasp forces, and achieving the maximum clamp force, earlier. This earlier reaction to slip does result in better, more stable control of the grasped tissue, with lower tissue displacement and slip towards the rear of the grasper for the same global displacement (See Fig.3.9 and 5.11), especially during the earlier stages of retraction before the maximum clamp load is reached.

The other major aspect for comparison of these two systems is an assessment of how feasible it would be to implement them within surgical practice. Currently the major barrier to employing both these sensors in a robotic surgical device is the ability to package them within the small form factor required for a robotic surgical grasper (8 mm wide x 10-20 mm in length), as they are currently over double the width. However, with current sensing technologies it would be possible to position at least two magnetic hall effect sensor nodes (MLX90393, Melexis), along the length of the grasper, making it possible to detect slip differentials between the front and rear of the grasper, as required for the front to back method. In comparison, fitting 3 displacement sensors across the

width of a robotic surgical grasper, for sensing incipient slips caused by the variation of normal force, currently seems much less feasible, though recent advances in magnetic sensing technology might make it possible in the near future [2].

As well as the issue with the scale of the grasper designs the current lab based investigations are very idealised. The manipulation of tissue during retraction currently only occurs parallel to the grasper jaws, whereas in surgical practice there will be additional lateral and rotational motions that the sensor system, and control algorithm, will need to be able to account for. Due to the larger number of islands, separated along 2 axis, of the side to side sensor, it is suspected that with some further optimisation of the control algorithms this method would be much more robust to these additional movements, as it could be adapted to sense incipient slips both laterally and longitudinally along the grasper face, though further work is required to confirm this.

In summary, the side to side method, based around normal force variations, provides a more reliable and robust method for detecting incipient slip across the full range of test conditions investigated, and has also been successfully demonstrated for the early detection of slip when grasping porcine liver tissue. However, when used for the automation of the grasping action the front to back method and sensor, based on utilising the deformable properties of tissue to create incipient slip, applied lower forces during the early retraction, whilst producing a similar time of macro slip. This occurred because the reaction of the normal force based sensor was premature for the low stiffness material, which has a slow slip propagation. In other cases though, for example with higher stiffness materials, this might be preferable, as a faster, more immediate response, is required to cope with the high rate of slip propagation. Ultimately a combination of the two methods would likely provide a more effective slip sensing system than either in isolation. The sensors at the front and rear of the grasper could be used to estimate how fast slip is propagating, then the controller can use this information to determine how aggressively the system should respond to incipient slips, when they are detected across the width of the curved grasper face by the side to side method. However, due to technology miniaturisation issues this may not be currently feasible, though work is ongoing to try and overcome

these manufacturing limitations.

6.3 Comparison With Alternative Slip Sensing Systems

Although there is a variety of slip sensing systems this comparison will only focus on those with surgical applications, as the grasping and slip of soft, deformable, lubricated materials is significantly different from the grasping of rigid objects, which the large majority of non surgical systems are focused towards.

To date the most developed grasper slip detection system for robotic surgical applications, within research, is that created by *Burkhard et al.* [3]. This sensor uses a technology based on hot-wire anemometry to monitor variations in heat flux as an indicator of the magnitude, and direction, of tissue slip. This system has been successfully integrated within a robotic surgical grasper, comparable in size to industry standards, and has been demonstrated to be effective at detecting slip for a variety of porcine tissues. In addition, it has been proven to help reduce the occurrence of tissue slip events during a representative manipulation task, when employing trained surgeons on a commercially available robotic surgical platform.

Although direct comparison with this system is challenging due to the different analysis methods used, there are several fundamental differences between the two sensing methods that have been identified. Firstly, the thermal based slip sensor has no moving parts to it, unlike our incipient slip sensors, this helps to simplify manufacturing, and likely reduces the probability of failure during use, which could result in serious complications if grasper islands/parts are lost within the body. There is also likely to be less perceived input lag, due to the moving silicone base below the rigid upper gripper surface (See Fig. 3.2 & 4.2). During the initial stages of retraction the silicone base and island will also move, therefore the expected tissue movement might be slightly delayed from the surgeon's point of view, however, further work is required to understand if this will be an issue in-situ. The second major difference is the number of sensing nodes utilised, the additional nodes across the surface, combined with the grasper design, allow the sensors presented

in this thesis to detect slip earlier, as well as provide a greater understanding on the rate of the slip propagation to the controller. This can help to improve how the control algorithm reacts to slip events, reducing the occurrence of tissue movement, allowing greater control to be maintained. However, utilising multiple sensing nodes does increase the manufacturing challenge of trying to fit multiple sensors within a surgical graspers small form factor. Lastly, the sensor from [3] requires direct contact between the sensing elements and the tissue being grasped, whereas for two sensor designs presented in this thesis the circuitry for the sensor elements (hall effect sensor/SITS coils) can be kept isolated from the biological tissue, and only the magnets/copper disc targets are exposed to the biological tissue and the possibility of fluid ingress. This not only helps to protect the circuitry during surgery, but also makes sterilisation simpler, allowing graspers to be more readily utilised for multiple operations.

One possible interesting solution to detecting slip would be to combine the two technologies, utilising the thermal sensor from [3], but with multiple nodes positioned along the length of the grasper. This could allow for a sensor system with no moving parts, that can detect slip events early, and if metal pillars are used to conduct heat between the sensing elements and the tissue, and vice versa, then it might also be possible to minimise their exposure to the biological environment too.

The only other significant surgical slip sensing system identified in literature is that developed by *Khadem et al.* [4]. This system utilises a load cell, contained within the joint actuation unit, to measure the grasping forces via the tension in the cable, and a 6 DoF force/torque sensor at the interface between the robot arm and tool, to monitor the retraction forces. The gripping force is adjusted depending on the current retraction force to remain within a predefined safe grasping zone to prevent slip. The main disadvantage of this system, compared to the approaches presented here, is that it requires significant prior knowledge of the tissue being manipulated, and so is unable to adjust to new tissues, or variations in the operating environment e.g. fluid varying the frictional properties. However, it does offer one major benefit over our systems, in that all of the sensors and electronics are external to the patient's body, making it much easier to integrate with

current robotic surgical platforms, and simplifying the instrument sterilisation process.

6.4 Evaluation against the Mechanics of Slip Theory

The results were also assessed in relation to the theory around the mechanics of how slip initiates, and then progresses, that the grasper designs were based on. This was done to ensure that the grasper faces were performing as intended, through comparing them to the theories around which they were designed.

Amanton's law states that the frictional force is only proportional to the normal force, and the coefficient of friction. The Convex grasper face, where the normal force is varied using a curved surface (similar to a Hertzian contact), clearly follows this law as can be seen from the results in figures 2.4 & 2.5. The colour maps show significantly more slip towards the outer edges, where the normal forces, and therefore frictional forces, are lower, as intended, based on Amanton's law. However, a similar but much smaller level of displacement is also observed towards the outer edge of the flat All Hex grasper face, despite the normal force and CoF being the same across the full grasper face. This is the result of edge effects, the unclamped tissue outside the area of the grasper face has no friction acting on it, and so is free to move, the movement of this unconstrained tissue outside the grasper causes shear forces to propagate to the tissue at the edge of the grasper-tissue contact quicker than for the rest of the grasper contact, leading to slightly more displacement towards the outer edge.

The results from the sensors in the Convex instrumented grasper (Fig. 4.5) show a similar agreement with Amanton's law, with the left and right sensed islands, where the normal forces are lower, slipping before the centre island. The results from the liver samples also show a similar expected correlation, but due to the uneven thickness of the porcine liver samples one edge of the sample can slip significantly before the other.

The Centre-hex grasper face also shows the expected relationship with Amanton's law. The smooth unpatterned areas towards the outer edge, where the CoF is much lower, slip before the central section, displayed by the clear curve in the colour map in figure 2.4.

The other major theory that governs slip is Coulomb's model of friction, which states that the frictional force is independent of the sliding velocity, when the contact is slipping. So once macro slip occurs, given that the normal force remains constant, the frictional force should also remain constant. Therefore after macro slip the sensor displacement should remain stable. However, several of the results do not appear to follow this model. Towards the end of some of the retractions (Fig. 3.5 & Fig. 4.5), there is a rapid increase in the front sensors island displacement, not in line with the Coulomb model. This is caused by the tissue slipping off the rear islands, as shown in figure 3.5, where the displacement of the rear island starts to rapidly decrease as the front island's displacement increases. When the tissue starts to slip off the rear island the contact area decreases resulting in an increase in the normal force acting on the remainder of the grasper contact, thus increasing the frictional force. Given that the retraction velocity is constant the shear force acting on the front islands will therefore also increase, increasing the strain on the moveable silicone elastomer of the grasper islands, thus increasing their displacement.

6.5 Assessment of Research Objectives

Section 1.3 detailed several research objectives, below is a summary of how each of these was addressed:

Develop a system for simulating the surgical grasping and retraction of tissue, that is capable of directly monitoring the tissue slip occurring at the grasper face

A simulated surgical grasper was developed that was able to robustly and repeatedly reproduce the clamping and retraction of tissue, and tissue simulants, with representative retraction speeds and force control. In addition the analysis method for directly monitoring tissue slip, using digital image correlation, provided a reliable indication of the tissue slip and movement occurring across the entirety of the surface, helping to provide a good understanding of the basic slip mechanics. The tissue simulants developed also provided a repeatable test sample that allowed for easy comparison between various methods and

grasper faces, whilst providing a similar enough representation of biological tissues for the development of the methods towards its end use case in surgery. However, there were several limitations of this system, the grasping action was parallel rather than scissored, like a standard surgical grasper, and the system could only reproduce retractions in a direction directly parallel to grasper, whereas in surgical practice there will be additional lateral and rotational motions involved in tissue manipulation.

Investigate the slip mechanics of soft, lubricated, deformable materials like tissue, and how variations in grasper design can influence the development of incipient slips

Two different methods of inducing incipient slip were investigated, varying the normal force across the surface, and varying the coefficient of friction across it, both of these were based on Amanton's law of friction. Analysis of these identified that the variation of the normal force produced much better results for inducing incipient slip, as the variation of the coefficient of friction reduced the overall coefficient of friction too much, affecting the overall grip performance. An additional method of inducing incipient slip was also identified from this work, due to the deformable nature of soft tissue the tissue towards the front of the grasper has to move and deform first before the tissue behind can start to move, creating a slip differential between the front and rear that can be monitored.

Utilising the knowledge of slip mechanics develop an instrumented grasper(s) capable of inducing and then detecting incipient slip of soft tissues

Two novel slip sensors were created to monitor the two different slip phenomena identified in the slip mechanics investigation. The first of these looked to detect the slip differential between the front and rear of the grasper, caused by the tissue's deformable properties. The second used a curved surface to create a normal force distribution across the width to induce slips towards the outer edges. Both of these graspers used a series of independent moveable islands, with sensors placed under specific islands, to allow slip differentials of the tissue across the surface to be monitored. They were both able to reliably detect slip well before macro slip occurs over a range of test conditions that simulated surgical

grasping and retraction tasks. The sensor system developed that employed the variation of normal force was found to be more robust, detecting slip earlier and across a greater range of test conditions, specifically those utilising higher stiffness tissue simulants. This system was also demonstrated to be effective at detecting incipient slip of porcine liver tissues.

Develop an algorithm for the automatic detection and mitigation of slip events during robotic surgery, and demonstrate its ability to reduce the forces applied to tissue during grasping, whilst preventing the occurrence of slip

For both sensor systems separate automation algorithms were developed. For the front to back sensor there is a simple fixed step change in the clamp force whenever incipient slip is detected, whilst the side to side sensor uses a proportional control to maintain a consistent ratio between the velocity of the sensor islands at the edge and the middle of the grasper, so that they are both moving with the tissue at a similar speed. Both systems were successfully demonstrated for use in automating the force control of the grasper, producing similar grasp performance to a grasper applying the maximum clamp force, in terms of the time of macro slip and the shear force required to induce it, whilst using lower gripping forces during the early stages of retraction, likely reducing the occurrence of tissue trauma. The automated front to back system appeared to apply much lower impulse during the retraction, but it is suspected this is largely because the side to side grasper detects slip, and thus reacts, much earlier, providing more control and less tissue displacement early in the retraction, but slightly increasing the possibility of tissue trauma.

6.6 Future Work

Although the work presented here provides, and demonstrates, two promising concepts for the early detection of slip events during robotic surgery, there is still an extensive amount of work required to progress these systems to a point that they could be effectively utilised within surgical practice. The next major stages of development are detailed below:

- **Integration within a robotic/laparoscopic grasper** - This is currently the most significant barrier to these technologies. Although the developed sensors provide a strong proof of concept, they are significantly larger than a standard robotic surgical grasper, and utilise a parallel, rather than a scissor motion, to grasp tissue. For detecting slip differentials between the front and rear of the grasper, caused by the deformable properties of the tissue, commercially available sensors could easily be integrated into a standard robotic surgical grasper, with sufficient nodes, to make early slip detection possible. This would then make it possible to test the sensor system and sensing method at the correct scale, whilst also utilising the scissor motion for grasping. However, as stated previously, fitting sufficient sensing nodes across the width of the grasper, to detect incipient slips caused by variation of the normal force distribution, is currently unfeasible. Further miniaturisation and development of displacement sensing technologies is required before a to scale grasper for this method can be developed.
- **Expanded tissue testing** - To date only porcine liver samples have been trialled with one of the sensing methods (side to side method). Although these results were very promising, a much wider set of tissue testing is now required to fully understand the limitations and capabilities of the grasper systems. Results already demonstrate that both methods are sensitive to tissue properties, with the front to back method being heavily influenced by changes in the tensile properties of the tissue, whilst the side to side method can encounter issues if the tissue doesn't compress sufficiently for the islands at the outer edges of the grasper to engage sufficiently.
- **Investigation of more complex manipulation tasks** - The current testing set up only evaluates the sensor's performance when the direction of retraction is directly parallel to the grasper jaws. However, during surgery there will be significantly more lateral and rotational movement than the sensor, and the associated slip detection algorithms, will need to be able to account for. The current test rig will need to be adapted so that different slip/retraction directions can be properly

assessed, before the system is then trialled on more representative surgical manipulation tasks e.g. peg to peg and phantom organ manipulation tasks [5].

- **Improvement of detection and control algorithms** - Although the detection and mitigation algorithms developed are effective, there is still significant room for improvement. The sensors utilised have the ability to detect motion in three axis, but currently only one of these is utilised for slip detection. Monitoring these extra axes of movement could provide additional useful information that dictates how the system detects or reacts to slip. For example, as stated in Chapter 4, the displacement in the z direction, normal to the grasper face, could provide an indication of the level of sensor island engagement to help dictate which sensors should be given priority during slip detection. The combination of the two methods developed, as discussed in Section 6.2, could also be utilised to improve how the system reacts to slip events, employing knowledge of both the slips across the width, as well as the rate of slip propagation, to improve the way in which the system chooses to mitigate slip events. In addition the slip detection algorithms utilised both rely on the use of basic threshold monitoring to identify when slip is starting to occur, an alternative option would be to try and utilise machine learning and pattern recognition to predict when incipient slip is about to occur, as there could be other indicators within the sensor signals that it is not possible for humans to identify. However machine learning does involve some major complications with this particular scenario, as gathering sufficient training data that has a clearly defined slip indicator for the localised slips is very challenging.
- **Develop a more reliable method of understanding the "ground truth"**- Although the current DIC method gives a good indication of when different areas of the tissue first start to slip, the results are still not directly comparable to the sensor measurements. The DIC is monitoring slip at the opposite face of the tissue to the instrumented grasper, where the tissue is only gripped against a low friction acrylic plate. This smooth counter-face will slip before the tissue that is gripped by the instruments grasper, meaning there is a small disconnect between the DIC

measurements and the sensor data. One method of overcoming this disconnect is through investigating how tissue slips when grasped by a completely smooth instrumented grasper, as there would be minimal difference in the initiation of tissue slip between the two opposing faces as they would both have similar coefficients of friction.

- **Investigate other application routes** - The main focus of this research was towards the development of a slip sensor for use in the grasping and manipulation of soft biological tissues during robotic surgery. However, the large majority of research into slip sensors in general has focused on the grasping of non-deformable, dry rigid objects [6]. The sensor presented here could have a range of other use cases in addition to surgery, for the more generalised grasping of soft deformable materials, investigation into alternative applications could find a variety of fields that this system could be applied to, e.g. food processing and agriculture.

6.7 Conclusions

The research presented here demonstrates two possible concepts for the detection, and mitigation, of tissue slip events during surgery. The slip mechanics of soft, wet, deformable materials, similar to biological tissues, were first evaluated, this then formed the basis for the two sensing approaches developed. Two prototype grasper faces were produced that operated off the two slip phenomena identified from the slip mechanics study. The first sensor employed the deformable properties of the tissue to create a measurable slip differential between the front and rear of the grasper, whilst the second used a curved grasper surface to create a variation in the normal, and thus frictional, force across the width of the grasper face, leading to the outer edges slipping preferentially. The efficacy of both of these methods for the detection and automatic mitigation of slip has been successfully demonstrated using silicone tissue simulants, with the latter also proven effective for slip detection of porcine liver samples too. The method looking to detect incipient slip across the width has proven to be more robust, detecting incipient slip reliably over the full

range of test conditions, though a combination of both techniques would likely prove to be the most effective solution for improving surgical grasping. Further work is now required to miniaturise this technology so that it can fit within a standard robotic surgical grasper, before analysing it over a wider range of representative test conditions, more closely simulating those used in surgical practice. Ultimately though this work provides a strong basis for the future development of slip sensing technologies for robotic surgical applications, providing two novel sensing methods which could prove effective at helping to automate surgical grasping tasks to help minimise slip events, reduce the occurrence of tissue trauma caused by excessive grasping loads, and reduce surgeon fatigue.

References

- [1] A. I. Margovsky, R. S. A. Lord, and A. J. Chambers. The effect of arterial clamp duration on endothelial injury: An experimental study. *ANZ Journal of Surgery*, 67(7):448–451, July 1997.
- [2] Theo Le Signor, Nicolas Dupre, and Gael F. Close. A Gradiometric Magnetic Force Sensor Immune to Stray Magnetic Fields for Robotic Hands and Grippers. *IEEE Robotics and Automation Letters*, 7(2):3070–3076, April 2022.
- [3] Natalie T. Burkhard, J. Ryan Steger, and Mark R. Cutkosky. The Role of Tissue Slip Feedback in Robot-Assisted Surgery. *Journal of Medical Devices*, 13(2):021003, June 2019.
- [4] Seyed Mohsen Khadem, Saeed Behzadipour, Alireza Mirbagheri, and Farzam Farahmand. A modular force-controlled robotic instrument for minimally invasive surgery - efficacy for being used in autonomous grasping against a variable pull force: Modular force-controlled robotic instrument. *The International Journal of Medical Robotics and Computer Assisted Surgery*, 12(4):620–633, December 2016.
- [5] Tamas D Nagy and Tamas Haidegger. A DVRK-based Framework for Surgical Sub-task Automation. *Acta Polytechnica Hungarica*, 16(8):18, 2019.
- [6] Wei Chen, Heba Khamis, Ingvars Birznieks, Nathan F. Lepora, and Stephen J. Redmond. Tactile Sensors for Friction Estimation and Incipient Slip Detection – Towards Dexterous Robotic Manipulation: A Review. *IEEE Sensors Journal*, pages 1–1, 2018.